A Phase Plane based perspective of Energetics of Large Scale Tropical Convection

By

Vijit Maithel

A dissertation submitted in partial fulfillment of
the requirements for the degree of

Doctor of Philosophy
(Atmospheric and Oceanic Sciences)

at the
UNIVERSITY OF WISCONSIN-MADISON
2023

Date of final oral examination: 6/28/2023

The dissertation is approved by the following members of the Final Oral Committee:
Larissa Back, Professor, Atmospheric and Oceanic Sciences
Angel Adames-Corraliza, Assistant Professor, Atmospheric and Oceanic Sciences
Stephanie Henderson, Assistant Professor, Atmospheric and Oceanic Sciences
Tristan L'Ecuyer, Professor, Atmospheric and Oceanic Science
Sam Stechmann, Professor, Mathematics
Dan Vimont, Professor, Atmospheric and Oceanic Science

Abstract

A Phase Plane based perspective of Energetics of Large Scale Tropical Convection

by Vijit Maithel

Rainfall and convection in the tropics has huge impacts on the lives and livelihood of almost 40 percent of the global population that resides there. However, we still lack a complete understanding of the full spectrum of convective variability that is observed in the tropics. One such component of this spectrum is the cyclic increase and decrease in rainfall at sub-seasonal scales in the tropics. Such cyclic patterns, termed as convective life-cycles, have been observed ubiquitously throughout different regions in the tropics across a range of different timescales. This suggests that such cyclic evolution is fundamental to tropical convection and how it interacts with its environment. Further, global climate models seem to find it difficult to replicate such variability realistically. This makes it even more important for us to better understand the underlying mechanisms and where the models are going wrong.

In this dissertation, I aim to provide a phase plane based framework to understand the different aspects and mechanisms associated with such cyclical modes of variability. The phase plane based framework presented in this study is built upon the moist static energy (MSE) budget framework. It provides a new way to visualize and extend the application of MSE budget. We test and verify the usefulness of this framework as a process-oriented diagnostic tool by applying it to different observational and reanalysis data sets, with

the hope that future work can adapt this to be applied to understand model biases and errors.

Chapter 2 introduces novel phase angle diagnostics to understand convective evolution. The phase angle is physically related to the notion of gross moist stability (GMS). It allows us to track the daily evolution of GMS which was not possible earlier due to the highly variable nature of the metric at shorter timescales. Chapter 2 also highlights that convective life-cycles are strongly linked to the evolution of moisture and can be considered as moisture recharge-discharge cycles. Results show that these recharge-discharge cycles are a type of moisture mode driven primarily by advection of moisture by the convective circulation. Interestingly, the cycles over different regions in the tropics seem to have a similar timescale. Chapter 3 applies the GMS phase plane to analyze easterly waves in the Eastern Pacific. We observe that easterly waves also show a cyclic evolution on the phase plane driven by advection of MSE similar to recharge-discharge cycles. However, not all cyclic evolution on the phase plane is associated with easterly waves events. This helps extend the applicability of the phase plane based framework to other tropical wave modes and for understanding moisture modes in general.

In chapter 4, we focus on a more lagrangian perspective of the ubiquitous convective evolution by introducing a new MSE variance phase space. The use of MSE variance allows us to understand convective evolution in terms of convective aggregation. The results highlight that large-scale convective aggregation in the real world is in the form of aggregation-disaggregation cycles. The results also highlights the important role of

advection of MSE in maintaining and driving aggregation-disaggregation cycles which has been relatively less studied compared to radiative feedbacks.

Acknowledgements

I would like to take this opportunity to acknowledge that this PhD is not just the research work presented in this thesis but is also a product born out of how people around me have influenced and contributed to my life. I would like to thank my advisor Larissa Back for giving me the opportunity to pursue this PhD in the first place. She has been a great mentor throughout this journey. In addition to all the support and guidance with our research, I particularly appreciate how she has given me the opportunity to develop each of the research projects in my own way.

I would like to thank all my committee members - Ángel Adames-Corraliza, Dan Vimont, Sam Stechmann, Stephanie Henderson, and Tristan L'Ecuyer. Their comments and inputs over the years have helped improve the scope of this research work greatly. I would also like to take this opportunity to thank all the faculty members at AOS. Through discussions and classes, I have learned a lot from them about not just the subject but also the different ways to be a great scientist, teacher, mentor, and person. I would also like to thank Pete, Christi, Dee, Carolyn, Sue, and Chelsea for their support with tech and administrative issues throughout my time at Madison.

I would also like to thank all my previous mentors and teachers as well. There are too many to name but they have all played a big part in driving me to be interested in science and research in general. I would particularly like to thank J. Srinivasan and Ashwin Seshadri, my undergraduate thesis mentors. They introduced me to atmospheric science and science research, and that positive experience is the biggest reason I decided to apply for grad school.

I would like to thank all my friends and extended family for their support, and camaraderie. Special mention to Pooja, Sreenath - Akshaya, Abhilash, Sapan, Hardik - Zeel, and Mayukh who have been like my family away from home in Madison. I would like to thank Miguel, who has been an awesome office mate through all these years and has

gone through all the ups and downs of graduate student life with me. I would also like to mention Zach and Kuni, previous members of Back research group, who were always willing to share their time and advice to help me figure out what I want to do in life. I would also like to mention Victor, Rosa, HC, Rudra, and Juliet. Even though many of them came to the department after me, in many ways they made me feel welcome in the department and that I belong here.

Lastly, this list will be incomplete without mentioning two groups of people closest to me. First is TDA – Anadi, Chandu, Abeer – Shraddha, Pai, Patil, Karthik, Jyot, Soni, Lath, Barda, Bose, and Akhil – Manali. Thank you for somehow always making me feel that we are back at BITS where anything is achievable, no problem too big, and most importantly no moment too small or overbearing to not share with friends. And second is my family, specially my parents, Beena and Sameer Maithel for being my biggest source of support and inspiration throughout my life. They have been an infallible failsafe for countering every problem in my life, always knowing what exactly I need whether I know it myself or not. I would not be able to complete this journey without all of you.

There are many more people that I have had the pleasure of interacting with, learning from, traveling together, performing music with, playing basketball, badminton, volleyball, organizing events with and just shared my life with in general that I am unable to mention here. But please know that I deeply cherish and feel immensely grateful for all those moments when I think of what and who all have contributed to help me succeed in my life.

Contents

List of Figures

Chapter 1

Introduction

1.1 Background

Weather in tropics is perhaps best characterized by the broad range of spatio-temporal scales over which convection and precipitation can vary. These can range from size of a single cloud to systems like the Intertropical Convergence Zone (ITCZ) which span the whole planet; from clouds that grow and decay in a matter or minutes to cloud bands in ITCZ that move with seasons. This is all a consequence of the complex two way interactions between convection and the large-scale environment which causes organization of convection at different scales. Therefore, understanding these interactions and the rainfall variability it causes is of key importance for the lives and economic activity of almost 40 percent of the world population which resides in the tropics.

Convection generates circulation and clouds which impact the large scale environment, by 1) releasing latent heat when water vapor condenses to liquid water in clouds, 2) moving around moisture and temperature, 3) heating or cooling from interaction of clouds and water vapor with the incoming solar and outgoing longwave radiation. In return, the large scale environment also controls convection by 1) controlling the stability of the atmospheric column making it more favorable or unfavorable for convection, 2) drying up the rising convective parcel as it entrains and mixes with the environmental air, 3) providing necessary conditions or a push to trigger convection. All these factors happen simultaneously, at different speeds and scales giving rise to the large range of variability that we observe.

Role of moisture has been found to be particularly important in understanding the nature of these interactions. Although other theories which do not include moisture have found some success in explaining tropical variability, they also have some serious limitations. Among these, most notable is the dry shallow water model in an equatorial β plane by Matsuno (1966), which showed existence of equatorial wave solutions in the tropics. Wheeler and Kiladis (1999) showed that space-time spectra of observed tropical convective variability does closely lie around the dispersion curves from Matsuno's dry model. However, there are also some key differences like the phase speed of the waves in dry theory being unrealistically fast, some unexplained peaks in the observed spectrum, etc. (review Kiladis et al., 2009). These differences are expected to arise because of role of moisture and its impact on how these dynamic modes are coupled with convection (Adames, 2022, Adames et al., 2019, Raymond and Fuchs, 2007, ,etc.).

The evolution of column moisture can be studied prognostically using the column integrated moist static energy (MSE) budget (Equation 1.1).

$$\frac{\partial\langle Lq\rangle}{\partial t} \approx \frac{\partial\langle h\rangle}{\partial t} = -\langle\omega\partial h/\partial p\rangle - \langle\mathbf{v}\cdot\nabla h\rangle + \langle Q_R\rangle + S \tag{1.1}$$

Where, $h \equiv c_pT + gz + Lq$ represents MSE, c_pT represents the temperature in energy units, Lq represents moisture in energy units, gz is the geopotential energy, Q_{R} represents radiative heating, S represents net surface flux, $\mathbf{v}$ represents horizontal winds, ω represents the vertical velocity and $\langle\,\rangle$ means mass weighted vertical integral between the 1000 and 100 hPa pressure levels.

The MSE budget can be used to study column moisture in the tropics because the temperature tendency tends to be very small owing to the weak temperature gradient (WTG) approximation (Sobel and Bretherton, 2000, Sobel et al., 2001). As a result, the MSE tendency primarily tends to follow the moisture tendency, and sources and sinks of MSE can be considered as sources and sinks of moisture. The WTG approximation has been found to be well applicable to the tropics at pretty much all timescales longer than 2 days. Using the MSE budget also has the following advantage over moisture budget. The tendency term in the MSE budget is of comparable scale to other terms in the budget. In contrast, in the moisture budget, the moisture tendency is generally orders of magnitude smaller compared to other terms in the dominant balance. That makes it difficult to use

the moisture budget equation to understand how tendency is related to sources and sink of moisture and that is why the MSE budget is preferable .

Equation 1.1 tells us that the following can act as sources and sink of column MSE or column moisture. Vertical advection, $\langle \omega \partial h/\partial p \rangle$ which represents the transport of MSE due to convergence or divergence. Horizontal advection, $\langle \mathbf{v} \cdot \nabla h \rangle$ which represents the horizontal transport of MSE by the circulation when horizontal MSE gradients exist. Radiative heating in the column, $\langle Q_R \rangle$ which adds or removes MSE due to radiative processes and feedbacks including water vapor radiative feedbacks, as well as cloud radiative feedbacks. And net surface fluxes, S which is the sum of latent and sensible heat fluxes (LH and SH respectively).

Some of the earliest works utilizing MSE and MSE budgets date back to Riehl and Malkus (1958), and Yanai et al. (1973) which successfully used early observations to develop key insights about the structure of clouds and large-scale circulation in the ITCZ. Yanai et al. (1973) in particular was the first study to outline the framework to calculate cloud mass flux profiles and MSE budgets by combining observational data and parameterization scheme. They were able to show that shallow convection moistens the large-scale environment to make deep convection possible and that there is large-scale slow downwelling in the tropics at any given instant of time with upward motion restricted to a limited number of deep convective cores.

Neelin and Held (1987) computed column MSE budgets to explain large-scale surface convergence in the tropics based on thermodynamic profiles. The success and complexity

of the results were remarkable given the simplicity of the model. Another key contribution of the paper is to define and develop the gross moist stability (GMS) parameter which could be used as a quantitative diagnostic tool to study thermodynamic mechanisms in tropical convection. The GMS represents the efficiency of MSE export during convection. The paper highlighted thermodynamic controls on tropical convection and the ability of MSE budgets and GMS to diagnose these controls. Raymond et al. (2007), and Raymond et al. (2009) further improved upon the GMS framework by defining a normalized GMS, a verison of which will be used in this study and will be introduced later.

Despite its success, the Neelin and Held model and other subsequent models built on that framework like Neelin and Zeng (2000), also had some big limitations, particularly in explaining day-to-day or faster timescale variability of convection. The models only account for a single baroclinic mode because of which they are unable to account for variability in vertical motion profile shape. Back and Bretherton (2006) showed that vertical motion profile shape is very critical for understanding whether GMS is negative or positive, and that a single GMS value can not explain the full range of tropical convective variability realistically.

Use of MSE budgets has only been more popularly adopted recently, over the last 20 years, given that the underlying framework has been around since much before that. This was made possible due to the ability to compute these budgets from gridded datasets like reanalyses to evaluate the relevant mechanisms and build a process level understanding. Back and Bretherton (2005) was the first paper to do so, computing MSE budgets

from ERA-40 and NCEP Reanalysis data to look at processes driving wind speed - precipitation relationship. Since then, MSE budgets and GMS have been widely used to investigate the thermodynamics of tropical convection using observational data (Inoue and Back, 2015, 2017, Masunaga, 2013, Masunaga and L'Ecuyer, 2014, Sobel et al., 2014, etc.), reanalysis data (Back and Bretherton, 2006, Inoue et al., 2021, Mayta and Corraliza, 2023, Peters et al., 2008, Yu et al., 1998, etc.), and in convective models of varying complexity (Andersen and Kuang, 2012, Bretherton et al., 2005, Maloney, 2009, Raymond, 2000, Sessions et al., 2010, Wing and Emanuel, 2014, etc.). MSE budgets have been particularly useful in improving our understanding of the Madden Julian Oscillation (MJO)(Madden and Julian, 1971) which is one of the leading modes of tropical variability (Andersen and Kuang, 2012, Kiranmayi and Maloney, 2011, Maloney, 2009, Sobel et al., 2014, Wolding and Maloney, 2015, Wu and Deng, 2013, etc.). Apart from the MJO, MSE budgets and GMS have also been used to examine WTG simulations (Raymond and Fuchs, 2007, Raymond and Sessions, 2007, Sessions et al., 2010), moisture modes (Raymond et al., 2009), tropical cyclogenesis (Juračić and Raymond, 2016), monsoons (Adames and Ming, 2018, Srinivasan, 2001), ITCZ (Back and Bretherton, 2006, Yu et al., 1998), quasi-equilibrium simulations (Neelin and Yu, 1994, Yu and Neelin, 1997), convective self-aggregation (Arnold and Randall, 2015, Bretherton et al., 2005, Masunaga et al., 2021, Wing and Emanuel, 2014), convectively coupled waves (Yasunaga et al., 2019), and convective life-cycles or moisture recharge-discharge cycles (Inoue and Back, 2015, 2017, Inoue et al., 2021, Maithel and Back, 2022, Masunaga and L'Ecuyer, 2014).

In this dissertation, we will focus on characterizing and understanding the variability

associated with convective life-cycles or moisture recharge-discharge cycles, which are a mode of cyclical variability found ubiquitously throughout the tropics. We are also interested in delving deeper into the properties and extending the application of the GMS phase plane framework, which had been developed as a diagnostic tool to visualize these recharge-discharge cycles. The subsequent sections in this chapter provide a quick, and probably incomplete introduction of the recharge-discharge cycles and the GMS phase plane framework. The main aim being here to motivate the broader physical insights about large-scale tropical convection that this dissertation tries to build upon rather than present a thorough literature review. A more complete introduction with review of the background literature for the respective topics is included in each of the subsequent chapters.

1.2 Recharge-Discharge cycles : A ubiquitous cyclical pattern

Convective life-cycles are statistical cycles of increasing and decreasing precipitation at sub-seasonal timescales. These have been observed in satellite based datasets (Inoue and Back, 2017, Masunaga and L'Ecuyer, 2014), reanalysis (Inoue et al., 2021, Wolding et al., 2020, 2022), and field campaign data (Hannah et al., 2016, Inoue and Back, 2015, Mapes et al., 2006). Further, these have been observed throughout the tropics over different ocean basins (Inoue and Back, 2017, Inoue et al., 2021, Maithel and Back, 2022). We will show in Chapter 2 that convective life-cycles can also be interpreted as moisture

recharge-discharge cycles and that the two terms can be used interchangeably. We will use the term convective life-cycles to refer to this cyclic variability till chapter 2 and then switch to using recharge-discharge cycles.

These cycles differ from other dynamical cyclic modes of convective variability in the tropics like the MJO, convectively coupled waves, etc. in that they are not associated with a particular time or spatial scale by definition. Instead they can be identified as cyclic patterns in time series data when passed through a simple 24 hour running mean filter and analyzed through a lagrangian framework. So technically, any of the dynamic cyclic modes can be considered as convective life-cycles since they also display cycles of increasing and decreasing precipitation. However, since no timescale is being filtered out, convective life-cycles actually represent a cyclic mode of evolution when variability from all the various timescales is mixed together. Interestingly, as we will present in Chapter 2 later, these cycles seem to have a similar timescale and similar evolution of MSE budget terms in different regions (Maithel and Back, 2022). This is despite the fact that different regions are known to be dominated by different dynamic mode for eg. MJO (30-60 day timescale) in Indian and West Pacific Ocean, while easterly waves (2-10 day timescale) dominate Eastern Pacific and Atlantic Ocean basins. This suggests that the cycles represent some fundamental mechanisms with which convection evolves and organizes which is resulting in emergence of a similar pattern when different timescales are mixed together. Mapes et al. (2006) also discuss about a prototypical convective life-cycle which can be seen at different time scales having a similar structure, noting

that it is different from the different dynamic modes which will generally have different structures at different timescales.

The fact that these cycles represent very fundamental ways in how convection interacts with its environment, make it important that our weather and climate models can represent these mechanisms correctly. Since these mechanisms are related to convective evolution at sub-seasonal timescales, inaccuracies in representing these mechanisms can also be a big source of error in long term forecasts. Wolding et al. (2020, 2022) show how global climate models and different reanalysis datasets can disagree in being able to represent such cyclic evolution realistically. This calls for a need for more process oriented diagnostics (POD) to help understand and diagnose where exactly the models may be going wrong. This dissertation aims to contribute towards that need, though additional steps are needed to further develop our diagnostics into something used by modeling centers, since this research will deal more with proposing and verifying new diagnostics. Applying the diagnostics to various models will be a natural future direction for this work.

1.3 GMS phase plane

Recharge-discharge cycle waves can be visualized by employing different lagrangian frameworks each of which tries to track the evolution using some physical property rather than in space (eulerian). In this work, we make use of a GMS phase plane (Inoue and Back, 2015, 2017, Masunaga and L'Ecuyer, 2014) to do so. However, Wolding et al. (2020)

have shown similar cyclic evolution using a column saturation fraction - precipitation phase space, and Wolding et al. (2022) use a dilute - undilute plume bouyancy phase space. Each method can have its own strengths and weaknesses, and tends to put more emphasis on different mechanisms.

The GMS phase plane is constructed by taking the divergence of dry static energy (DSE) on the x-axis vs divergence of MSE on y-axis. Thinking about it more physically, the x-axis of the GMS phase plane represents the amount of convection or precipitation, whereas y-axis of the GMS phase plane aims to represent the column MSE tendency. Convective life-cycles show up as counter-clockwise elliptical orbits on such a phase plane. A characteristic of the GMS phase plane is that GMS is the slope of the line connecting the origin to a point on the phase plane. It should be noted that none of the three frameworks are completely from a lagrangian perspective in that a travelling wave in space without growth or decay will also appear as a cycle on the phase space. So one should maybe consider the cycles on the GMS phase plane as part translatory and part evolutionary. We try to modify and present a more lagrangian phase space, focusing more on evolution of wave rather than its translation in chapter 4.

The GMS phase space will be analyzed in more detail in Chapter 2, but for the argument being presented here, what is important is that it represents a way to visualize how MSE tendency and precipitation evolve with respect to each other. They are related to each other because MSE tendency represents moisture tendency under WTG approximation. Further, since moisture is tightly coupled to precipitation in the tropics (Bretherton

et al., 2004, Raymond, 2000), moisture tendencies can drive precipitation tendencies and hence describe how precipitation changes with time. Counter-clockwise evolution on the phase plane is a natural consequence of this relationship showing that positive MSE tendency leads to an increase in precipitation and vice versa. Therefore, any systematic evolution on the GMS phase space like that of convective life-cycle implies that the two assumptions related to WTG approximation and moisture-precipitation coupling are valid. And inversely, systematic counter-clockwise evolution on the GMS phase plane describes convective variability that is being driven by moisture.

In that regard, convective life-cycles can be considered to represent the impact of moisture - precipitation coupling on convective organization in the tropics, showing that moisture variability leads to cyclic growth and decay of precipitation at sub-seasonal timescales ubiquitously throughout the tropics. We will discuss a little bit about the relation of these cycles with the dynamics in chapters 3 and 4, but that is an important question that warrants more systematic analysis than what is presented in this thesis. Recent work by Adames-Corraliza and Mayta (2023), Mayta and Corraliza (2023) do present observational and theoretical evidence for dynamic modes that could be related to this type of ubiquitous variability.

1.4 Dissertation outline

Putting everything together, this dissertation broadly aims to explore the energetics of generic large-scale convective variability in the tropics which is in the form of sub-seasonal

cycles of precipitation. We will use and build new diagnostics based on the GMS phase plane framework to characterize this convective variability. It should be noted that such cyclic evolution on the phase plane is expected to be a direct consequence of a strong moisture-precipitation coupling in the tropics. In that regard, this dissertation explores the characteristics of generic convective variability in the tropics driven by moisture-precipitation coupling.

Chapter 2 will focus on extending our understanding of the evolution of MSE budget terms during different phases of convective life-cycles, and how they contribute to its evolution. It introduces a new phase angle diagnostic to understand changes in GMS during convective life-cycle evolution. Further, it aims to compare results across different datasets and different regions in which such convective life-cycles have been noted in previous studies. Results from a theoretical moisture mode model are also compared with observations to verify that this cyclic variability is indeed behaving like a moisture mode.

Chapter 3 explores the idea that cyclic variability on the GMS phase plane is a type of moisture mode by looking at whether Easterly waves in the Eastern Pacific, which are another type of moisture mode, also show up as counter-clockwise cycles on the phase plane. We also verify whether the Easterly wave cycles show similar patterns as Chapter 2 in how the various MSE budget terms contribute to its evolution.

Chapter 4 aims to focus more on the total growth and decay of the convective life-cycle recognizing that propagation of a wave in space can also look like growth and decay

on the GMS phase plane. We do so by presenting a novel MSE variance phase space diagnostic that makes use of spatial variance of MSE and is unaffected by the apparent growth and decay of MSE due to a propagating wave mode. Such a framework also draws parallels between these life-cycles, convective aggregation, and convective self aggregation, showing that large scale convection tends to cyclically aggregate and disaggregate in space. Contribution of the various MSE budget terms to these aggregation-disaggregation cycles is explored.

Finally, chapter 5 presents the broad conclusions and the key new findings from this dissertation.

The three main chapters from this thesis, chapters 2,3, and 4, correspond to or will correspond to three independent peer reveiwed publications. Chapter 2 has already been published as Maithel and Back (2022), while chapter 3 will be converted to a manuscript for submission in Geophysical Research Letters (GRL) after adding some more analysis. Chapter 4 is a close to final draft for submission in Journal of Climate..

Chapter 2

Moisture Recharge-Discharge Cycles: A Gross Moist Stability based Phase Angle perspective

2.1 Introduction

Convective phenomena in the tropics are the result of complex interactions between convection itself, and the large-scale environment. These phenomena, observed at different spatial and temporal scales, can often be associated with at least one of the two broad type

[1]Material in this chapter is an exact version of: Maithel, V., and L. Back, 2022: Moisture Recharge–Discharge Cycles: A Gross Moist Stability–Based Phase Angle Perspective. *J. Atmos. Sci.*, 79, 2401–2417

of instabilities; the moisture mode instability which is due to the relationship between moisture and precipitation (Raymond and Fuchs, 2007), and the instabilities associated with the various convectively coupled linear wave modes (Kiladis et al., 2009, Matsuno, 1966). Moisture mode-based theories have found great success in explaining the slower convective modes, in particular the Madden Julian Oscillation (MJO; Adames and Kim, 2016, Fuchs and Raymond, 2017, Raymond and Fuchs, 2009, Sobel and Maloney, 2013, and others). Moisture modes have also been associated with convective life-cycles (Inoue and Back, 2017, Inoue et al., 2021). However, current climate models have had a hard time simulating these interactions between moisture and circulation (Stevens and Bony, 2013), and the convective variability that results from it accurately, eg. MJO (Ahn et al., 2017, Hung et al., 2013, Jiang et al., 2015, Kim et al., 2014), and convective life-cycles (Wolding et al., 2020). Therefore, there is a need for good process oriented diagnostics to study the role of moisture (and hence moisture modes) and compare theory, observations and climate models.

Budgets of column moist static energy (MSE) or moist entropy have proved remarkably useful in studying the evolution of moisture from a process level. These budgets have helped understand how interactions between radiation, surface fluxes, and advection impact organization of convection at different time and spatial scales (Andersen and Kuang, 2012, Back and Bretherton, 2006, Beucler and Cronin, 2016, Bretherton et al., 2005, Juračić and Raymond, 2016, Kiranmayi and Maloney, 2011, Maloney, 2009, Masunaga and L'Ecuyer, 2014, Wing and Emanuel, 2014, Yasunaga et al., 2019, and many

others). Gross moist stability, Γ (GMS) comes out as a natural parameter and a diagnostic tool from some of these analyses, and helps address the need for process-oriented diagnostics to some extent. GMS represents the efficiency of MSE export or import in the column by advection, and is defined as the ratio of energy added or removed by the circulation divided by the amount of convection (Neelin and Held, 1987, Raymond et al., 2009). Despite its effectiveness, use of GMS is complicated because it is a difficult quantity to calculate. When the amount of vertical motion is close to zero, the GMS ratio is pushed towards infinity making its use difficult as a diagnostic tool. Although there are methods to overcome these limitations in calculating GMS (e.g. Hannah and Maloney, 2014), studying the time evolution of GMS itself, specially at shorter time resolution is still challenging. Convective cycles are one such phenomena which is particularly plagued by this issue.

Convective cycles have been observed in satellite based datasets (Inoue and Back, 2017, Masunaga and L'Ecuyer, 2014), reanalysis (Inoue et al., 2021, Wolding et al., 2020, 2022), and field campaign data (Hannah et al., 2016, Inoue and Back, 2015, Mapes et al., 2006) during which convection undergoes statistical cycles of increase and decrease in large-scale upward vertical motion at time scales much longer than those associated with a typical mesoscale convective system life-cycle. The ubiquitous nature of these convective cycles suggests that the mechanisms responsible for its evolution are fundamental to convection in the tropics. Furthermore, current climate models have a hard time simulating this type of variability accurately (Wolding et al., 2020). Therefore it is important to understand the role of various column processes during the different phases of the convective cycle.

During a complete cycle, large-scale upward vertical motion anomalies will transition between negative and positive values leading to GMS values becoming infinite when the magnitude of upward vertical motion is small. This restricted the scope of previous studies trying to understand these cycles through a GMS based framework (Inoue and Back, 2015) by forcing them to confine their analysis to only one half of the cycle. This paper expands on the GMS based framework developed in Inoue and Back (2015) and tackles these issues by defining an alternative parameter to represent the role of GMS, namely the GMS phase angle.

Previous studies (Inoue and Back, 2015, 2017, Inoue et al., 2021) utilize a GMS phase plane to study these convective cycles. The GMS phase plane, defined as the divergence of dry static energy (DSE) on the x-axis vs divergence of MSE on y-axis (Inoue and Back, 2015, Masunaga and L'Ecuyer, 2014), provides a geometric visualization of convective cycles in the form of elliptical orbits with GMS being the slope of the line connecting the origin to a point on the phase plane (Fig. 2.1). Then, a phase angle can be defined on the phase plane corresponding to the GMS value for a point, effectively converting the unbound slope magnitude into a finite ranged angle value. Though the transition from GMS value to GMS phase angle is not a linear transition, nevertheless, the physical interpretation of the phase angle values is similar to GMS. This paper proposes GMS phase angle as a new diagnostic tool that can be used to study these cycles in detail and compare theory, observations, and models.

During a convective cycle, when convection increases in strength, Inoue and Back (2015)

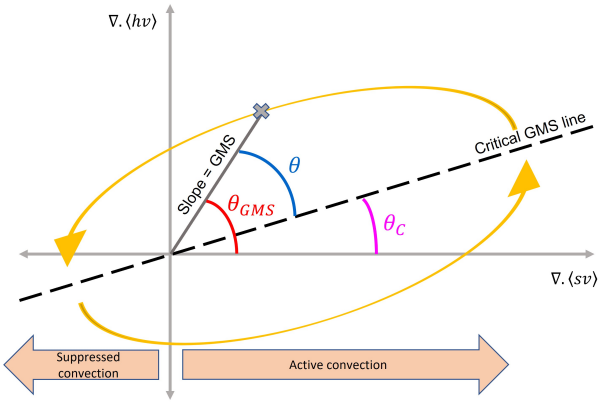

FIGURE 2.1: Schematic showing the GMS phase plane and the various phase angles. The GMS phase angle,θ_{GMS} (red) represents the MSE advection terms. Critical GMS phase angle, θ_c (pink) represents the column radiation and surface flux terms. Life-cycle phase angle, θ (blue) is the difference between the two and represents the angle with respect to the critical GMS line. θ is related to the MSE tendency term in the MSE budget. Arrows in yellow show the trajectory of a typical RD cycle on the phase plane.

refer to it as the amplifying phase and when it decreases in strength, they refer to it as the decaying phase. In terms of MSE, the increase and decrease in convective strength coincides with increase and decrease in column MSE. In the free troposphere, under the Weak Temperature Gradient approximation (WTG; Sobel and Bretherton, 2000, Sobel et al., 2001) variations in temperature are very small in the tropics. As a result, variations in column MSE are primarily associated with increase or decrease of column moisture. Therefore, the convective life cycles can also be considered as moisture or column MSE recharge discharge cycles in this regard. The context in which the term, recharge discharge cycles is being used here could be a bit different to how it has been used in previous studies (eg. Chikira, 2014). By recharge discharge, we refer to changes in column moisture or MSE and the processes that contribute to it in context of describing the physical state of the large scale environment, and not it terms of recharge discharge of convective instability associated with convective plumes. From here on we will use convective life cycles or just

convective cycles and recharge discharge (RD) cycles interchangeably.

We write the MSE budget equation as:

$$\frac{\partial\langle Lq\rangle}{\partial t} \approx \frac{\partial\langle h\rangle}{\partial t} = -\langle\omega\partial h/\partial p\rangle - \langle\mathbf{v}\cdot\nabla h\rangle + \langle Q_R\rangle + S \tag{2.1}$$

where h represents MSE, Lq represents moisture in energy units, Q_{R} represents radiative heating, S represents net surface flux, $\mathbf{v}$ represents horizontal winds, ω represents the vertical velocity and $\langle\,\rangle$ means mass weighted vertical integral between the 1000 and 100 hPa pressure levels. Based on the MSE budget, changes in column moist static energy or column moisture can be associated with vertical advection ($\langle\omega\partial h/\partial p\rangle$), horizontal advection ($\langle\mathbf{v}\cdot\nabla h\rangle$), radiative heating in the column ($\langle Q_R\rangle$), and the net surface fluxes (S) which is the sum of latent and sensible heat fluxes (LH and SH respectively).

The diabatic terms (radiative and surface fluxes) which can be approximated as a linear feedback of convective strength (Bretherton and Sobel, 2002, Su and Neelin, 2002), act as a line of separation between the two phases on the GMS phase plane which Inoue and Back (2015) called the critical GMS (black dashed line in Fig. 2.1). Critical GMS represents the efficiency with which diabatic terms change the column MSE. For points on the line, advection of MSE balances the diabatic terms and MSE tendency is zero. For points below this critical line, the right hand side of equation 1 is positive leading to increase in moisture and convection, and for points above the line the right hand side is negative leading to decrease in moisture tendencies (fig. 2.2a) (Inoue and Back,

2015, 2017). This interplay between MSE advection and the diabatic terms govern the convective variability during the life-cycle and is broadly consistent with the nature of mechanisms possible for moisture evolution under WTG (Chikira, 2014).

The question then arises, how does this interaction between the advective terms and the diabatic terms change during the course of the cycle and how does this impact the evolution of the RD cycle itself? Inoue and Back (2015) look at this question in the TOGA COARE dataset (Webster and Lukas, 1992) by defining a drying efficiency parameter which is similar to the notion of effective GMS (e.g. Bretherton and Sobel, 2002, Hannah and Maloney, 2014, Su and Neelin, 2002, and others). It combines the effect of advective terms on column MSE tendency with the effect of radiative feedbacks and surface fluxes. Results from Inoue and Back (2015) are restricted to only the anomalously high convective part of the cycle due to limitation of using GMS based variables. They find that the diabatic terms have a destabilizing impact on the column that supports growth of moisture anomalies during both the amplifying and decaying phase (support convection). Horizontal and vertical advection have a varying impact importing MSE into the column during the amplifying phase phase (support convection) and exporting MSE out of the column during the decaying phase (inhibit convection). They also argue vertical advection is more dominant in the amplifying phase and horizontal advection is more dominant in the decaying phase of the life cycle. Alternatively, Inoue et al. (2021), using ERA-Interim data, show that horizontal advection is more important for predicting growth or decay of precipitation during the cycle including the amplifying phase, hypothesizing that the presence of other wave modes is responsible for the importance of vertical

advection in Inoue and Back (2015). Horizontal advection is found to be more important than vertical advection in other slower modes too including damping of MJO amplitude (Wolding et al., 2016).

It should be mentioned that interpretations of the MSE budget for a cyclic or wave mode also depend on the frame of reference. Amplification or decay in a Lagrangian view corresponds to horizontal propagation of the wave in an Eulerian framework. Analysis in previous work (Inoue and Back, 2015, Inoue et al., 2021, Wolding et al., 2020) and in this study follow a Lagrangian point of view which corresponds to a propagating wave mode in the Eulerian view.

A simple theoretical model for the advective terms during the convective life-cycle is presented in Inoue and Back (2017) based on idealised linear moisture mode theory. The parameters of the simple model, which can be calculated based on observations, do a good job of simulating the elliptical orbits on the GMS phase plane and indicate the relevance of moisture for convective life-cycle variability. Inoue et al. (2021) also highlight the similarity between the assumptions in moisture mode studies and their analysis of convective life-cycles based on MSE budgets, and argue that same mechanisms as moisture modes are applicable more broadly for explaining convective variability in the tropics beyond just the Madden Julian Oscillation (MJO). Other studies have also looked at and found moisture dynamics to play an important role in explaining different aspects of tropical convective variability associated with different tropical wave modes (review by Adames and Maloney, 2021).

Our present study looks in particular at the role being played by radiative fluxes, surface fluxes, vertical advection and horizontal advection during different phases of the RD cycle using the GMS phase angle framework. Since these cycles have been observed ubiquitously, we are particularly interested in what these results will imply about the processes related to a more general variability of convection in the tropics. We are especially interested in studying the time evolution of the cycle more explicitly than has been done in past work with the help of time derivative of phase angle. We perform the analysis for TOGA COARE data, satellite-based data and reanalysis data to compare the RD cycles and underlying processes observed in all three data sets. Observations are also compared with an idealized model of the life cycle consistent with moisture modes to understand the contribution of moisture dynamics in governing convective variability associated with the life cycles.

Section 2 describes the datasets and data processing techniques used in this study. Section 3 presents the basic equations and the theoretical framework for the phase angle parameters and the simple model based on moisture mode theory. Section 4 presents the features and characteristics of RD cycles when analyzed using the GMS phase angle framework. Further discussions are presented in section 5, followed by concluding remarks in section 6.

2.2 Data and Methods

This study uses observational and reanalysis datasets to study the evolution of column integrated moisture tendency and moist static energy budgets (eq. 2.1) during RD cycles. The first part of the study is carried out using a version of field campaign data from TOGA COARE (Webster and Lukas, 1992) which was constrained to conserve column integrated mass, and energy quantities (Zhang and Lin, 1997). This dataset, spanning the four month long intensive observation period from 1 November 1992 to 28 February 1993 with a 6 hour time resolution is also passed through a 24 hour running mean filter to remove the effects of diurnal cycle and ensure that the WTG approximation is valid (Inoue and Back, 2015, Yano and Bonazzola, 2009).

The second part of the study uses a mix of satellite based datasets and ERA-Interim reanalysis data (Dee et al., 2011) to study RD cycles over different spatiotemporal scales. We utilize a daily time series data over 8 years from 2000 to 2007 to be able to compare results directly with Inoue and Back (2017). Satellite based datasets are used for precipitable water, radiative heating, as well as latent and sensible heat surface fluxes using the same data treatment process as Inoue and Back (2017). Precipitable water is provided by Remote Sensing Systems and is derived from the TRMM Microwave Imager (TMI; Wentz et al., 2015), Special Sensor Microwave Imager (SSMI; Wentz et al., 2012) and Advanced Microwave Scanning Radiometer for Earth Observing System (AMSR-E; Wentz et al., 2014). The radiative heating estimates are derived using the Hydrologic Cycle and Earth's Radiation Budget (HERB; L'Ecuyer and Stephens, 2003, L'Ecuyer and

Stephens, 2007) algorithm from TMI. The surface flux data was obtained from SeaFlux (Curry et al., 2004). The diurnal cycle and seasonal cycle are removed from data for all three variables and the data is regridded to a 2° x 2° horizontal resolution spatial domain. More detailed information about these data procedures can be found in section 3 of Inoue and Back (2017).

Our study differs from Inoue and Back (2017) by making use of ERA-Interim reanalysis data (Dee et al., 2011) to calculate the advective terms in the moist static energy budget rather than calculating them as budget residuals. Horizontal wind fields, along with the temperature and moisture fields are used from ERA-Interim to calculate horizontal and vertical advection explicitly which Inoue and Back (2017) did not do. The ERA-Interim data from 2000 to 2007 is also converted to a daily time series at a 2° x 2° spatial resolution, and the diurnal cycle and seasonal cycle is removed to match the satellite-based datasets. Additionally, we also pass all the data through a 10 - 90 day Lanczos bandpass filter with 75 weights to further remove any other short term and long term variability apart from the one already removed as part of the diurnal and seasonal cycle. The bandpass filter helps reduce the noise and displays the convective cycle signal better in the longer time series. Changing the number of weights does not impact the results significantly (not shown). The length of the bandpass filter is chosen arbitrarily and does not impact the results qualitatively (not shown).

For similarity, we focus our study on the four main tropical ocean basins defined in Inoue and Back (2017). These are defined by selecting grid points, with mean precipitation

greater than 5mm per day, between 5°S - 5°N, 60° - 90° E for Indian Ocean (IO); 5°S - 5°N, 150° - 180°E for Western Pacific (WP); 0° - 15°N, 190° - 250°E for Eastern Pacific (EP); and 0° - 15°N, 300° - 360°E for Atlantic Ocean (AO).

2.3 Theoretical Framework

2.3.1 GMS and Drying Efficiency (Inoue and Back, 2015)

Because advection of MSE can also change with changing amount of convection, in addition to changing gradients of MSE, it makes sense for many purposes to normalize column MSE advection per unit of convection. This introduces GMS, Γ ($= \nabla \cdot \langle h\mathbf{v} \rangle / \nabla \cdot \langle s\mathbf{v} \rangle$) in our analysis as the MSE budget becomes:

$$\frac{\partial \langle Lq \rangle / \partial t}{\nabla \cdot \langle s\mathbf{v} \rangle} = -\frac{\nabla \cdot \langle h\mathbf{v} \rangle}{\nabla \cdot \langle s\mathbf{v} \rangle} + \frac{\langle Q_R \rangle + S}{\nabla \cdot \langle s\mathbf{v} \rangle} \tag{2.2}$$

Here, s represents dry static energy (DSE), $\nabla \cdot \langle s\mathbf{v} \rangle$ represents total advection of DSE, and $\nabla \cdot \langle h\mathbf{v} \rangle$ is the total advection of MSE given by the sum of vertical and horizontal advection of MSE. DSE advection, $\nabla . \langle s\mathbf{v} \rangle$ can be used as a metric for amount of convection in the normalization above. The dominant balance in the DSE budget (eq. 2.3) is between the advective term and convective heating, LP (P is amount of precipitation):

$$\nabla \cdot \langle s\mathbf{v} \rangle = \langle Q_R \rangle + LP + SH \tag{2.3}$$

Since the column radiative heating and surface fluxes are proportional to P, the terms on the right hand side in eq. 2.3 can be combined together and $\nabla.\langle s\mathbf{v}\rangle$ can be linked to amount of precipitation. Inoue and Back (2015) define the right hand side of eq. (2.2) in terms of the drying efficiency parameter, $\Gamma - \Gamma_C$ where Γ_C is the critical GMS defined as $\Gamma_c = (\langle Q_R\rangle + S)/(\nabla.\langle s\mathbf{v}\rangle)$. While Γ represents the impact of advective terms in the MSE budget, Γ_C represents the impact of the diabatic fluxes (column radiation and surface flux).

$$\frac{\partial\langle Lq\rangle/\partial t}{\nabla\cdot\langle s\mathbf{v}\rangle} = -(\Gamma - \Gamma_c) \tag{2.4}$$

During the convectively active phase ($\nabla\cdot\langle s\mathbf{v}\rangle > 0$) of the cycle, when drying efficiency is negative moisture anomalies increase, and when drying efficiency is positive moisture anomalies decrease. This makes drying efficiency a useful diagnostic tool. However, as highlighted earlier, the usefulness of drying efficiency is restricted because the value is not well defined when amount of upward vertical motion (as defined by dry static energy advection) is small, as is often the case in tropics which is close to radiative-convective equilibrium.

2.3.2 Transitioning to phase angles

This issue is tackled by defining phase angle parameters on the GMS phase plane. As mentioned previously, GMS and GMS-like quantities which represent the slope of a line on the GMS phase plane can be easily transformed into an angle value (Fig. 2.1). This is done by computing the arc tangent of the relevant GMS like quantity. The resulting angle value can be easily interpreted physically in terms of GMS using the phase plane,

and at the same time it is well defined throughout the time series and can be used for other analysis.

Since the critical GMS line acts as the boundary between the recharge and the discharge phase, the life cycle phase angle, θ is defined as the angle between the line connecting a point to the origin and the critical GMS line (blue angle in Fig. 2.1). The life cycle phase angle, θ value then represents whether a point lies below the critical GMS line or above it, and is analogous to drying efficiency in Inoue and Back (2015). Geometrically from Fig. 2.1,

$$\theta = \theta_{\text{GMS}} \; - \; \theta_c \tag{2.5}$$

where,

$$\theta_{\text{GMS}} = \arctan\left(\frac{\nabla \cdot \langle h\mathbf{v}\rangle}{\nabla \cdot \langle s\mathbf{v}\rangle}\right), \; and \tag{2.6}$$

$$\theta_c = \arctan\left(\frac{\widehat{\langle Q_R\rangle + S}}{\nabla \cdot \langle s\mathbf{v}\rangle}\right) \tag{2.7}$$

Here, θ_{GMS} is called the GMS phase angle, and θ_c is called the critical GMS phase angle, and $\widehat{\langle Q_R\rangle + S}$ represent linearly regressed diabatic fluxes ($\langle Q_R\rangle + S$) on $\nabla.\langle s\mathbf{v}\rangle$. The GMS phase angle represents the efficiency of the advective term in transporting MSE and the critical GMS phase angle represents the efficiency of radiative heating and surface fluxes terms.

Eq. (2.5) makes use of the observation that the diabatic fluxes can be well approximated through a linear regression line (Inoue and Back, 2017) to calculate the life cycle phase angle. An alternate method can be to calculate a single arc tangent value of the full right hand side of eq. (2.2). Life cycle phase angle values calculated through both the methods are closely correlated with one another (not shown). Using eq. (2.5) has the advantage that impact of advective and diabatic terms can be calculated explicitly.

The critical GMS phase angle, θ_c calculated as per eq. (2.7) is a constant for a given diabatic flux time series and does not impact how the life cycle phase angle will evolve with time. However, the underlying diabatic flux terms can vary in time. These can be represented by defining a time varying diabatic flux phase angle, θ_{diab} using the following equation.

$$\theta_{\text{diab}} = \arctan\left(\frac{\langle Q_R \rangle + S}{\nabla \cdot \langle s\mathbf{v} \rangle}\right) \tag{2.8}$$

Additionally, using eq. (2.9), the GMS phase angle can be further broken down into vertical GMS angle, θ_V and horizontal GMS angle, θ_H to represent the contribution of vertical and horizontal advection respectively:

$$\theta_V = \arctan\left(\frac{\langle \omega \partial h/\partial p \rangle}{\nabla \cdot \langle s\mathbf{v} \rangle}\right),\ \textit{and}\ \theta_H = \arctan\left(\frac{\langle \mathbf{v} \cdot \nabla h \rangle}{\nabla \cdot \langle s\mathbf{v} \rangle}\right) \tag{2.9}$$

Because angles do not add up like scalars, the vertical and horizontal angles will not add up to give the GMS phase angle, unlike vertical and horizontal GMS which add up to

give total GMS. However, defining the vertical and horizontal GMS angles will allow us to study each of these terms individually in the phase angle framework.

It should be noted that the initial arc tangent values which will range from $-90°$ to $90°$ cannot differentiate between the right (convectively active) and the left half (convectively inactive) of the phase plane. To do so the arc tangents values are modified such that the final phase angle values range from $-180°$ to $180°$. Then the phase angles cover the entire phase plane uniquely. Schematics in Fig. 2.2 show the range of the various phase angles and the corresponding area on the plane spanned the respective angle values.

2.3.3 Physical interpretation of phase angle parameters

Physically, phase angles can be interpreted just like GMS, in terms of energy transport. For example, a negative θ_{GMS} implies that the system lies below the x-axis (Fig. 2.2b). As a result, divergence of MSE (y-axis) is negative in that state and the system is importing MSE through advection. Similarly, a negative θ value will represent that the system is below the critical GMS line and hence is in the recharging phase. Fig. 2.2 represents the relation between various phase angle values and their contribution to MSE budget. Furthermore, the magnitude of phase angle values can be used to diagnose the efficiency of the system. Higher phase angle magnitudes imply high values of MSE advection (y-axis magnitude) for small convective strength (x-axis magnitude). Therefore, these are states during which convection is highly efficient at importing or exporting MSE (large GMS magnitude). The vertical and horizontal GMS phase angles can further be understood

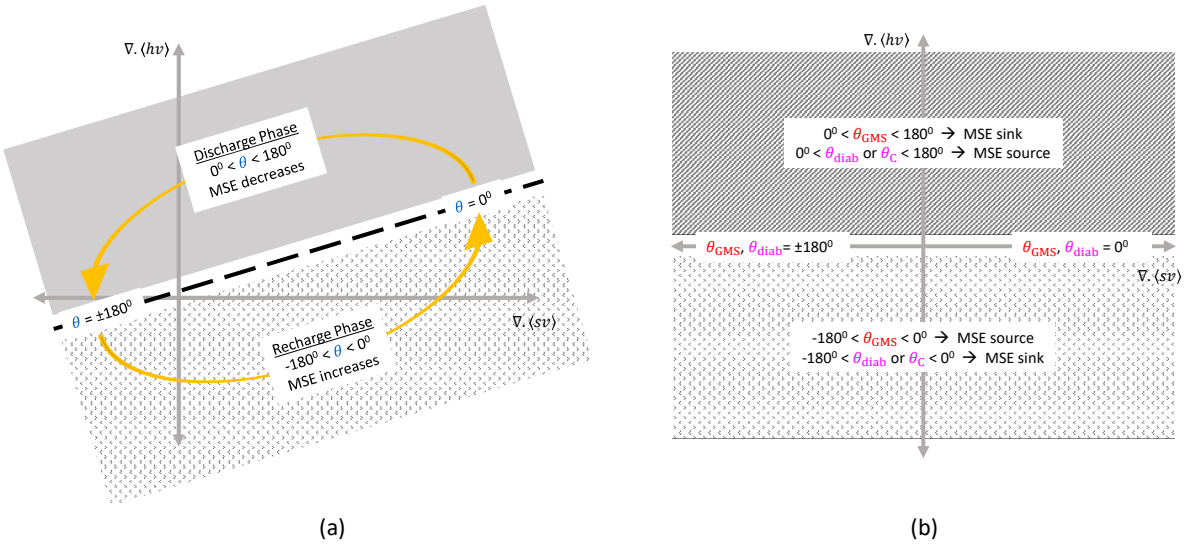

FIGURE 2.2: Schematic showing the various phase angles on the GMS phase plane and their contribution to MSE budget. a) Relation between life cycle phase angle,θ (blue) and the recharge discharge phases. Yellow arrows represent the direction of evolution of a typical cycle. b) Role of critical GMS phase angle, θ_c (pink), and GMS phase angle, θ_{GMS} (red) as source and sink of MSE for different locations on the phase plane.

physically in terms of vertical motion profile shape variability and horizontal transport of moisture across gradients respectively. These are discussed in more detail in section 5.

The relation between amplifying and decaying convective phases with the life cycle phase angle values can be further visualized in a manner similar to Fig. 4 in Inoue and Back (2015) for drying efficiency values. Precipitation rate and metrics of changes in precipitation rate are plotted against both drying efficiency and life cycle phase angle in TOGA COARE data to show that drying efficiency can easily be substituted with life cycle phase angle as the parameter used to study convective life cycles. Binned values of life-cycle phase angle are plotted on the x-axis and are arranged in an increasing order from $-180°$ to $180°$ to represent a composite life cycle. Bins are created for every 8.33%

percentile range containing 39 samples in each bin for TOGA COARE data. Following Fig. 4 from Inoue and Back (2015), Fig. 2.3 shows bin averaged absolute precipitation rate (top row), change in precipitation rate (bottom row), and probability of increase in precipitation rate (middle row) as functions of binned drying efficiency (left) and life cycle phase angle (right). The four vertical lines represent the corresponding location of the same state in the other parameter framework. Owing to the small number of samples in each bin, the error bars corresponding to the 95% confidence interval about the bin mean are relatively large and have been omitted to make the figure clearer. Instead, the average length of the error bars is mentioned in the figure captions. We determine the number of independent samples in the time series data by determining the e-folding timescale from the time lag auto correlation function. Inoue and Back (2017) show that similar characteristics are also seen in a larger independent dataset which will not have the same issue of under sampling.

As one transitions from amplifying to decaying convective phase, we expect that the absolute precipitation rates should peak at this transition as it is the end of the amplifying phase. Moreover, there should be a sharp drop off in the probability of increase of precipitation rate as the cycle goes from amplifying to decaying phase of convection. In terms of changes in precipitation rate, δP will change from positive in amplifying phase to negative during decaying phase. This is observed as drying efficiency values change from negative to positive in Fig. 2.3, as also shown in Inoue and Back (2015). Similar trends are seen as life cycle phase angle value changes from negative to positive, showing the strong relation between phase angle values and the two phases of the cycle. This

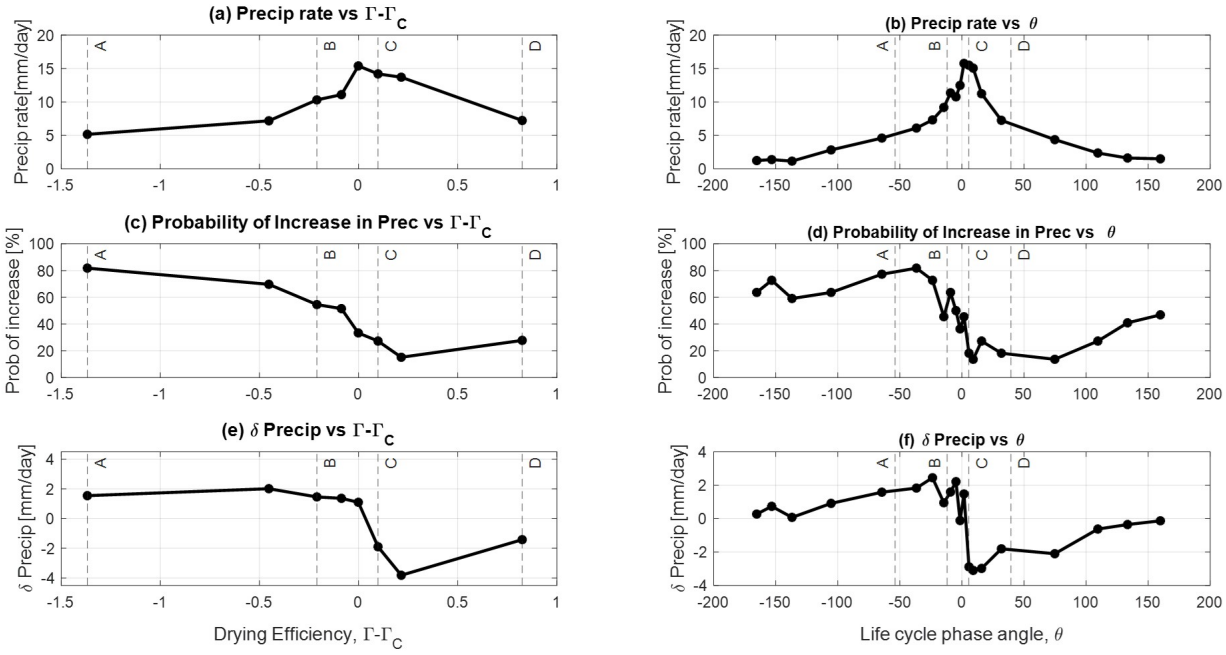

FIGURE 2.3: Precipitation rate (mm/day) (top), probability of increase in precipitation rate with time (middle), and change in precipitation rate (mm/day) (bottom) in TOGA COARE data as a function of binned values of drying efficiency, $\Gamma - \Gamma_C$ (left; a,c, and e. Reproduced from Inoue and Back, 2015) and life-cycle phase angle, θ (right; b,d,and f). A, B, C, and D are corresponding locations of the same physical state in the different frameworks. Average error bar length for each subplot is as follows: a) 4.2 mm/day, b) 3.7 mm/day, c) 36%, d) 48%, e)3.6mm/day, f) 3.5mm/day.

also points towards the advantage of using phase angle instead of drying efficiency. In case of drying efficiency, the analysis is forced to be restricted between -1.5 to 1. This corresponds to a small range in terms of phase angle value as shown by the vertical lines. Therefore, with the use of phase angles, the analysis can be easily carried out and plotted for the entire cycle.

Figure 2.4 represents the evolution of the vertical profiles of a) anomalous moisture (top) and b) anomalous moisture tendencies (bottom) as a function of the composite life cycle. The line plot shows the value of the vertically integrated moisture anomaly for the total

column. The anomalous moisture tendencies are positive throughout most of the troposphere during the increasing convective phase (negative x-axis). This results in the total column being anomalously moist towards the end of the amplifying phase. In contrast, the decaying convective phase (positive x-axis) is dominated by negative moisture tendencies throughout the troposphere and result in an anomalously dry column at the end of the decreasing phase. The exact vertical structure of moisture anomalies is more detailed and consistent with previous studies (Inoue and Back, 2015, Wolding et al., 2022). However, in terms of evolution of column moisture, the convective life-cycle is behaving like a moisture recharge discharge cycle, as expected from eq. (2.1). Fig. 2.3 and 2.4 together also imply that precipitation and column moisture are closely related to each other. This condition along with WTG balance, forms the essence of the moisture mode criteria presented in Mayta et al. (2022). This further supports the idea that moisture dynamics are important for this convective mode.

2.3.4 Idealized model of convective cycle

Inoue and Back (2017) discuss the interpretation of the time dependent and the time independent GMS associated with life cycles using an idealized model to represent the vertical advection term. They show that vertical advection displays elliptical orbits on the GMS phase plane when its variability is modelled from simplified moisture mode solutions that have an imaginary component in the vertical GMS. They also show that the time independent or the background GMS is the fixed value associated with the slope of the major axis of the ellipse and the time dependent GMS varies as the system evolves

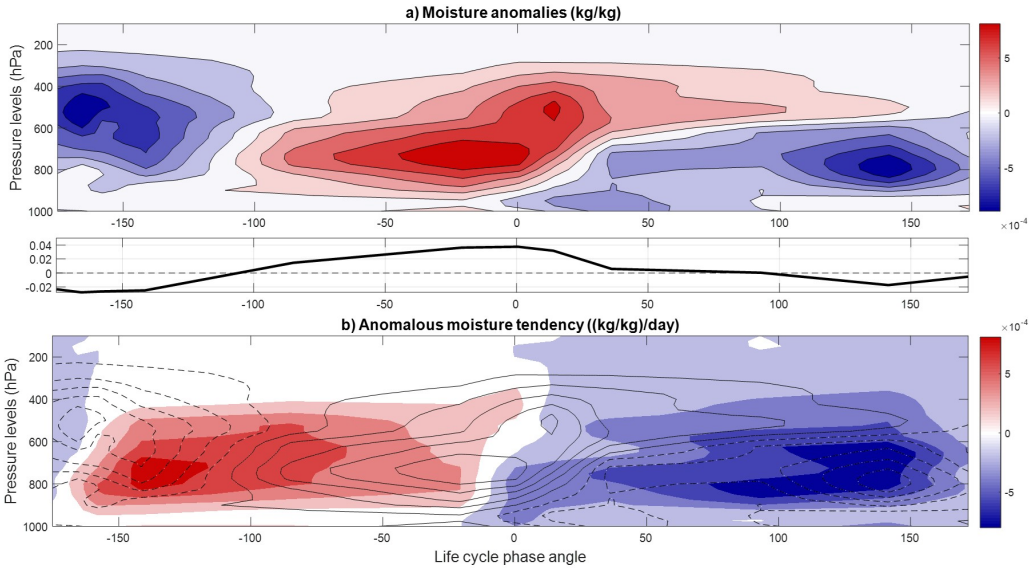

FIGURE 2.4: Anomalous moisture profiles (kg/kg) (top) and anomalous moisture tendencies (kg/kg/day) (bottom) as a function of binned life cycle phase angle values. In the bottom panel, solid and dashed contours represent positive and negative moisture anomalies from the top panel respectively and color shading represents the moisture tendencies. Line plot shows the mass weighted vertical integral of moisture anomaly profiles in (a). Negative values on x-axis correspond to the recharge phase and positive values represent the discharge phase.

during the cycle moving along the elliptical orbits. They also highlight that since only the background GMS is related to stability of the moisture mode, the moisture mode is stable for positive values of time independent GMS and vice-versa. Moreover, it is also possible to have negative time dependent GMS values even in a stable moisture mode. Similar interpretation of negative GMS values is discussed in Raymond et al. (2009) for non-steady state conditions like the ones under which RD cycles would also be classified.

As discussed earlier, column moisture anomalies are important for the evolution of precipitation in moisture mode theories. Further, the tight coupling between column moisture anomalies and precipitation anomalies (e.g. Bretherton et al., 2004) implies that precipitation changes can be modelled in terms of precipitation anomalies in the moisture mode

framework. Following Inoue and Back (2017), an idelaized model can be expressed as

$$\frac{\partial P'}{\partial t} = -(\Gamma_{\text{eff,r}} + i\,\Gamma_{\text{eff,i}}) \times P' \tag{2.10}$$

where P' is precipitation anomaly, and $\Gamma_{\text{eff,r}}, \Gamma_{\text{eff,i}}$ are the real and imaginary model parameters associated with growth or stability of the system and mode propagation respectively. The model permits solutions of the form

$$P'(x,t) = \hat{P} \exp\left[ikx + (\sigma_r + i\sigma_i)t\right] \tag{2.11}$$

where $\hat{P}$ is an amplitude, k is a zonal wavenumber, σ_r, σ_i represent real and imaginary frequencies respectively. We can assume $\Gamma_{\text{eff,r}} = 0$ since the precipitation has to be non zero and finite over a long time series. Based on this setup, equations for the vertical and horizontal advection terms can be derived (not shown) which express how vertical and horizontal advection will evolve for a solution of the form of eq. (2.11) and are given below (Inoue and Back, 2017).

$$\langle \frac{\omega \partial h}{\partial p} \rangle_M \simeq \hat{P}\left[\,\Gamma_{v,r} \cos\Gamma_{\text{eff},i}\; t \;+\; \Gamma_{v,i} \sin\Gamma_{\text{eff},i}\; t\right] \tag{2.12}$$

$$\langle \mathbf{v} \cdot \nabla h \rangle_M \simeq \hat{P}\left[\,\Gamma_{h,r} \cos\Gamma_{\text{eff},i}\; t \;+\; \Gamma_{h,i} \sin\Gamma_{\text{eff},i}\; t\right] \tag{2.13}$$

Subscript M represent vertical and horizontal advection as calculated from the simple

model. $\Gamma_{v,r}$ and $\Gamma_{h,r}$ are the real part of model parameters, and are related to the background (time-independent) vertical and horizontal GMS, whereas $\Gamma_{v,i}$, $\Gamma_{h,i}$, and are the imaginary parts of model parameters associated with the time dependent GMS. Further, these parameters can be estimated from observed data as per the following equations:

$$\Gamma_{v,r} \simeq \frac{\overline{\langle \frac{\omega \partial h}{\partial p} \rangle \times \nabla \cdot \langle s\mathbf{v} \rangle}}{\overline{\nabla \cdot \langle s\mathbf{v} \rangle}^2} \quad , \quad \Gamma_{h,r} \simeq \frac{\overline{\langle \mathbf{v} \cdot \nabla h \rangle \times \nabla \cdot \langle s\mathbf{v} \rangle}}{\overline{\nabla \cdot \langle s\mathbf{v} \rangle}^2} \tag{2.14}$$

$$\Gamma_{v,i} \simeq -\Gamma_{\text{eff},i} \frac{\overline{\langle \frac{\omega \partial h}{\partial p} \rangle \times \frac{\partial \nabla \cdot \langle s\mathbf{v} \rangle}{\partial t}}}{\overline{\left(\frac{\partial \nabla \cdot \langle s\mathbf{v} \rangle}{\partial t} \right)^2}} \quad , \quad \Gamma_{h,i} \simeq -\Gamma_{\text{eff},i} \frac{\overline{\langle \mathbf{v} \cdot \nabla h \rangle \times \frac{\partial \nabla \cdot \langle s\mathbf{v} \rangle}{\partial t}}}{\overline{\left(\frac{\partial \nabla \cdot \langle s\mathbf{v} \rangle}{\partial t} \right)^2}} \tag{2.15}$$

Here, the overbar denotes a time average, and $\Gamma_{\text{eff},i}$ represents the frequency of the life-cycle equal to $2\pi/n$, where n is the number of days it takes to complete a full cycle. The approximate value of n is calculated from data based on values of $\partial\theta/\partial t$ as outlined in the next section. The model parameters in eq. (2.14,2.15) are calculated using the complete TOGA COARE time series, and their value is used in eq. (2.12,2.13) to generate a sample time series for the advective terms as per the simple model. Readers are referred to section 5b in Inoue and Back (2017) for more details and full derivation of the idealized model being used here.

The simple model for the advective terms is combined with a linear model for the diabatic terms (eq. 2.16) which has been shown to be a good approximation at the timescale associated with these RD cycles (Inoue and Back, 2015, 2017). The slope of the critical

GMS line is represented by $\tan(\theta_c)$ in eq. (2.16).

$$(\langle Q_R \rangle + S)_M \simeq tan\theta_c \, \nabla . \langle s\mathbf{v} \rangle \tag{2.16}$$

2.4 Results

2.4.1 TOGA COARE results

The characteristics and evhttps://www.overleaf.com/project/6238b79508c4704f95fc64d2olution of different phase angle components through different phases of the RD cycle are plotted in Fig. 2.5 and 2.6, and the average 95% confidence interval is specified in the figure captions. Figure 2.5 shows the bin averaged value of different phase angle components on the y-axis as a function of binned values of life-cycle phase angle on the x-axis. It should be noted that for the purpose of plotting Fig. 2.5, values on the y axis have been adjusted to be in the range going from $-90°$ to $90°$. Values lesser or greater than this range were shifted to be between $-90°$ to $0°$ and $0°$ to $90°$ respectively. Doing so allows easier interpretation of the y axis in terms of efficiency of MSE import or export. As discussed previously, the $0°$ angle values represents least efficiency and $\pm 90°$ values represent maximum efficiency. Therefore, displacement from $0°$ on the y-axis in Fig. 2.5 means that the phase angle component is more efficient at importing MSE for negative values, and more efficient at exporting MSE for positive values.

This figure is similar to Fig. 5 from Inoue and Back (2015) having the corresponding

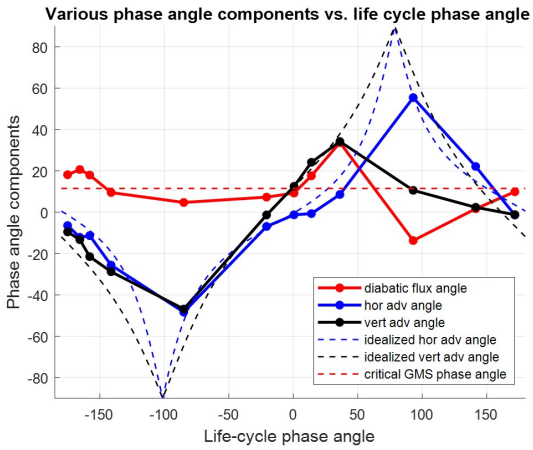

FIGURE 2.5: Various phase angle values as a function of binned life-cycle phase angle, θ for TOGA COARE data; horizontal phase angle (blue), vertical phase angle (black), diabatic flux angle (red), critical GMS phase angle (red dashed), idealized model horizontal advection phase angle (blue dashed), idealized model vertical advection phase angle (black dashed). Negative values on x-axis correspond to the recharge phase and positive values represent the discharge phase. Average error bars showing the 95% confidence interval for the bin means are : vertical phase angle - 19.65, horizontal phase angle - 19.59, diabatic flux angle - 14.53.

phase angle counterparts on the two axes rather than GMS values. Because of the use of phase angles, Fig. 2.5 present a full composite life-cycle and not just the convective half represented in Inoue and Back (2015).

It is observed that the radiative and surface flux terms (solid red curve) stay around a small positive phase value throughout most of the life-cycle. This complements the finding of Inoue and Back (2015) that the diabatic terms closely follow the regression line and are well approximated as a linear feedback at these timescales. The positive critical GMS phase angle value (dotted red line) implies that overall the diabatic terms complement the existing MSE anomaly in the column. They add MSE to the column when column MSE anomaly is positive and remove MSE from the column when anomaly is negative. Further, the diabatic fluxes are larger when the existing anomaly is larger.

In comparison, both horizontal and vertical advective phase angles (blue and black curves respectively) show a cyclic nature, and to some extent are in phase with the life cycle phase angle. The vertical and horizontal phase angles (y-axis) have negative values when the life-cycle phase angle (x-axis) is negative and vice-versa. In terms of energy advection, this implies that both horizontal and vertical advection add MSE when the RD cycle is in the recharge phase and remove MSE when the cycle is in the discharge phase. Additionally, the efficiency of the advective terms is also well correlated with that of the overall cycle with the advective terms being less efficient for life cycle phase angle values around 0° and $\pm 180^\circ$.

The close relationship between the cyclic nature of the RD cycle and the advective terms points towards an important role being played by the advective terms in governing the evolution of the life cycle. This is analysed more closely by calculating the time derivatives of various phase angles explicitly using a central difference scheme on the phase angle time series. Phase portraits as shown in Fig. 2.6 are plotted with the computed derivatives. Figure 2.6 has the same binned values of life-cycle phase angle on the x-axis as Fig. 2.5. However, the y-axis shows the time tendency of the respective phase angle component, or in other words the contribution to life-cycle phase angle tendency from the respective component. Therefore, the positive values on y-axis imply an increase in life-cycle phase angle value and vice versa. This is also qualitatively shown through the arrows on the x-axis in these plots. The arrows point towards the direction in which life-cycle phase angle values will tend to evolve under the influence of that particular term.

Taking the time derivative of eq. (2.5), the time tendency of life cycle phase angle can be represented as $d\theta/dt = d\theta_{\mathrm{GMS}}/dt$. Therefore, the time tendency of vertical and horizontal advection phase angles contribute directly to the time tendency of the life cycle phase angle as they are a part of θ_{GMS}. The critical GMS phase angle, being a constant, does not contribute to the time evolution. However that does not mean that the time evolution of the diabatic terms has no effect on the evolution of life cycle phase angle. As discussed later in this section, there is an indirect, or a non prognostic effect of the diabatic flux phase angle time tendency on the life cycle phase angle through its influence on the critical GMS angle.

Figure 2.6a shows the time tendency of the life-cycle phase angle as a function of binned life-cycle phase angle values. It is observed that the life-cycle phase angle has a positive time tendency and continues to increase throughout the life cycle. This is consistent with our visualization of the composite life cycle as an elliptical orbit moving in the counter-clockwise direction with phase angle going from $-180°$ to $180°$. This is an alternate way compared to the vector plots used in Inoue and Back (2017) to visualize the evolution of life-cycle on the GMS phase plane. There is also a slow-fast behavior associated with the life cycle evolution which is observed here. The life cycle evolves slowly near phase angle values $\pm 180°$ and $0°$ (vertices of the ellipse), shown by the smaller tendency values near these points and faster between them. This slow fast behavior can be associated with existence of equilibrium points in the system and is discussed in more detail in section 5a. Additionally, Fig. 2.6a can also be used to get an estimate of the time period for a composite life cycle by integrating the inverse of life cycle angle tendency over a full

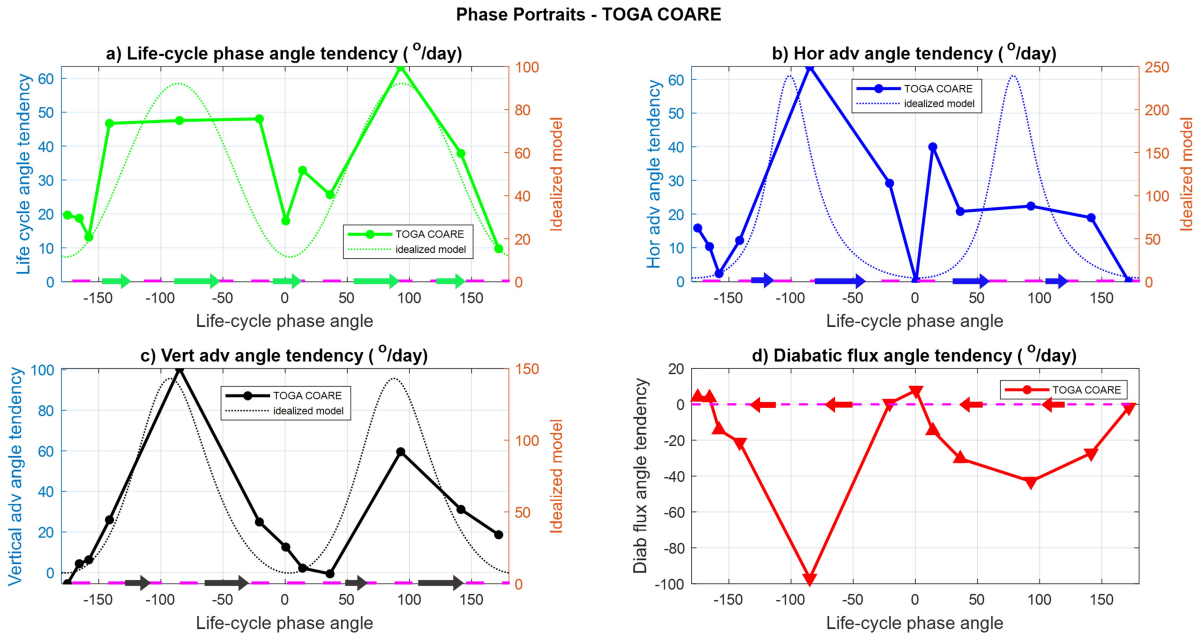

FIGURE 2.6: Phase portraits ($\dot{x}$ *vs* x) of various phase angles as function of binned life-cycle phase angle, θ for TOGA COARE data; a) life cycle phase angle tendency, $\frac{\delta\theta}{\delta t}$ (green), b) horizontal advection phase angle tendency, $\frac{\delta\theta_H}{\delta t}$ (blue), c) vertical advection phase angle tendency, $\frac{\delta\theta_V}{\delta t}$ (black), d) diabatic flux phase angle tendency, $\frac{\delta\theta_{diab}}{\delta t}$ (red). Corresponding values calculated from the idealized model are plotted for a,b, and c in dotted lines with magnitudes on the y-axis on the right side. Arrows on the x-axis represent the impact of the corresponding term on the value of θ on the x-axis. Average length of error bars representing the 95% confidence intervals are : a) 69.7, b) 64.6, c) 68.7, d) 69.6

cycle. Doing so gives the time period of a composite life cycle in TOGA COARE data to be around 11 days.

Figure 2.6b and 2.6c show that the contribution to life cycle phase angle tendency by the horizontal and vertical advection phase angles respectively is very similar to the angle tendency in Fig. 2.6a. The slow fast behavior seen in the life-cycle phase angle tendency is also replicated in the phase portrait of the advective terms. Therefore, the advective terms seems to be acting as the drivers of the RD cycle. Although it is difficult to

determine which between vertical and horizontal advection is the more dominant factor based on this figure alone, neither seems to be negligible in comparison to the other. More detailed discussion on the role of horizontal advection vs. that of vertical advection and their physical interpretation is given in section 5.

Figure 2.6d shows the negative bin averaged time tendency of the diabatic flux phase angle, which includes the radiative and surface flux terms. A negative tendency is plotted because of the difference in sign of the diabatic terms in eq. 2.2. The diabatic flux phase angle tendency does not directly impact the life cycle phase angle as discussed above. However, it does describe the scatter distribution from which the regression slope is being calculated. If the diabatic flux was distributed such that it fits the regression line perfectly then the diabatic flux angle tendency would be zero as diabatic flux evolves along the same line. Therefore, non zero diabatic flux angle tendencies represent departures from the linear approximation. These non linearities impact the calculation of the regression slope and can therefore support changes in the life cycle phase angle value in the direction shown by the arrows in Fig. 2.6d.

Based on Fig. 2.6d, it is observed that the diabatic flux angle tendency supports a leftward evolution of the life cycle phase angle over almost the entire RD cycle. Therefore the second order effect of the radiative and surface flux feedbacks seems to be to resist the observed direction in which the life cycle evolves and slow it down. This resistance is more like a frictional force which opposes the natural evolution of the system but will not cause the system to move in the opposite direction by itself. Similar results have been found in

previous studies (Andersen and Kuang, 2012, Kiranmayi and Maloney, 2011). The first order impact of the radiative and surface flux feedbacks is the critical GMS line slope being positive which represents the diabatic terms acting as a stronger MSE source as convection gets stronger. Long wave cloud convective feedback (lower outgoing radiation for more convection), and wind induced surface heat exchange feedback (WISHE; higher surface fluxes for more convection) are some dominant mechanisms that can result in this positive slope.

Results from the idealized model for TOGA COARE data (described in section 3d) are represented as dotted lines in figures 2.5 and 2.6. Since the diabatic terms in the simple model are modelled as a line, the diabatic flux angle tendency is zero and there is no dotted line counterpart for Fig. 2.6d. The model seems to do quite well in replicating all major features in the two figures. There is a high qualitative agreement between the dotted and solid lines in both the figures. The major differences in shape of the curves can be attributed to the fact that TOGA COARE data has been binned whereas the model time series is not binned. Even quantitatively, the model performs quite well. For Fig. 2.6a, 2.6b, and 2.6c the dotted lines are plotted following the y-axis on the right hand side. Although there is a difference in magnitude between the two axes and parts of the cycle in moisture mode appear to be much faster than the observation, the faster parts are compensated by the slower parts such that the overall timescale of the life cycle is same in the model and observations. Therefore, the idealized model has a great success in replicating the RD cycle behavior. Further insights and interpretations based on the simple model are discussed in section 5.

2.4.2 Results from ERA - Interim and Satellite based datasets

In addition to examining TOGA COARE data, RD cycles are also investigated across different tropical ocean basins using a mix of data products from reanalysis and satellites, as outlined in section 2. The mixed dataset helps test the robustness of these features by studying a longer time series data as well as giving a look at geographic variability. Unlike for TOGA COARE data, the MSE budget in this mixed dataset is not closed because data from different sources is used for different terms. Therefore, precipitable water tendency is used to calculate MSE tendency (left hand side of eq. 2.1) and the life cycle phase angle instead of eq. (2.5). Doing so also allows us to calculate the budget residual and its corresponding phase angle to keep the budget closed. With the 10-90 day filter, using precipitable water tendency to caluclate MSE tendency is a reasonable assumption as WTG approximation is valid at these timescales. 5% percentile bins are used for analyzing the mixed dataset. Each bin has more than 4000 samples in all different ocean basins.

Similar to Fig. 2.5, Fig. 2.7 shows the characteristics of the different phase angle components as a binned function of life-cycle phase angle for the four active ocean basins outlined earlier. The 95% confidence interval for the bin mean value is also represented through the error bars. The diabatic flux angle (red) has a small, positive value throughout most of the life cycle in all ocean basins, similar to TOGA COARE data. This means that the diabatic terms support the existing MSE anomaly in the column during all phases of the life cycle. Horizontal advection (blue) also has a very robust behavior across the different

ocean basins and is well correlated with the life-cycle phase angle as discussed previously for TOGA COARE data. One of the key differences among the ocean basins and with TOGA COARE data is seen in the vertical advection angle (black).

It is interesting to note that the curve for vertical advection angle looks similar in pairs; one being the Indian Ocean - Western Pacific basin, and other Eastern Pacific - Atlantic Ocean basin. In the Eastern Pacific and Atlantic Ocean basins, the vertical advection angle has a very small slope, and looks more similar to the diabatic terms rather than horizontal advection. In contrast, in the Indian Ocean and Western Pacific basins, the vertical advection angle is seen to have a relatively stronger role, particularly for negative life-cycle phase angle values on x-axis. This difference between the two groups could possibly be related to geographic variability in vertical motion profiles in these regions as observed in previous studies (Back and Bretherton, 2006), and is discussed more in the next section. The vertical advection term in all four ocean basins is also very different from TOGA COARE data. This has also been noted in previous studies and could be a result of differences in the scale of the disturbance being observed in the two datasets (Inoue et al., 2021). The Kelvin wave signal could be more dominant in TOGA COARE data, and the MJO or Intra-Seasonal Oscillations (ISO) signal could be more dominant in the mixed dataset.

Never the less, even though the relationship is not as strong as in TOGA COARE, we can still observe that the negative to positive transition in vertical advection phase angle is weakly in phase with the negative to positive transition of life-cycle phase angle on

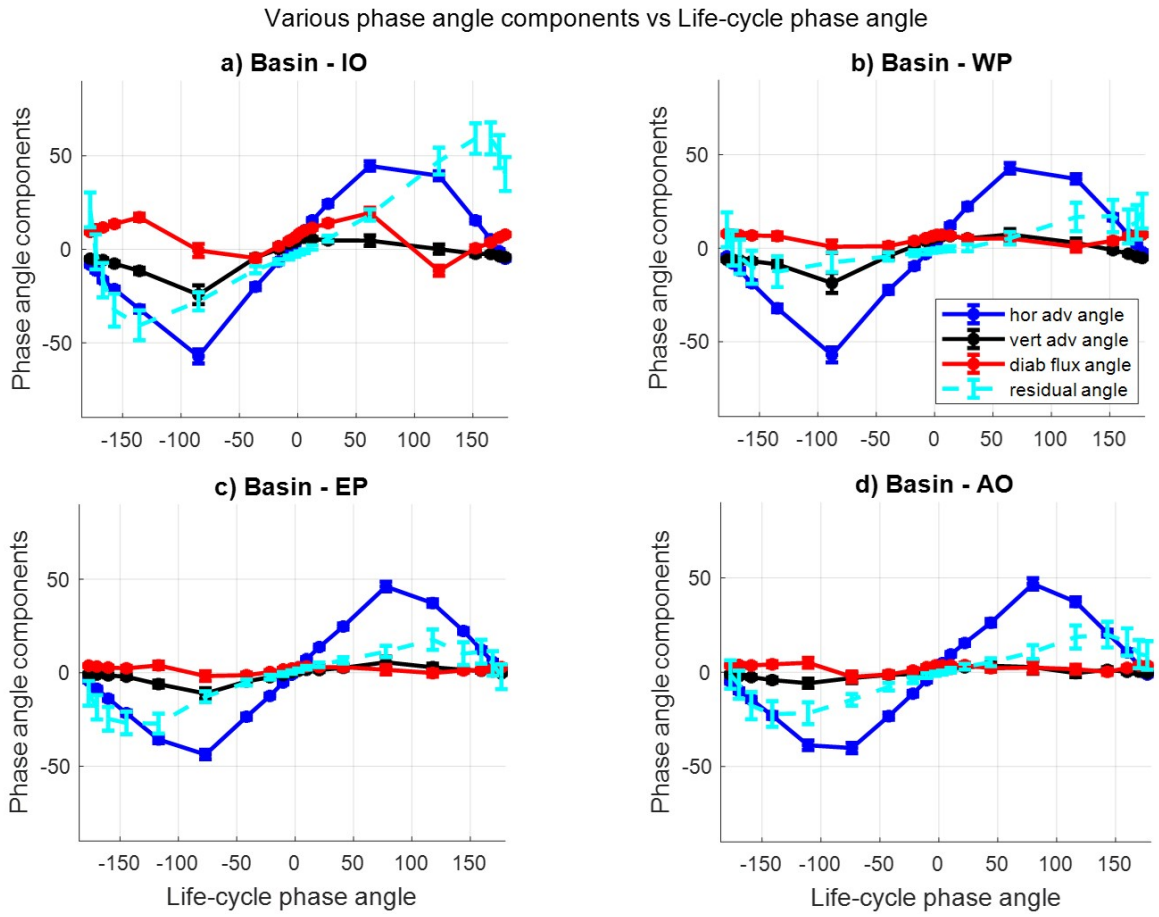

FIGURE 2.7: Same as Fig. 2.5 but with satellite and reanalysis mixed data over different tropical ocean basins; a) Indian Ocean (IO), b) Western Pacific (WP), c) Eastern Pacific (EP), d) Atlantic Ocean (AO). For each subplot a residual phase angle is also plotted in cyan corresponding to the residual term in the MSE budget from eq. 1. error bars represent the 95% confidence interval for each bin mean value.

x-axis in all four ocean basins. It is observed that the residual term (cyan) also has the systematic relationship with life-cycle phase angle like the advective terms. Interestingly, the uncertainties associated with the bin mean residual are also the largest compared to other terms.

Phase portraits of relevant parameters with 95% confidence intervals across different ocean basins are shown in Fig. 2.8. Qualitatively, the phase portraits for the satellite-reanalysis

mixed dataset look similar to those for TOGA COARE. As expected, a positive tendency of the life-cycle phase angle (Fig. 2.8a) is observed in all ocean basins corresponding to counterclockwise life-cycle evolution on the phase plane. The same feature is seen for the two advective term tendencies as well in all four ocean basins. Horizontal advection angle tendencies are shown in Fig. 2.8b and vertical advection tendencies are shown in Fig. 2.8c. The slow fast life-cycle behavior seen in TOGA COARE data is also observed robustly in all ocean basins. A similar pattern as TOGA COARE is also observed for the diabatic flux angle tendency (Fig. 2.8d) in all ocean basins representing their resistive effect on RD cycle evolution.

The time evolution of vertical advection phase angle has a significant impact on the life cycle phase angle tendency in Fig. 2.8 despite the vertical advection phase angle not showing a strong relationship in Fig. 2.7. Further, the similarities in Fig. 2.6 and Fig. 2.8 suggest that similar mechanisms might be relevant for both TOGA COARE and mixed dataset in this aspect even though the scale and mode of the disturbance being observed is different between the two. The main difference between the mixed dataset and TOGA COARE phase portraits seems to be in the magnitude of the phase portraits.

The time period of the composite cycle in satellite data is around 40 days ($\pm$2 days for all basins), which is much larger compared to 11 days in TOGA COARE. One possible reason for this could simply be on account of the fact that the mixed dataset is a much longer time series compared to TOGA COARE. This would allow longer timescales to be more visible in the mixed dataset compared to TOGA COARE. When the 10-90 day

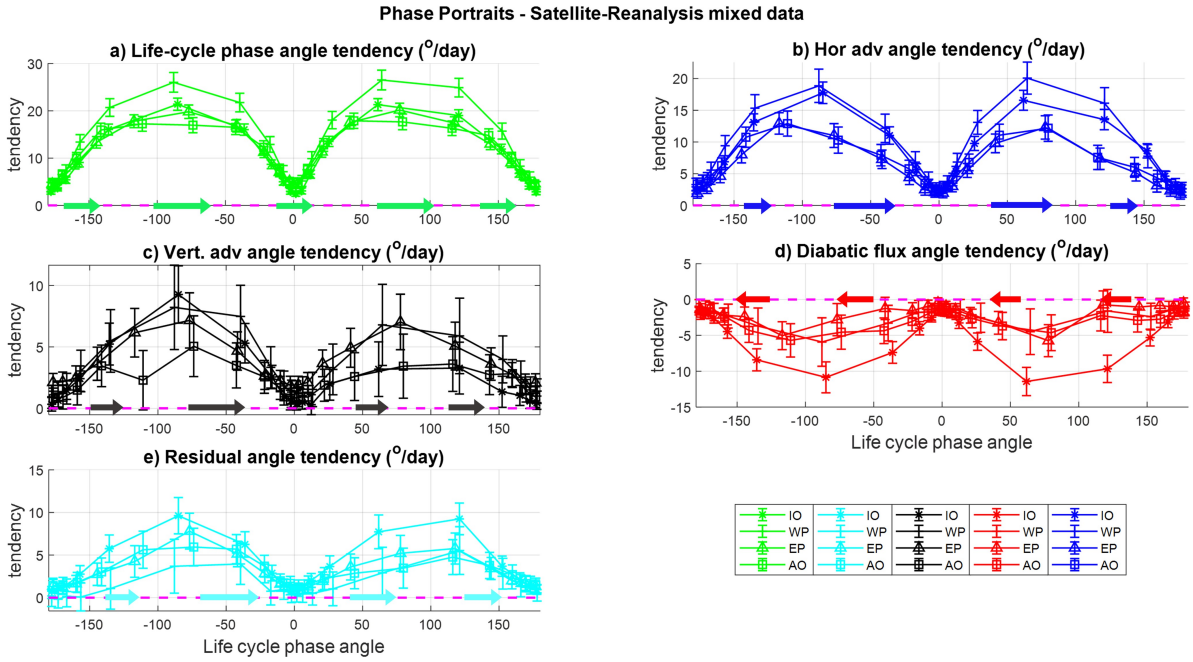

FIGURE 2.8: Same as Fig. 2.6 but with mixed data over different tropical ocean basins; Indian Ocean (IO), Western Pacific (WP), Eastern Pacific (EP), Atlantic Ocean (AO). e) is the phase portrait of the residual phase angle for all four ocean basins.

band pass filter used for mixed data is removed, the phase portraits still qualitatively remain the same but the time period of the cycle changes to around 65 days for all ocean basins (not shown). Conversely, when a fast filter is used (4-20 day band pass filter) the time period of the cycle reduces to 11-15 days in the four ocean basins with the same qualitative results.

A source of residual in the satellite data could be based on the fact that in this study radiation budgets are calculated from data at each pixel, and are not spatially averaged over the ocean basin. L'Ecuyer and Stephens (2003) note that there can be considerably higher uncertainties in the radiation budget at individual pixel level compared to the regional mean. Another reason of uncertainty in the satellite data could be related to the

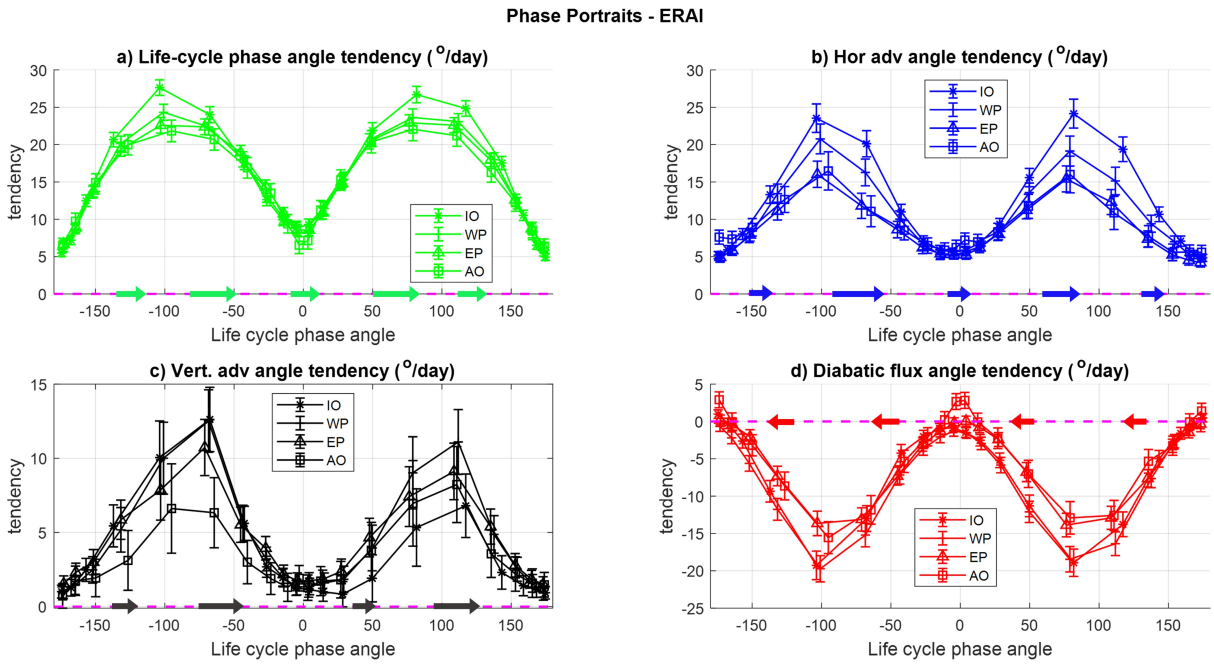

FIGURE 2.9: Same as Fig. 2.8 but with reanalysis data only from ERA-Interim over different tropical ocean basins; Indian Ocean (IO), Western Pacific (WP), Eastern Pacific (EP), Atlantic Ocean (AO). The diabatic fluxes are calculated as a residual from the MSE budget so no separate residual phase angle.

fact that satellite observations measure the state at a particular instant in time, and for many regions in the tropics, satellite overhead passes could be too few in number to be able to calculate daily means accurately. In contrast, the advection terms from reanalysis will be based on daily averages leading to a higher residual. Even TOGA COARE data is at a six hour resolution. This could also lead to some of the observed differences in the mixed data compared to TOGA COARE. The effect of some of these uncertainties could be better understood by only looking at reanalysis data rather than a mix of satellite and reanalysis data.

Figure 2.9 shows the same plots as Fig. 2.8 but only with reanalysis data from ERA-Interim. To better constrain the diabatic flux terms in reanalysis, these are calculated as

a residual in eq. (2.1) since the circulation is better constrained in reanalysis compared to radiative fluxes. With a higher time resolution, daily means from reanalysis data compare better with those from TOGA COARE data than satellite data. Also, with the diabatic terms being calculated as a residual, there can be more certainty at the individual pixel level. The phase portraits in Fig. 2.9 are very similar to the ones in Fig. 2.8, both qualitatively and quantitatively. Just like the mixed dataset, results from reanalysis data differ from TOGA COARE results mainly in terms of their magnitude. The time scale of the life cycle in reanalysis data is also around 40 days, similar to the time scale in mixed data.

Although reanalysis data seems to do a good job in representing this cyclic variability here and in previous studies, there can also be multiple areas of concern. Wolding et al. (2022) show that there are considerable differences in the convective cycles in different reanalysis products. In particular, lack of observations in marine atmospheric boundary layer leads to poor constraints on thermodynamic variables in lower troposphere in the reanalysis Pincus et al. (2017). Wolding et al. (2022) note that this could also contribute to the differences between reanalysis and observations contributing to the residual in figures 2.7 and 2.8. In that case, the residual will be dependent on reanalysis model parameterization and reanalysis increment which could help explain the systematic relationship being seen in the residual term.

Despite the data limitations and inaccuracies, the reanalysis data and observations both do show a cyclic behavior. Compositing over life cycle phase angle, overall we observe

similar mechanisms contributing to the evolution of the composite cycle in terms of column MSE budget. The invariance of key patterns in different data sets and over different regions suggest that these mechanisms are relevant at different time and spatial scales. Coupling between moisture and convection and the resulting dynamics from that coupling could be a viable place to start in understanding this better.

2.5 Discussion

2.5.1 Recharge discharge cycles - a dual equilibrium system

The idealized model for the moisture RD cycles is successfully able to replicate the life cycles in TOGA COARE data. The idealized model consists of the interactions between the linearized diabatic term and the advection terms consistent with moisture mode dynamics. On the GMS phase plane, this is visualized through the line representing the diabatic term, and elliptical orbits for the advective terms in Fig. 2.1. Points of intersection between the line and the ellipse are points where the diabatic terms and advective terms are equal to each other. The MSE budget (eq. 2.1) is balanced at these points and the time tendency of column MSE, $\partial\langle h\rangle/\partial t$ will be zero. Therefore, these are the equilibrium states for the idealized model. In terms of phase angle values, the points of intersection will be the 0° and 180° life cycle phase angle values. And indeed, we see equilibrium point like behavior as the system evolves slowly near these phase angle values in data. The life cycle phase angle tendency is smaller and closer to zero in phase

portraits around these values in not only TOGA COARE (Fig. 2.6) but also in mixed (Fig. 2.8) and reanalysis only datasets (Fig. 2.9).

Arrows in figures 2.6a, 2.8a, and 2.9a also show that both the equilibrium points are half stable points. The system is attracted towards the equilibrium on the left side and is pushed away from the equilibrium on the right side. Therefore the equilibrium states do not appear to be fully stable (attracting from all directions) or unstable states (pushing away in all directions).

The equilibrium point at 0° phase angle corresponds to a wet state with enhanced convection, and the equilibrium point at 180° phase angle corresponds to a dry state with suppressed convection. On a simpler level, physically the wet equilibrium state could be expected to exist based on quasi equilibrium type of ideas and self organization of convection as discussed in Peters and Neelin (2006), Wolding et al. (2022). They argue that a slow buildup of convective instability due to large scale processes and its fast dissipation by convection results in a system that is attracted towards a high critical column water vapor value or a wet equilibrium state. Based on our results, we hypothesize that at intraseasonal timescales the large scale advective terms modify the self organizing behavior around the wet state critical point by introducing the dry state critical point. Because of mass continuity, a convecting atmosphere also controls the amount of subsidence in other areas. At the intraseasonal scales, advection of MSE between the convecting and subsiding regions is able to drive the drying of the convecting region below the critical

column water vapor value. Therefore, the critical point no longer behaves as an attractor for all perturbations. Rather there are drying perturbations which are supported by advective terms that lead to transition of the system from the wet state critical point to the dry state critical point. We expect the magnitude of the dry state to be controlled by the magnitude of the wet state. Averaging over such cycles and moving to a larger scale should result in an overall wet state for the tropics consistent with quasi equilibrium ideas.

2.5.2 Role of horizontal vs vertical advection

Phase portraits in figures 2.6, 2.8, and 2.9 show the contribution of horizontal and vertical advection terms to evolution of the RD cycle across the different datasets. Qualitatively, the two advective terms show a similar behavior, and quantitatively the tendency due to vertical advection is a bit smaller in magnitude but not negligible. This is somewhat in contrast with results of Inoue et al. (2021) who find horizontal advection to be the main driver of convective variability associated with these RD cycles. We explore why this may be below.

Our results suggest that vertical advection has a non negligible contribution to the time evolution of life cycle phase angle. Figure 2.7 shows that the vertical phase angle is small compared to the horizontal phase angle. Further it shows only a very weak correlation with the total phase angle in most of the ocean basins. This matches with the finding in Inoue et al. (2021) that vertical advection does not do a good job in predicting the state of the system on the GMS phase plane. However, looking explicitly at the evolution of the

cycle by computing the time tendency of the life-cycle phase angle reveals that vertical advection is playing a non negligible role there. In other words, vertical advection may not do a very good job of indicating whether the cycle is currently in the recharge or the discharge phase. However, given the current phase, it has a significant contribution to how it will evolve with time and on shape of the cycle. This is perhaps because of the intrinsic relationship between vertical motion profile shape and efficiency of MSE transport through vertical advection in the column. GMS based phase angles then, as a metric, are much better adapted at focusing on this aspect of the recharge discharge cycle behavior and the inherent properties of convection including vertical advection.

2.5.3 Ubiquitous nature of horizontal advection

Convective behavior associated with the RD cycles is observed ubiquitously throughout the tropics, both in this work, as well as previous studies (Inoue and Back, 2017, Inoue et al., 2021, Wolding et al., 2020). Perhaps more surprising is the ubiquitous nature of horizontal advection (Inoue et al., 2021). Due to geographic variations in moisture gradients and the circulation, it is not necessary to expect horizontal advection to have similar patterns or similar timescales in different ocean basins. The ubiquitous nature then suggests that horizontal advection during these recharge discharge cycles is dominated by the part of the circulation which is intrinsically linked to the local convective features, and can thus be expected to be uniform across the different ocean basins. In that case, convection could be playing a dominant role in governing the large scale environment at these scales rather than the other way around.

A possible way to test this could be by decomposing the horizontal advection into being associated with a local and non local flow (appendix A of Wang et al., 2016). Local flow is the part of horizontal circulation which can be attributed to divergence and vorticity of the circulation associated with local convection within the box. In contrast, the non local flow is the part of circulation which is attributed to divergence and vorticity caused by convection elsewhere. Horizontal advection then represents how these transport MSE in the presence of moisture gradients or anomalies (temperature gradients are small in the tropics following WTG approximation).

We hypothesize that horizontal advection during these RD cycles is dominated more by the local flow part, and intrinsically linked to local convection. Horizontal advection due to this local flow will include advection of MSE by the divergent part of local flow (also termed as lateral entrainment in Raymond and Zeng (2005)), and advection of MSE by the rotational part of the local flow. In such a scenario, the non local horizontal advection just pushes around moisture anomalies. When the amount of vertical motion is low, the non local horizontal advection can push the cycle in the recharge or discharge phase (similar to findings of Inoue et al., 2021). However, once the local vertical motion is non negligible, further evolution of convection, and hence moisture, is dominated by the vertical advection and the local horizontal advection. Future work computing this local and non local horizontal advection explicitly during recharge discharge cycles, similar to Wang et al. (2016), can help test these ideas further.

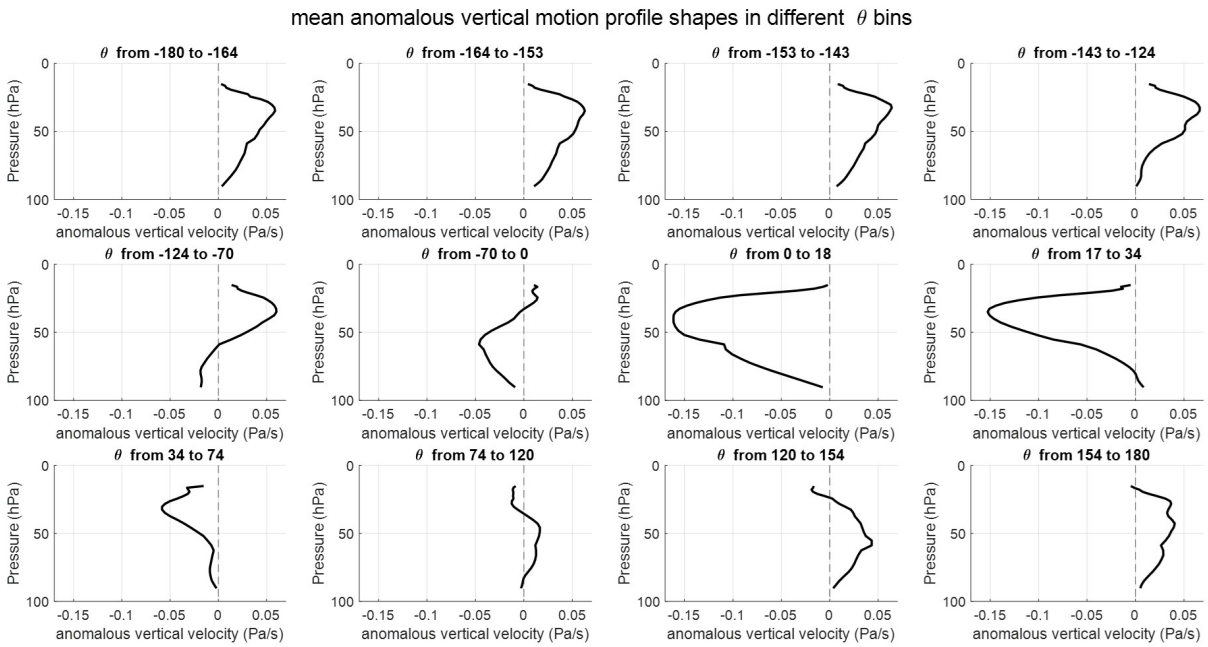

FIGURE 2.10: Vertical profiles of mean vertical velocity (Pa/s) composited over life cycle phase angle, θ bins from the x-axis in figures 2.5, and 2.6. Positive vertical velocities indicate descent and negative values indicate ascent. θ values between $-90°$ to $90°$ is the convectively active phase, and θ greater than $90°$ and less than $-90°$ is the convectively inactive phase.

2.5.4 Role of vertical motion profile shape variability and vertical tilt

We expect the recharge phase to have bottom heavy vertical profiles leading to negative GMS values and import MSE into the column. Oppositely, the discharge phase should have top heavy vertical motion profiles leading to positive GMS values and export of column MSE (Inoue and Back, 2015). Anomalous vertical motion profiles during TOGA COARE averaged over binned life cycle phase angle values are shown in Fig. 2.10. Life cycle phase angle values greater than $90°$ and less than $-90°$, which correspond to the convectively inactive part of the cycle, primarily show subsidence. During the convectively

active part of the cycle, vertical motion profiles are more bottom heavy during negative life cycle phase angles (recharge phase), and transition to a more top heavy profile during positive life cycle phase angle (discharge phase) as expected. Transition of vertical motion profiles from bottom heavy to top heavy, also referred to as 'vertical tilt', has also been observed to be important in other types of tropical convective organization. Inoue et al. (2020) find that the fast moving convectively coupled wave modes like the Kelvin waves, Inertial gravity waves, and the Mixed Rossby Gravity waves all show more significant vertical tilt compared to the slower moisture modes like MJO.

This vertical tilt is very important for the half stable nature of the equilibrium state discussed earlier. After reaching the peak moisture anomaly at the wet equilibrium state, if vertical motion profile continues to be bottom heavy then any drying perturbation will eventually die out rather than grow to push the system towards the dry equilibrium state. Therefore, vertical motion profile shape variability is key for driving the cyclic behavior seen in these RD cycles.

Varying vertical motion profile shape implies a vertical GMS value that is time dependent. In the idealized model, time dependent GMS is associated with a non zero $\Gamma_{\text{eff},i}$ and $\Gamma_{v,i}$ in eq. (2.12). $\Gamma_{\text{eff},i}$ in turn is associated with the propogation of the wave mode in the idealized model. Therefore, vertical tilt can also be important for propagation of faster moisture dominated modes like the convective cycles in TOGA COARE.

2.6 Conclusion

This study aims to develop a better understanding of the role of vertical advection, horizontal advection, and diabatic fluxes in the evolution of moisture recharge discharge cycles and compares these in the TOGA COARE data, satellite data, and reanalysis data. To do so, we define and study various phase angle parameters on the GMS phase plane. The phase angle parameters are analogous to GMS, and represent efficiency of MSE transport by a particular term in MSE budget. They have the advantage that the phase angle values does not go to infinity even if the denominator in GMS becomes very small. Therefore, the phase angle is particularly effective in studying the recharge discharge cycles which are also associated with a cycle of changing GMS values.

The results show the following basic characteristics associated with moisture recharge discharge cycles.

- Diabatic fluxes, which include column radiation and surface fluxes, support the existing MSE anomalies throughout different phases of the cycle.
- When vertical and horizontal advection are acting as a source of MSE, the cycle is in the recharge phase with moisture and precipitation increasing with time. In contrast, when vertical and horizontal advection are acting as a MSE sink, the cycle is in the discharge phase with moisture and precipitation decreasing with time.
- The cycle exhibits a slow fast behavior. The system evolves slowly near two equilibrium points and faster between them. One of the two equilibrium states correspond

to an anomalously moist state with enhanced convection, and the other equilibrium state corresponds to an anomalously dry state with suppressed convection. Near both the equilibrium states, the advective and diabatic flux terms in the MSE budget cancel each other resulting in a small MSE tendency, and slow evolution of the system.

- Both vertical and horizontal advection terms are observed to act like drivers of the RD cycle. Although the impact of the vertical advection term is a bit smaller compared to horizontal advection, it is not negligible. Consistent with previous studies, we find that vertical advection is not a robust indicator of whether the cycle is in the recharge or the discharge phase. However, time evolution of vertical advection does play a significant role (along with evolution of horizontal advection) in driving the evolution of the overall cycle.

- The tendency of diabatic fluxes has an indirect effect on the evolution of the cycle. It is found to resist the observed evolution of the overall recharge discharge cycle and slow it down. The diabatic fluxes themselves amplify the existing MSE anomaly in the system, but the sensitivity of convection to diabatic fluxes slows down the convective evolution during the recharge discharge cycles, consistent with previous studies.

These features are mostly consistent across the various datasets used in this study, ranging from the shorter time scale TOGA COARE data to the longer time series data from satellites and reanalysis covering different tropical ocean basins. The consistency of the

results across different data sets, and the different ocean basins suggests that similar mechanisms are important for understanding the RD cycles over different regions and at different scales. The evidence showing the limitations in our current models in getting this type of variability correctly (Wolding et al., 2020) calls for further research in this area. A starting point could be looking deeper into evolution of moisture and moisture dynamics. The data satisfies many of the key criteria to be classified as a moisture mode. Further, an idealized model based on the same key assumptions as moisture modes is found to replicate the features of the RD cycles in TOGA COARE data accurately. This indicates the importance of moisture and moisture mode like mechanisms in understanding RD cycles and general evolution of convection throughout the tropics despite the differences in scales and dominant wave modes.

Chapter 3

Analysis of Easterly Wave Events during the OTREC Field Campaign using ERA5 Data and GMS Phase Plane

3.1 Introduction

Chapter 2 and other previous studies provide evidence for moisture recharge-discharge cycles to be an inherent mode of variability of the tropical convective circulation (Inoue and Back, 2017, Inoue et al., 2021, Maithel and Back, 2022, Wolding et al., 2022). Challenges in successfully modelling such variability in global climate models (Wolding et al.,

2020) provides incentive for further research in understanding the underlying physics and implications of this variability for our weather and climate. In particular, we still lack a complete understanding about how this generic variability mode might be related to other large-scale convective modes that we know of.

Moisture recharge-discharge cycles have been linked to moisture modes. Inoue and Back (2017) showed that the Madden-Julian Oscillation (MJO) events during the DYNAMO field campaign follow counter-clockwise elliptical trajectories on the gross moist stability (GMS) phase plane similar to recharge-discharge cycles. Inoue et al. (2021) highlight that the basic physical assumptions behind moisture modes including the WTG approximation are also valid during recharge-discharge cycles. Maithel and Back (2022) show how an idealized moisture mode model with realistic parameters could replicate the cyclic variability in TOGA COARE field campaign. This raises the question whether other convective modes that are known to behave as moisture modes like Easterly Waves, Equatorial Rossby waves, etc. (Mayta and Corraliza, 2023, Mayta et al., 2022) also display characteristics of recharge-discharge cycles? If yes, then are recharge-discharge cycles just another way of representing the other moisture modes or do they also account for convective variability that can not be explained by the other convectively coupled wave modes?

A key feature of recharge-discharge cycles is it's evolution along counter-clockwise orbits on the GMS phase plane (Inoue and Back, 2015, 2017). During the recharge discharge cycles, positive moist static energy (MSE) tendency is linked with increasing precipitation,

and negative MSE tendency is linked with decreasing precipitation. The counter-clockwise direction of the orbit in particular is a direct consequence of this relationship. Weak temperature gradient (WTG) (Sobel et al., 2001) and moisture precipitation coupling (Bretherton et al., 2004) are the two main approximations which make this possible. The two approximations also form the physical basis for defining the criteria for moisture modes (Mayta et al., 2022). This implies that other modes of convective variability under the family of moisture modes should also show up as counter-clockwise orbits on the GMS phase plane. Inoue and Back (2017) showed that this is true for MJO events. However while MJO is a slower mode, comparable in timescale to recharge-discharge cycles, other moisture modes like Eaterly wves, or Rossby waves are much faster and evolve differently compared to MJO.

This chapter aims to look at the following two questions. First, do the relatively faster moisture modes, like the easterly or equatorial rossby waves also look like counter-clockwise orbits on the GMS phase plane? Second, is convective evolution during these wave modes driven by advection of MSE similar to recharge-discharge cycles generally? We choose the Organization of Tropical East Pacific Convection (OTREC) field campaign (Fuchs-Stone et al., 2020) study area in the Eastern Pacific basin for our analysis. OTREC field campaign took place in the months of August and September 2019, during which 22 research flights were flown to measure environmental conditions during different stages of convective development over boxes in Eastern Pacific and Caribbean.

The dominant mode of large scale convective variability in the Eastern Pacific region is

easterly waves, accounting for almost 50% of the total variability (Rydbeck and Maloney, 2015). Mayta and Corraliza (2023) show that Easterly waves in Eastern Pacific satisfy the moisture mode criteria and are expected to amplify through the moisture vortex instability mechanism (MVI) (Adames and Ming, 2018). MVI suggests that waves grow because of the convective vortex transporting MSE across meridional gradients. This implies that it is driven by horizontal advection. While previous studies have looked at filtered time series composites to understand the characteristics of Easterly waves, in this study we use phase plane diagnostics on unfiltered data for individual Easterly wave case studies. We will focus on the three Easterly wave events identified during the OTREC time period for this study. This will help extend the phase plane based framework presented in Chapter 1 and explore it's application for studying other large-scale modes in the tropics.

The rest of this chapter is organised as follows. Section 2 describes the data and methods used in this study. Section 3 presents the main results, and Section 4 gives the discussion, summary and direction of future work.

3.2 Data and methods

ERA 5 data (Hersbach et al., 2020) is used in this chapter to carry out the GMS phase plane analysis. Temperature, humidity, vertical velocity and horizontal wind profiles are used to compute the column integrated MSE, water vapor, MSE tendency, water vapor tendency, and vertical and horizontal advection of both MSE and DSE. The gridded

time series has a spatial resolution of $0.5^\circ \times 0.5^\circ$, and time resolution of 6 hours. The column integrated budget terms are passed through a 24 hour running mean filter, like in the previous chapter, to remove the effects of diurnal variability and ensure the WTG approximation is applicable. We focus our analysis to the same domain and time period as the OTREC field campaign. The Eastern Pacific domain box is between 3 - 11 N and 271 - 274 E, and the time period is August - September 2019. Since the dominant balance from the DSE budget is between precipitation and DSE advection, we will be using advection of DSE as a proxy for precipitation for all results in this chapter. We compute a domain mean MSE budget time series to represent convective evolution over the entire box with a single time series for each of the MSE budget terms.

Three Easterly wave events were identified passing through this box during the OTREC time period with peak precipitation on 7th August, 15th August, and 17th September respectively (Huaman et al., 2021). We choose a time period starting from two days before the peak precipitation to 3 days after peak precipitation to cover the full wave life-cycle for our case studies.

Contribution to maintenance and propagation on the phase plane

Previous studies analysing MSE budget evolution have focused on whether processes contribute towards amplifying or decaying existing MSE anomalies (maintenance term) and whether they are in phase with the overall MSE tendency (propagation term). Andersen and Kuang (2012) quantified these by projecting the MSE budget terms onto column MSE anomalies to get the maintenance term (Equation 3.1), and projected them onto

column MSE tendency to get the propagation term (Equation 3.2). A high propagation term represents that the term helps drive the cycle forward in time by changing its phase, while a strong contribution to maintenance term represents that the process is important for determining the amplitude of the cycle.

$$M_x = \frac{\|X' \cdot \langle h \rangle'\|}{\|\langle h \rangle' \cdot \langle h \rangle'\|} \tag{3.1}$$

$$P_x = \frac{\left\| X' \cdot \frac{\partial \langle h \rangle'}{\partial t} \right\|}{\left\| \frac{\partial \langle h \rangle'}{\partial t} \cdot \frac{\partial \langle h \rangle'}{\partial t} \right\|} \tag{3.2}$$

In Equation 3.1 and Equation 3.2, X represents a term from the MSE budget in Equation 2.1, $'$ represents the anomaly from a time mean, $\|...\|$ represents an integral over a time period.

3.3 Result

3.3.1 Easterly Waves during OTREC on GMS Phase Plane

We track and plot the evolution of individual easterly waves on the GMS phase plane to verify if they also have the form of counter-clockwise orbits as expected for a moisture mode. As mentioned previously, we focus on the three easterly waves were identified to have passed through the Eastern Pacific region (Huaman et al., 2021) during the period of OTREC field campaign.

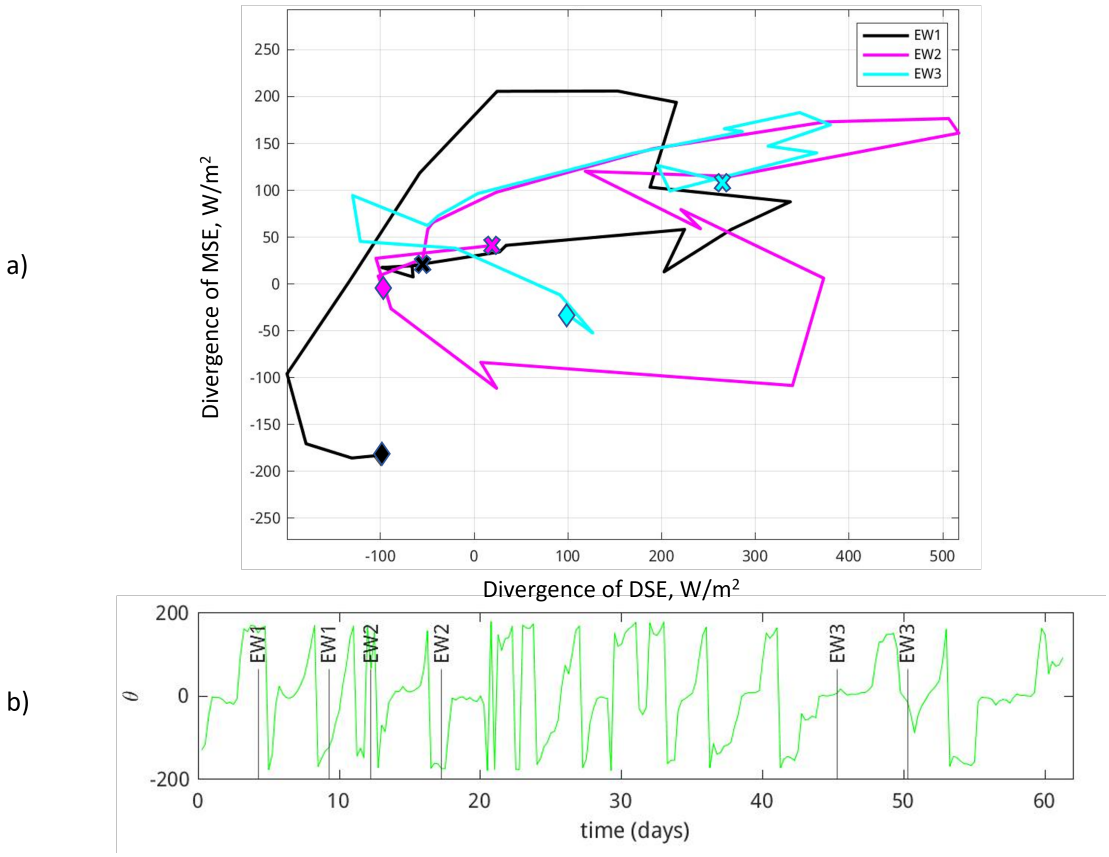

FIGURE 3.1: a) Trajectories of domain mean MSE divergence during the three passage of three easterly wave events on the phase plane. X-axis is the domain mean DSE divergence. Each color corresponds to a separate easterly wave. Cross symbol marks the start time of the easterly wave activity in the box, and diamond symbol marks the end time of easterly wave activity in the box. b) Complete time series of the life-cycle phase angle for the OTREC time period. Vertical lines mark the three easterly wave time periods.

Figure 3.1a shows the mean state of the domain box during the 5 days for each of the easterly wave events during OTREC. Each of the event is represented by a separate color. The trajectory starts at the cross pointer and ends at the diamond pointer. Overall, we can observe that each of the wave events do resemble somewhat of a counter-clockwise orbit on the phase plane. There are also some differences between each of the waves. Easterly waves 1 and 2 have a wider loop along the y-direction as compared to Easterly wave 3. Further, Easterly wave 1 trajectory has greater MSE advection magnitude during

the discharge phase, while Easterly wave 2 has a higher MSE advection magnitude during the recharge phase.

Figure 3.1b shows a time series of the domain life-cycle phase angle (defined in section 2.3.2) for the complete 2 month OTREC time period. We observe that cyclic evolution on the GMS phase plane, shown by phase angle value going from $-180°$ to $180°$, can be observed more generally in the time series and is not just exclusively observed during the passage of easterly waves. This suggests while easterly waves also show up as counter clockwise orbits on the phase plane, they are not the only phenomenon in Eastern Pacific which can cause such cyclic evolution.

3.3.2 Contribution of advective vs diabatic terms

From Chapter 2, we expect the elliptical shape of the cycle to be attributed more to the advective terms, while the diabatic terms vary more linearly for the composite recharge-discharge cycle(visualized in the schematic Figure 2.1). We explore whether this is also true for the individual case studies by plotting the trajectories corresponding to evolution of diabatic fluxes and the total MSE tendency in addition to MSE advection for each of the easterly wave events in Figure 3.2.

Each subplot in Figure 3.2 corresponds to one of the three easterly waves shown in Figure 3.1. Each blue line corresponds to the trajectory of MSE advection and is the same as those is Figure 3.1a. Red line shows the variability of the total diabatic fluxes during each of the easterly waves. We observe that generally the red line does vary more

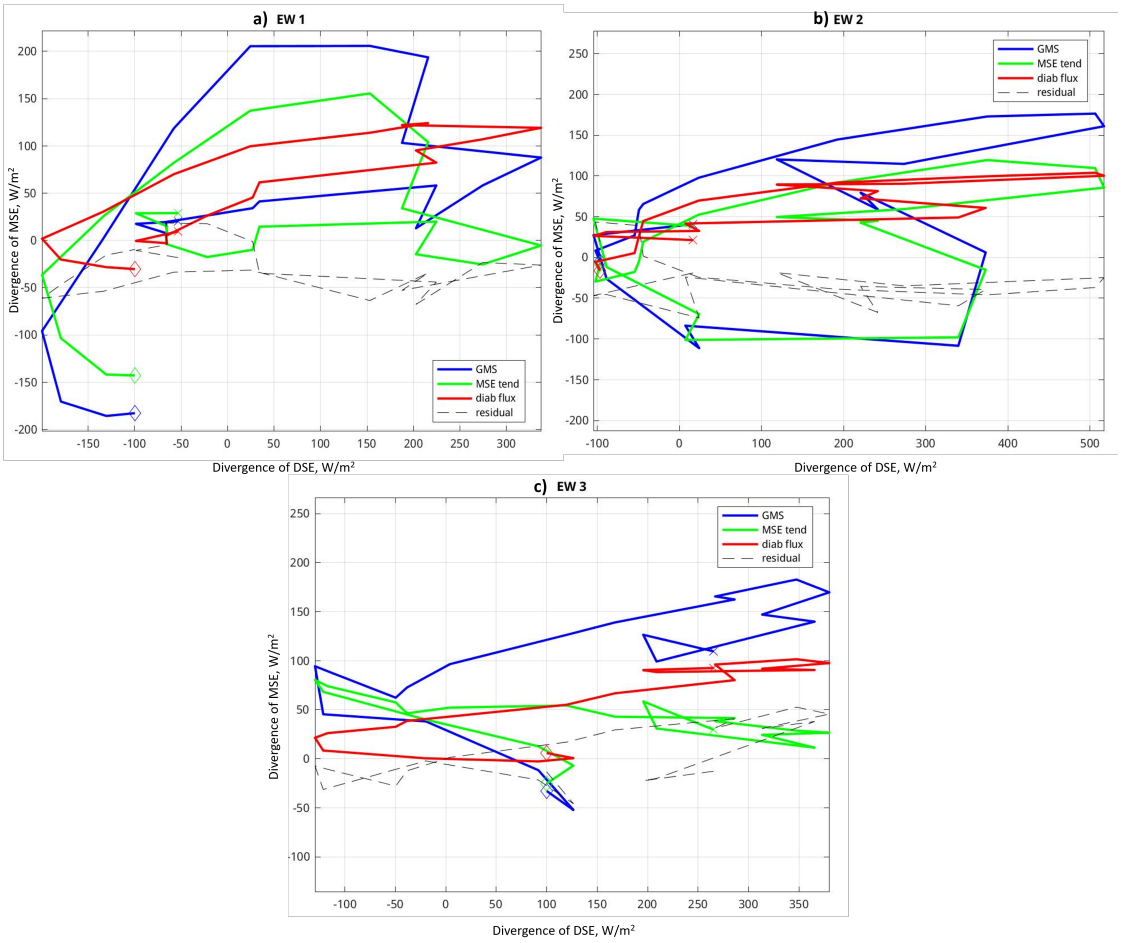

FIGURE 3.2: Phase plane trajectories of MSE divergence (blue), diabatic fluxes (red), - MSE tendency (green), and MSE budget residual (black dashed) during a) Easterly wave 1, b) Easterly wave 2, and c) Easterly wave 3 time period. X-axis in all plots is DSE divergence.

linearly and has a smaller magnitude compared to MSE advection for individual cycles consistent with previous results with composites.

Each green line corresponds to the trajectory of the overall MSE tendency term. In an ideal scenario where the MSE budget is exactly balanced, it should exactly follow the difference between the blue and red lines. Further, we expect MSE advection to be dominant in determining the total MSE tendency based on previous results in Chapter

2. For Easterly waves 1 and 2, the green line seems to be in qualitative agreement with the expected trajectory because of the resemblance in shape of the blue and green curves. However, for easterly wave 3 there seems to be greater qualitative differences. These differences can be accounted for by the fact that MSE budgets are not completely balanced in ERA 5 data. The MSE budget residual trajectory is plotted as a black dashed line in each plot. We observe that the residual, although non negligible here, is smaller than MSE advection. Also, the residual has a mostly constant value during Easterly waves 1 and 2 as compared to Easterly wave 3 when it varies with a positive slope. This explains the better agreement between the shapes of the blue and green curves during waves 1 and 2 compared to wave 3.

3.3.3 contribution to maintenance and propagation terms

From Figure 3.2, we might expect MSE tendency during Easterly waves 1 and 2 to be driven more by MSE advection compared to diabatic fluxes, while it is unclear what is happening during Easterly wave 3. We explore this question further through the maintenance and propagation term metrics introduced in section 3.2 above.

Figure 3.3 shows the mean contributions to maintenance and propagation from the advective, diabatic and the residual term for each of the three easterly wave events as well as the full two month OTREC time series. Overall we see quite a bit of similarity across the three easterly wave events and the full OTREC time period. MSE advection has a strong negative contribution to maintenance of MSE anomalies while diabatic fluxes positively

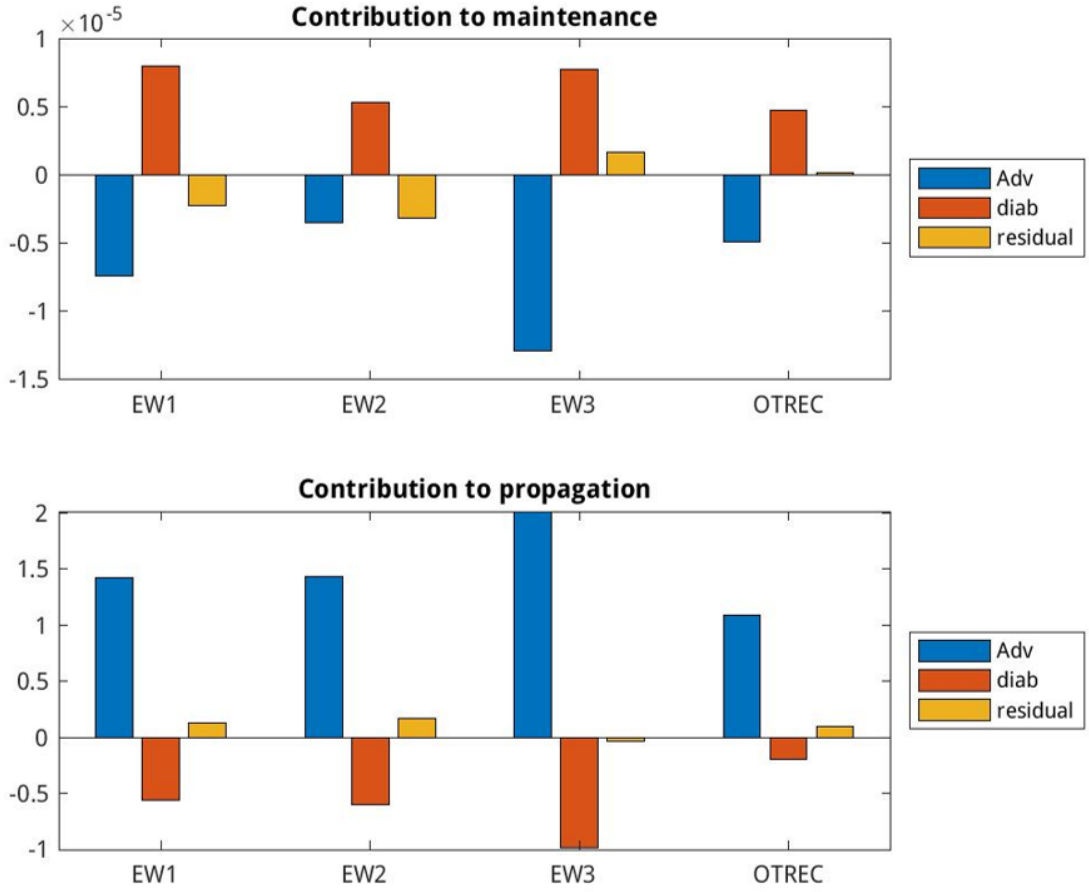

FIGURE 3.3: Mean contribution to maintenance of the cycle (top) and propagation of the cycle (bottom) during easterly wave 1 (EW1), easterly wave 2 (EW2), easterly wave 3 (EW3), full OTREC time period. For each time period contributions from MSE advection (blue), diabatic fluxes (red) and the MSE budget residual term (yellow) are plotted.

contribute to maintenance. This is broadly consistent with previous studies looking at composite Easterly waves in the Eastern Pacific (Mayta and Corraliza, 2023).

We also observe that MSE advection dominates the contribution to propagation, supporting results from Chapter 2 as well as previous studies that these easterly waves are primarily driven by advection of MSE. We also see a relatively smaller but substantial

negative contribution from the diabatic term to propagation of the cycle during the individual wave events. Comparatively, the contribution of diabatic terms to propagation over the full OTREC time period is negligible, suggesting that role of diabatic terms during the Easterly wave is being averaged out due to the non wave activity time periods. Residual term seems to have little impact on the maintenance and propagation terms here despite seeming to have a non negligible impact in Figure 3.2.

3.4 Discussion and Summary

In this chapter, we set out to primarily look at two things. First, do Easterly waves also have the counter-clockwise cyclic trajectory on the GMS phase plane. In particular, can we observe the cyclic evolution for individual easterly wave events as compared to working with composites. And second, what is the role being played by advection of MSE vs the diabatic fluxes in individual events? Is it similar to the results seen in composites? We identify the OTREC field campaign domain and time period to be suitable for these goals. We expect that because a counter-clockwise orbit on the phase plane is a direct consequence of the WTG approximation and moisture precipitation coupling in the tropics, different moisture modes, which also satisfy the same approximations, should exhibit a counter-clockwise trajectory.

Using easterly wave events during the OTREC time period as our case study, we find that easterly waves indeed do evolve along counter-clockwise trajectory on the phase plane (Figure 3.1). In addition to pointing towards the role of the moisture precipitation

relationship for this wave mode, this is also significant from the perspective that a cyclic signal can be picked up in data without explicitly filtering for the wave. Figure 3.1 simply comprises of a time series with 6 hour resolution which has been passed through a simple 24 hour running mean filter and nothing else. Although the trajectories may not seem very orbit like, but in this case we are also averaging over an area greater than size of the wave which may also be diminishing the signal. We also find that although easterly waves do correspond to cyclic trajectories, cyclic evolution is not dependent on whether an easterly wave is passing through the region or not. We can observe multiple moisture-recharge discharge cycles during the OTREC time period that do not coincide with easterly wave activity in the domain.

Further analysis of the three easterly wave events during OTREC also reveals other similarities with recharge-discharge cycles. We find that the individual cycles do seem to follow the simple schematic from Figure 2.1. Diabatic terms were found to vary more linearly, while the advective terms exhibited a more cyclic shape in easterly waves 1 and 2. The overall MSE tendency follows MSE advection. This pattern was seen to be weaker during Easterly wave 3, possibly due to larger and more systematic residual in the MSE budget during that time.

We project the MSE budget onto column MSE anomalies and column MSE tendency anomalies to quantify the contribution of the advective and diabatic terms to maintenance and propagation of the cycle respectively. We observe that overall the three easterly wave events behave very similarly to each other. MSE advection plays a dominant role

in driving the cycles through its positive contribution to propagation, while both MSE advection and diabatic terms play a role in maintaining MSE anomalies (Figure 3.3). This behavior is broadly consistent with the contribution seen over the full OTREC time period as well. One main difference that is seen is that diabatic terms over the individual Easterly waves seem to have a strong negative effect on propagation, which is not seen for the full time period.

Future direction for this work will involve expanding a little bit on the case study analysis being presented here to better understand the nature of the residual term in ERA5 data. A way to expand this work could also involve developing a new phase plane based metric to quantify the contribution to maintenance and propagation of the cycles. Based on the observation that as the cycle evolves through different phases, it goes through different GMS values, and therefore, different phase angle values. We can expect that propagation of the cycle is related to evolution on the phase plane in the angular direction. while maintenance of the cycle or its amplitude will be related to the evolution in the radial direction. In that case, we can decompose the velocity vector on the phase plane into its angular and radial component to measure contributions to propagation and maintenance respectively.

Chapter 4

Aggregation-Disaggregation cycles in ERA 5

4.1 Introduction

Convective aggregation is generally used to refer to clustering of clouds and convection in a non-random manner. Broadly, it can be a result of non-uniform boundary conditions forcing the domain, or it could be because of internal feedbacks between convection, moisture, and radiation. Idealized numerical models with uniform boundary conditions have been extensively used to study the characteristics of convective aggregation driven solely by these internal feedbacks, also referred as convective self-aggregation (Bretherton et al., 2005, Held et al., 1993). It is not completely clear what role or relevance the mechanisms behind self aggregation play when it comes to aggregation in the real world

where non uniform boundary conditions are present, and continuously varying in time (review by Holloway et al., 2017). However, there are some key characteristics that have been identified in how both self aggregation and aggregation can impact the spatial domain. Previous studies have showed that the domains consistently becomes drier, outgoing long wave radiation (OLR) increases, spatial gradients in column water vapor increase as they get more aggregated, both in idealized models (Bretherton et al., 2005, Holloway and Woolnough, 2016, Wing and Cronin, 2016, Wing and Emanuel, 2014, etc.), and observations (Bony et al., 2020, Stein et al., 2017, Tobin et al., 2012, Tsai and Mapes, 2022, etc.). This robust impact of aggregation on the large scale environment, combined with the dependence of aggregation on sea surface temperatures (SST) (Coppin and Bony, 2015, Cronin and Wing, 2017) make understanding convective aggregation extremely important to understand climate sensitivity (review by Wing, 2019).

To understand links between aggregation and self aggregation, we first need to understand the nature of convective aggregation in the real world and how it differs from the model world. Convection in idealized models starts off from a completely randomly distributed convective state. Then with time, the domain slowly transitions to a new equilibrium state with aggregated convection which stays aggregated for the remainder of the simulation. In contrast, in real world, convection will already be in an aggregated state due to the presence of external boundary conditions and internal feedbacks from previous convection. However, the extent of aggregation changes with time, and convection can also disaggregate. This will result in cycles of aggregation and disaggregation. Such cycles of changing amount of aggregation can also be observed in some idealized simulations (not

shown), but these have not been studied systematically in terms of what leads to such variability.

To measure the extent of aggregation, previous studies have used a variety of cloud clustering based metrics. Each of these metrics in some way or the other combine different cloud properties from satellite observations to quantify cloud clusters as the aggregation metric. Some prominent metrics in use are the Simple Convective Aggregation Index (SCAI, Tobin et al., 2012), organization index I_{org} (Tompkins and Semie, 2017), the Morphological Index of Convective Aggregation (MICA, Kadoya and Masunaga, 2018) etc. However, there can be some concerns about how well these metrics correlate with larger scale convective organization in the real world. For example, Sakaeda and Torri (2022) show that self aggregation based cloud metrics do not necessarily correlate well with MJO phases index with many metrics unable to show an increase in aggregation with enhanced MJO phase and some even showing that convection becomes less aggregated during MJO active phase. They highlight that these discrepancies primarily arise because of how these metrics can be biased towards particular cloud properties by construction (like cloud clusters becoming larger versus clusters becoming fewer) and individually may not fully capture all characteristics of cloud evolution in real world.

Such factors make it difficult to compare self aggregation with aggregation directly. However, since both models and observations have showed consistent and strong impacts on the large scale environment (Wing, 2019), there is potential to define aggregation based on state of large scale environment. One particularly strong, robust and easy to track

metric for doing so is spatial variability of column water vapor. Motivation for doing so is not only because column water vapor distribution has been shown to vary with aggregation significantly in both observations (Lebsock et al., 2017, Tsai and Mapes, 2022) and models (Bretherton et al., 2005, Wing and Emanuel, 2014), but is also based on empirical evidence showing strong dependence of precipitation on a critical moisture threshold (Bretherton et al., 2004) and existence of sharp water vapor margins for the Inter-Tropical Convergence Zones (ITCZ) (Mapes et al., 2018). Lebsock et al. (2017) have used and verified that spatial variance of column water vapor can be used as a metric for aggregation using satellite data. This provides strong support to the idea that self aggregation can be relevant for understanding convective variability in real world that is expected to be dominated by changes in moisture (Adames-Corraliza and Mayta, 2023, Tsai and Mapes, 2022). Other recent studies have also highlighted such moisture driven modes of convective variability being observed ubiquitously throughout the tropics (Inoue and Back, 2017), and the mechanisms behind them to be very inherent to how convection interacts with the large scale environment (Inoue et al., 2021, Maithel and Back, 2022).

All together, this suggests that studying evolution of moisture can be an indirect way of tracking aggregation. Owing to the weak temperature gradient approximation (WTG) (Sobel et al., 2001), evolution of moisture can be studied using moist static energy (MSE) budgets. While MSE budget (Equation 4.1) has been extensively used to study moisture driven convective variability, MSE variance budget (Equation 4.2) (Wing and Emanuel,

2014) has been extensively used to study self aggregation. MSE variance budget framework (Wing and Emanuel, 2014) makes use of the observation that self aggregation results in redistribution of moisture, and consequently MSE in the domain, into a bimodal distribution with anomalously moist and dry columns instead of being more uniformly distributed. This implies an increase in value of spatial variance of MSE with aggregation. Further, MSE variance budget (Equation 4.2) can be used to measure how different processes contribute to increase of MSE variance. It is derived by multiplying the the spatial anomalies of the terms in Equation 4.1 with anomalous column MSE at each time instant.

$$\frac{\partial \langle h \rangle}{\partial t} = \text{VADV} + \text{HADV} + \langle Q_R \rangle + SF + \text{Res} \tag{4.1}$$

$$\frac{1}{2}\frac{\partial \langle h \rangle'^{\,2}}{\partial t} = -\langle h \rangle' \text{VADV}' - \langle h \rangle' \text{HADV}' + \langle h \rangle' \langle Q_R \rangle' + \langle h \rangle' SF' + \langle h \rangle' \text{Res}' \tag{4.2}$$

$$\text{VADV} = -\langle \omega \partial h / \partial p \rangle$$

$$\text{HADV} = -\langle \mathbf{v} \cdot \nabla h \rangle$$

In Equation 4.1 and 2, $\langle ... \rangle$ represents mass weighted vertical column integral from surface to 100hPa, $'$ represents anomaly compared to the domain mean, h represents MSE, ω

represents vertical velocity in pressure coordinates, $\mathbf{v}$ is the horizontal wind vector, VADV and HADV stand for vertical and horizontal advection respectively, $\langle Q_R \rangle$ are the column radiative fluxes, SF are the surface sensible and latent heat fluxes, and Res stands for the residual term.

Using MSE variance budget, idealized modeling studies have found radiative feedbacks from clouds and water vapor to be the dominant mechanisms responsible for maintenance as well as initiation of self aggregation (Pope et al., 2021, 2023, Wing et al., 2017). Their role in helping maintain the self aggregated state once it is already aggregated can be particularly relevant for real world scenario. Befittingly, even in observations at large scales, anomalous column radiative fluxes have been shown to vary linearly with anomalous column moisture with a positive slope (Inoue and Back, 2017, Su and Neelin, 2002). This implies that radiative feedbacks act to moisten the already moist columns or further dry the dry columns, that is, it act as a positive feedback for aggregation. Moreover, the positive slope also implies that the feedback is expected to get stronger with larger anomalies. However, this only implies that radiative anomalies strongly covary with MSE or moisture anomalies. If they also do not covary strongly with MSE tendency, then they may not drive the evolution of MSE. Many recent studies looking at evolution of the aforementioned moisture driven convective variability modes in observations have found them to be driven strongly by advection instead, with radiation being important for maintenance (Inoue et al., 2021, Maithel and Back, 2022, Mayta and Corraliza, 2023).

This raises the main question being addressed in this study. Does convection in real

world also disaggregate whenever this positive maintenance factor weakens? Or does radiative feedbacks only contribute to determining the extent of aggregation whereas advective processes determine when things aggregate and disaggregate? We hypothesize that advection of MSE plays a large role in driving aggregation disaggregation cycles in observations. We use spatial variance of MSE as our metric of aggregation.

The rest of this chapter is structured as follows. Section 2 describes the data set being used and how the variance budget calculation is setup. It also introduces the novel variance phase space that we will use as our diagnostic framework. Section 3 presents the main results from the study, while section 4 presents the discussion, and section 5 presents the key conclusions.

4.2 Data and Methods

We use ERA 5 data (Hersbach et al., 2020) as our best guess for what is happening in the real world in this study. Temperature, humidity, horizontal winds, radiation, and sensible and latent heat surface fluxes are used from ERA 5 to compute the column integrated MSE and MSE budget term time series at each grid point. We use 6 hourly gridded data from 1980 to 2019 at a horizontal resolution of 0.5°. Column integrated quantities are computed by taking the vertical integral across 27 vertical levels between 1000hPa and 100hPa. Further the MSE variance budget terms are computed over 4 large domain boxes, each corresponding to the 4 main tropical ocean basins – Indian Ocean (IO) box spanning between 10 S - 5 N and 55 – 95 E, Western Pacific (WP) box spanning

5S – 10N and 150 – 180E, Eastern Pacific (EP) box spanning 0 – 15N and 195 – 265E, and Atlantic Ocean (AO) box spanning 0 – 15N and 315 – 340E. We use data at horizontal resolution of 0.5x 0.5 degrees and a time resolution of 6hr from 1980-2019 within each box. The time series at each grid point is further passed through a 24 hr running mean filter to remove diurnal variability from the data.

These domains are much larger than the 10 x 10 or 5 x 5 degree boxes used to evaluate the cloud based aggregation metrics in previous studies. In this study instead we are focusing on defining aggregation through its impact on the large scale distribution of MSE. Hence the need for larger domain size. Because of larger domain size, the domains can be expected to be closer to radiative convective equilibrium (RCE) more frequently (Jakob et al., 2019). Also this shifts the focus on aggregation at larger scales (like ITCZ) which evolves more slowly at sub-seasonal timescales making it more comparable to aggregation in idealized models. It should be noted that most of the existing literature on convective aggregation in real world instead is focused more on cloud and meso-scale.

The MSE variance budget terms are calculated as follows from the MSE budget time series data. First the spatial anomaly of MSE and each budget term is computed by subtracting the respective domain mean at each time step. Then the MSE budget term anomaly is projected onto the column MSE anomaly for each grid point. Finally, a domain mean of the projected term is calculated leaving a simple time series representing each of the four domain boxes for each term in equation. Figure 4.1 shows the spatial distribution of column MSE anomalies when the domain mean MSE variance is low (top),

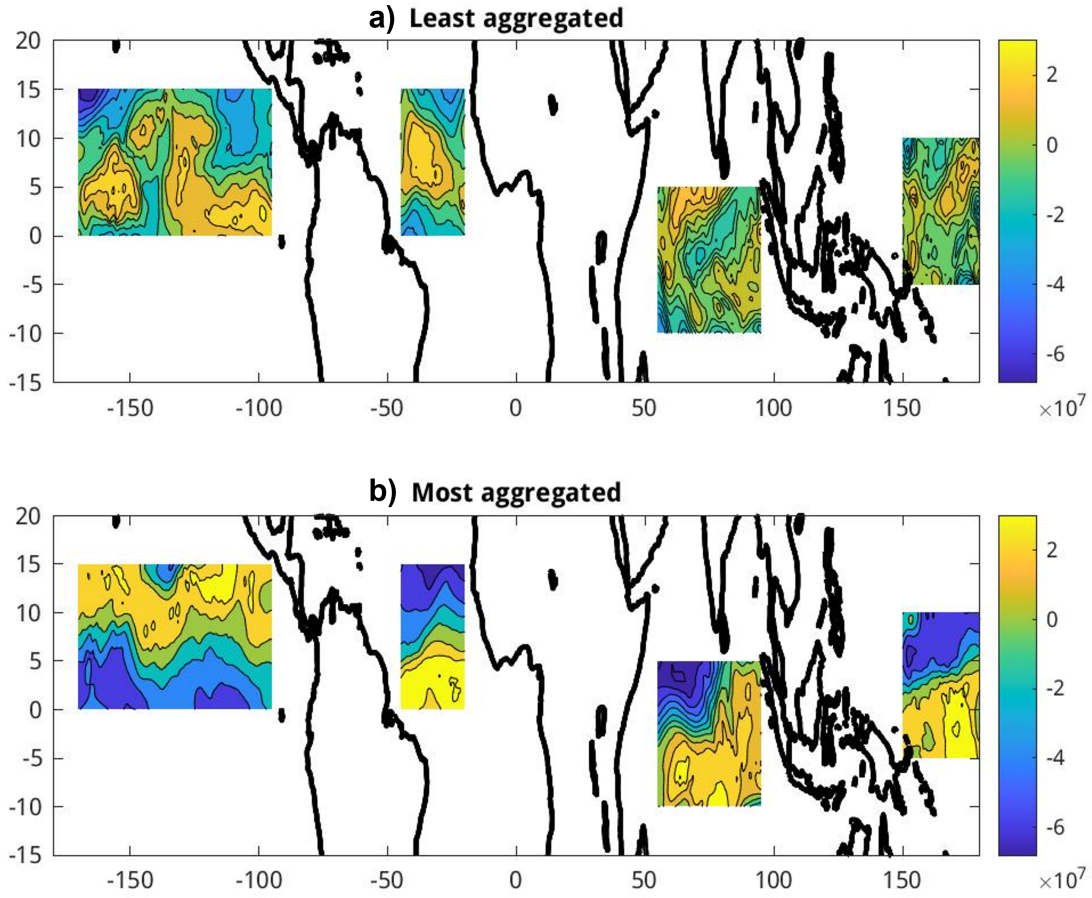

FIGURE 4.1: Spatial structure of the column MSE anomalies (J/m^2) in the four ocean basin domain being studied when a) domain is least aggregated, and b) domain is most aggregated. Both a) and b) follow the same colorbar.

and when the domain mean MSE variance is high (bottom) for each of our four boxes. A strongly aggregated domain in this framework looks like a strong ITCZ latitudnal band with sharp margins.

We also propose to use a novel MSE variance based phase space to visualize and understand aggregation – disaggregation cycles better. The phase space is formed by taking domain mean MSE variance on the x-axis and the tendency of the domain mean MSE variance on the y-axis. While the x-axis physically corresponds to extent or degree of

aggregation in the domain, y-axis represents whether the domain is getting more or less aggregated with time. A schematic of ideal aggregation-disaggregation cycle is shown in Figure 4.2a. The arrows depict that when the domain is aggregating in time, it transitions from less to more aggregated state, and when the domain is disaggregating, it goes from more to less aggregated.

4.3 Results

First we verify that the cyclic variability on the phase space, expected in Figure 4.2a is actually observed in the reanalysis data. To do so, we plot phase portrait for our two dimensional phase space showing vectors corresponding to the direction of evolution on the phase plane. The vectors are computed by first computing the time derivatives of the domain MSE variance and domain MSE variance tendency at each time step. Then, the phase plane is divided into 400 small rectangular bins (20 bins along each axis). Then we compute the bin mean time derivative of MSE variance (vector magnitude along x-axis) and the bin mean time derivative of MSE variance tendency (vector magnitude along y-axis) for each bin. The resulting vectors for each ocean basin are plotted in Figure 4.2 b-e. Only bins with more than 100 samples are plotted. We observe that the cyclic signal as visualized in the simple schematic in Figure 4.2a is reproduced very clearly in all ocean basins. This signifies that extent of large scale aggregation varies cyclically everywhere throughout the tropics in the form of these aggregation - disaggregation cycles.

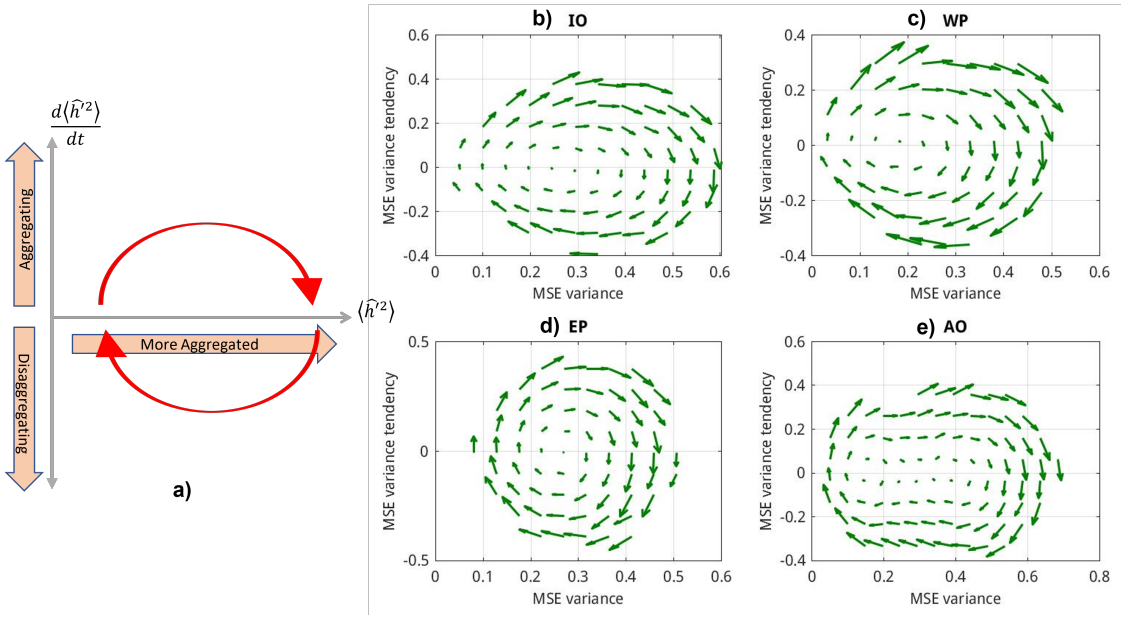

FIGURE 4.2: a) A simple schematic of the MSE variance phase space. X-axis is the domain mean MSE variance, and y-axis is the tendency of domain mean MSE variance. Red arrows represent what a typical aggregation - disaggregation cycle would look like. b)-e) vector plot showing the actual evolution on the MSE variance phase plane in reanalysis data for the four ocean basins - IO, WP, EP, AO respectively. For easier visualization, the phase plane has been divided into 400 equally spaced bins (20 along each axis) and bin mean values have been plotted. Only bins with more than 100 samples are shown.

The MSE variance phase plane helps differentiate between different phases of the aggregation disaggregation cycle. More and less aggregated phases are the right and left halves, and aggregating and disaggregating phases are the top and bottom halves respectively.

4.3.1 Contribution to maintenance and propagation of MSE variance anomalies for the complete cycle

We are interested in understanding what drives this cyclic behavior and how do the MSE variance budget terms vary during different phases of this cycle. One way to do so is to understand how each of the budget terms co-vary with MSE variance (in the x-direction)

and with MSE variance tendency (in the y-driection). This is same as asking how each term contributes to maintenance and propagation of these cycles respectively. This can be evaluated by projecting the MSE variance budget (Equation 4.2) onto the appropriate terms and computing the total projection for the full time series as given by the equations below.

$$M_x = \frac{\left\{\left|\hat{X}\right| \cdot \left|\widehat{\langle h\rangle'^2}\right|\right\}}{\left\{\left|\widehat{\langle h\rangle'^2}\right|^2\right\}} \tag{4.3}$$

$$P_x = \frac{\left\{\left|\hat{X}\right| \cdot \left|\widehat{\frac{\partial\langle h\rangle'^2}{\partial t}}\right|\right\}}{\left\{\left|\widehat{\frac{\partial\langle h\rangle'^2}{\partial t}}\right|^2\right\}} \tag{4.4}$$

In equations 3 and 4, X represents a term from the MSE variance budget in Equation 4.2, $\widehat{...}$ represents the domain mean, $|...|$ represents the time anomaly, and $\{...\}$ represents the mean of the underlying term across the full time series. This is analogous to the maintenance and projection terms calculated in Andersen and Kuang (2012) for the MSE budget. The propagation term (Equation 4.4) represents if the budget term anomalies are the same sign as MSE variance tendency. While the maintenance term (Equation 4.3) represents how the budget terms vary when the domain is more or less aggregated. Figure 4.3 shows the contribution of each term in all four ocean basins to the maintenance and propagation of the cycles.

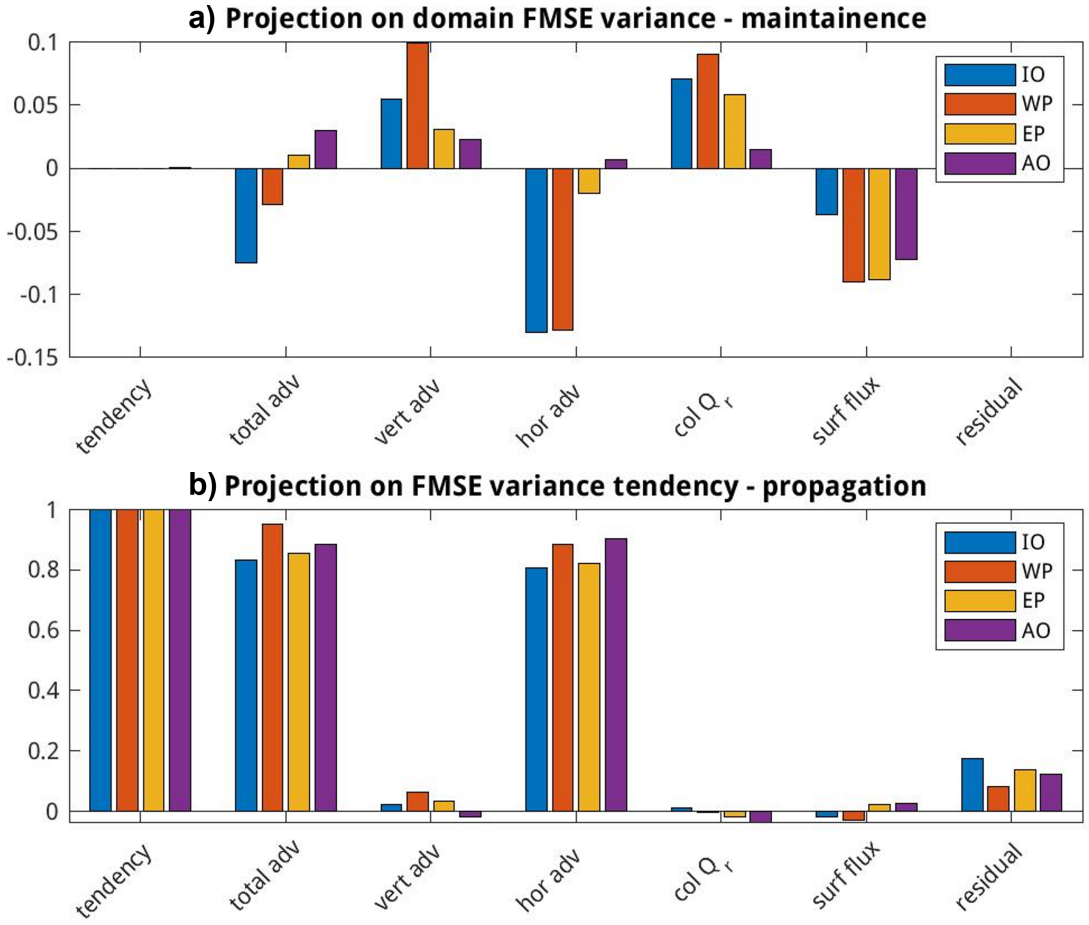

FIGURE 4.3: Bar plot showing the contribution of each MSE variance budget term from Equation 4.2 to a) Maintenance of MSE variance - computed as per Equation 4.3, and b) propagation of MSE variance - computed as in Equation 4.4. Different colors correspond to different ocean basins with IO in blue, WP in orange, EP in yellow, and AO in purple

Figure 4.3a shows that vertical advection and column radiation fluxes have a positive contribution while horizontal advection and surface fluxes have a negative contribution to maintenance of aggregation. Positive value implies that the MSE variance budget varies such that it anomalously favors further aggregation when the domain is already more aggregated or it anomalously supports disaggregation when the state is already less aggregated. This can happen due to processes which tend to moist the moist columns more strongly or dry the moist columns weakly as the domain gets more aggregated.

Oppositely, negative values represent that the MSE variance budget term varies such that it favors anomalous disaggregation when the domain is more aggregated or it supports anomalous aggregation in the domain when it is less aggregated. Overall, we see some amount of qualitative agreement between the different ocean basins even though there are also some stark quantitative differences. For example, surface fluxes are a strong negative term consistently throughout the tropics, however vertical advection and column radiation show larger changes in magnitude but have the same sign. Horizontal advection here seems to be a outlier in the sense that the sign of the term also seems to change between the ocean basins in addition to its magnitude. This is discussed further in the next subsection.

Propagation term shown in Figure 4.3b instead show that most of the contribution to propagation comes from horizontal advection. Positive value here means that the MSE variance budget term positively covaries with tendency. This will happen if the domain overall is in the process of aggregation or disaggregation at the same time when the budget term tends to support aggregation or disaggregation respectively. Oppositely, negative value denotes that the anomalous variance budget term is of the opposite sign to the total MSE variance tendency and the budget term tends to be disaggregating the system when overall it is aggregating or vice versa. A zero value denotes that there is no specific pattern between how the two co vary. It is observed that the propagation of the aggregation disaggregation cycles is almost exclusively because of horizontal advection in all ocean basins with other terms being close to zero.

This is significant because this implies that the diabatic terms, column radiation and surface fluxes, do not contribute in a specific way to how large scale aggregation will evolve in time in the real world. While their contribution may be non zero for individual cycles, but when considering multiple cycles, we observe that they do not statistically control how the cycles will evolve in time. This is potentially important for understanding how aggregation might change in the real world with climate change, and suggests that understanding the change in advective feedbacks will be more important to understand the time evolution, and frequency of aggregation instead of the radiative feedbacks.

4.3.2 Contribution to maintenance and propagation of MSE variance anomalies during different phases of the cycle

Because the values calculated as per Equation 4.3 and 4 include taking a mean over the full time series, it represents the overall contribution of each term averaged over all the different phases of the cycle. However we can understand the full contribution of each term during the different phases by using the MSE variance phase plane to only average over the same phase bins across different cycles.

Figure 4.4 shows contours of the bin mean values for each of the MSE variance budget terms in Equation 4.2 for Indian Ocean basin. The contours represent how each term in the variance budget varies across the different phases of the aggregation-disaggregation cycles. A positive variance budget term represents that the anomalously moist columns in the domain tend to further moisten as a result of that process or anomalously dry columns

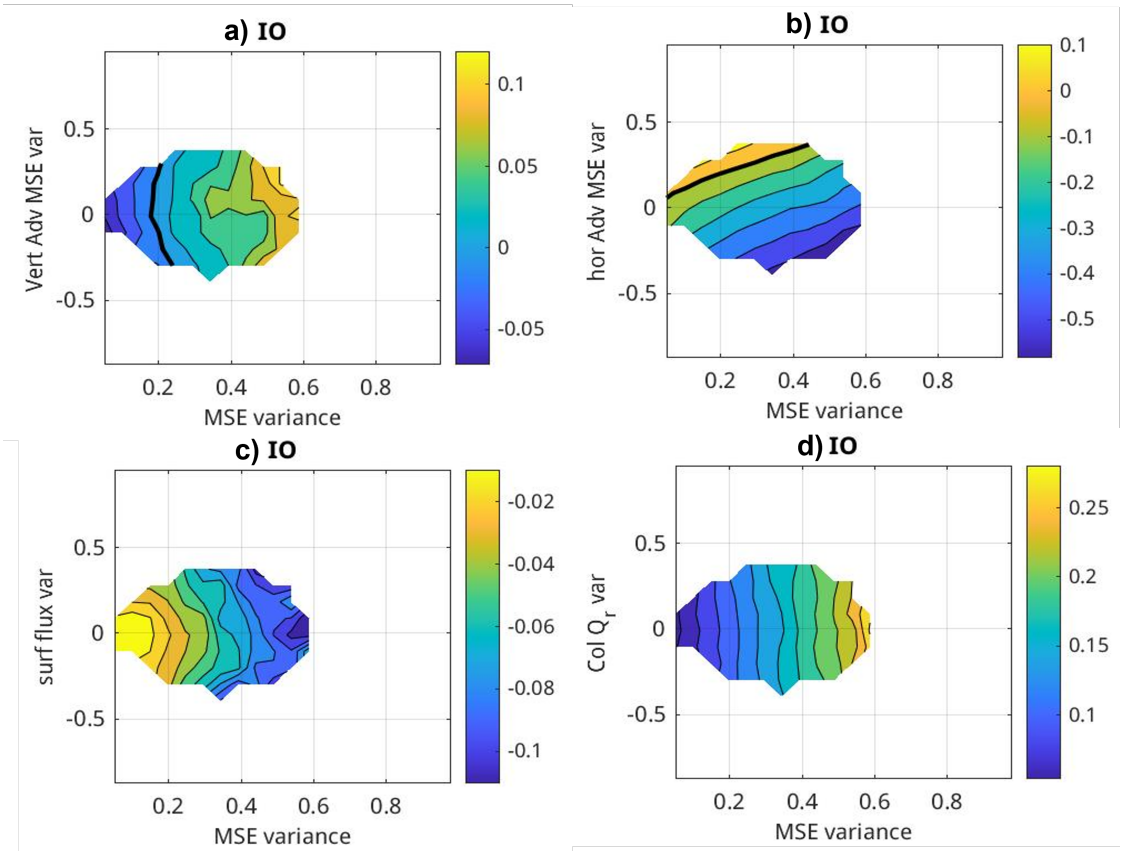

FIGURE 4.4: Bin mean contours of the different MSE variance budget terms from Equation 4.2 in the IO box showing how their contribution to MSE variance tendency varies across the variance phase space. a) contribution to variance tendency from vertical advection, b) contribution from horizontal advection, c) - contribution from surface fluxes, d) contribution from column radiative fluxes. Thick black contour represents the zero contour. Shading represents MSE profile.

will tend to further dry up. This implies that the term tends to favors aggregation. Consequently, negative variance budget term signifies that the term does not tend to support aggregation.

We observe that the column radiative and surface fluxes ubiquitously support and resist aggregation during all phases of the cycle. This is consistent with previous studies which have found long wave cloud radiative feedbacks to be dominant in tending to warm the already convecting columns. We observe that in ERA 5, surface fluxes tend to resist

aggregation during all phases of the cycle in all ocean basins. This suggests that surface fluxes are dominated by processes which tend to moisten dry regions compared to processes like the wind driven surface heat exchange feedback (WISHE) which will tend to moisten moist regions.

If we interpret the maintenance and propagation terms from the previous subsection as covariance between the budget term and the x and y axes respectively, then we can immediately understand why horizontal advection (Figure 4.4b) was the only contributor to propagation. It is the only term which varies in magnitude along the y-direction. The three remaining terms vary primarily along the x-direction making their contribution to propagation close to zero. Vertical advection, column radiation, and surface fluxes do not vary much between the aggregating and disaggregating phase for a given amount of aggregation. This ties back in with our initial hypothesis that diabatic terms can not sufficiently be the driving force behind the observed aggregation disaggregation cycles. Instead we observe that advection term can vary with the y-axis on the phase plane indicating that advection is important for driving these cycles.

We can further observe that vertical advection (Figure 4.4a) and column radiation fluxes (Figure 4.4d) become stronger positive feedbacks when domain is more aggregated, and surface fluxes (Figure 4.4c) and horizontal advection (Figure 4.4b) act as stronger negative feedbacks when domain becomes more aggregated explaining the positive and negative contribution of these terms to maintenance of MSE variance anomalies.

Similar figures for the other three ocean basins show that this behavior is oberved very consistently across the different regions (not shown). Changes in contour shapes between the different ocean basins can lead to the difference in values observed in freff43. For example, horizontal advection variance contours in Eastern Pacific and Atlantic Ocean boxes are more horizontal as compared to Indian Ocean or Western Pacific making its contribution to the maintenance term smaller in magnitude comparatively (not shown). This suggests that changes in magnitude of the contribution to maintenance of variance by the horizontal advection term are related to subtle differences in the phase relationship of horizontal advection with MSE variance rather than the horizontal advection term being different physically (like moistening instead of drying). Similarly, differences in vertical advection and radiation term can be associated with such subtle phase relationships rather than major physical differences suggesting that the maintenance and propagation bar plots (Figure 4.3) to understand energy budget evolution are very sensitive to how things are coupled with convection. Figure 4.4 can prove to be more easier to interpret in that regard.

4.4 Discussion

Changes in circulation between the most and least aggregated states

To better understand the physical processes behind how vertical and horizontal advection are contributing to MSE variance, we look at the structure of the 3 dimensional circulation

in our domain boxes when it is most and least aggregated. Panels in Figure 4.5 and 6 show 3-dimensional horizontal and vertical circulation on a 2-dimensional space respectively. Circulation is in contours and MSE profile is shown in shading as a function of binned column MSE on x-axis. By arranging the x-axis from 0 to 100 percentile, we can look at how the profiles change over dry and moist columns. Binned profiles are further composited over 10% of the times when the domain is most and least aggregated to show the differences as the overall domain becomes more or less aggregated.

4.4.0.1 Horizontal circulation

On this column MSE bin - height space, the geography of the domain has been distorted. Therefore, horizontal circulation has to be visualized as flow between dry and moist columns. This is calculated by computing the projection of horizontal wind vector at each grid point in the direction of MSE gradient. Collecting and plotting the bin mean of this projected vector then represents the average of horizontal winds in the direction of more moist columns at each location in the bin.

Looking at panels a and b in Figure 4.5, we observe that when the domain is least aggregated, the horizontal flow is negative meaning that flow is from moist to dry columns. Conversely, when the domain is more aggregated, the horizontal flow is from the dry to moist columns near the surface. This is consistent with recent studies presenting observational and theoretical evidence for horizontal moisture gradient driven moisture mode (Adames-Corraliza and Mayta, 2023, Mayta and Corraliza, 2023). These moisture

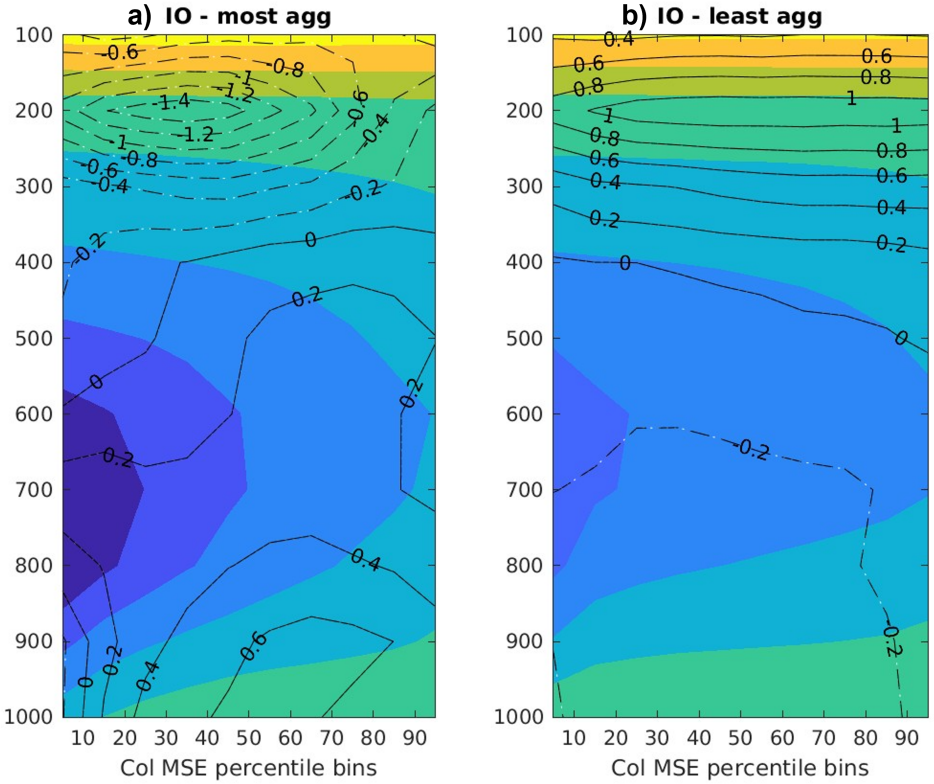

FIGURE 4.5: contours of anomalies in horizontal winds projected on MSE gradient for IO box composited over a) 10% of the times when the domain is most aggregated, and b) 10% of the times when the domain is least aggregated. Y-axis is height of the column, and x-axis represents deciles of column MSE arranged to go from dry to moist columns as you go left to right. Anomalies are computed with respect to a mean state that averages across the most and least aggregated cases. For a given column, positive anomalies of the projection denote that flow is toward moister columns. Solid contours show positive value and dashed contours show negative values.

modes were also found to be driven by horizontal advection. As per this theory, presence of strong moisture gradients in the domain spins up moisture mode eddies which act to even out the moisture mode gradient (Adames-Corraliza and Mayta, 2023). Therefore, existence of strong eddy flow from moist to dry columns should lead to small moisture gradients and a less aggregated domain, while absence of eddy flow should lead to build up of strong moisture gradients and a more aggregated state. This could be a possible

hypothesis for how horizontal advection can be driving the propagation of the aggregation-disaggregation cycles and explain the structure of horizontal circulation we observe in our results. If true, this suggests that our large-scale aggregation can be thought of in terms of a strong ITCZ or Hadley cell circulation, and other non planetary scale moisture mode variability acts as a disaggregation process. This implies that moisture modes themselves may not be an example of what aggregation looks like in the real world.

4.4.0.2 Vertical velocity profile changes and vertical advection

Variance due to vertical advection was found to contribute positively to maintenance of aggregation in Figure 4.3. Figure 4.4 showed that this happens because as the domain gets more aggregated, variance from vertical advection becomes more positive. This can be attributed to tendency of moist columns to be moistened more or for them to tend to dried less by vertical advection. Alternatively, the positive signal can also be related to dry columns in the domain having the tendency to dry more or moisten less by vertical advection. These changes can be due to a combination of 1) changes in the amount of vertical motion and/or 2) changes in the top-heaviness of the vertical motion profile and/or 3) changes in thermodynamic profiles affecting vertical advection without changes in the vertical motion.

Previous idealized modelling studies have highlighted the important role of increased low level subsidence in dry regions being an important positive feedback for aggregation by tending to export MSE from dry to moist columns (Muller and Held, 2012). Tsai and

Mapes (2022) also show that ascending vertical motion profiles in the moist columns tend to be more bottom heavy for more aggregated cases over Indian Ocean in MERRA-2 data. However, other previous studies also discuss how geographic variability in vertical motion profile shape implies geographical differences in how convection amplifies during such cyclical modes (Inoue et al., 2021). This then raises the question, are there specific patterns in vertical motion profile shape which can be observed consistently across the different ocean basins in this framework that can explain the positive contribution of vertical advection to maintenance of aggregation. Are these driven by vertical motion profile changes in dry regions or moist regions?

Change in vertical advection in IO box as the domain gets more aggregated is shown in Figure 4.6a. It can also be visualized by plotting the difference in bin mean advection between the most and least aggregated composites (black line in Figure 4.6b). We observe that for Indian Ocean, moist columns tend to be dried more by vertical advection in more aggregated cases. This is a negative feedback to aggregation. In contrast, dry columns tend to be moistened less by vertical advection in more aggregated cases, so this is a positive feedback on aggregation. Since overall vertical advection acts as a positive feedback in Indian Ocean, the dry columns being moistened less by vertical advection must dominate over the changes in moist columns. It is interesting to note that other ocean basins also consistently show a strong anomalous drying tendency in the drier columns. However, while moist columns get drier in IO and EP basins, they get moister in WP and AO (not shown). This discrepancy suggests that vertical advection changes

in the dry or the subsiding columns are more uniform across different regions, and more dominant in determining the overall behaviour.

To better understand whether changes in vertical advection come from changes in vertical motion profile or from changes in MSE gradient, we decompose vertical advection within each bin as follows.

$$\left\langle \omega \frac{\partial h}{\partial p} \right\rangle = \left\langle \overline{\omega} \overline{\frac{\partial h}{\partial p}} \right\rangle + \left\langle \overline{\omega} \frac{\partial h}{\partial p}_a \right\rangle + \left\langle \omega_a \overline{\frac{\partial h}{\partial p}} \right\rangle + \left\langle \omega_a \frac{\partial h}{\partial p}_a \right\rangle \tag{4.5}$$

Where, overbar denotes a time average across the most and least aggregated times and subscript a represents anomaly from the time mean. The decomposed terms are plotted as colored thin lines in Figure 4.6c. Since the mean profiles are constant between the most and least aggregated states, line corresponding to $\left\langle \overline{\omega} \overline{\frac{\partial h}{\partial p}} \right\rangle$ is zero (red). We observe that change in total advection is very closely followed by change in $\left\langle \omega_a \overline{\frac{\partial h}{\partial p}} \right\rangle$, which corresponds to anomalous changes in vertical motion profiles acting on a time mean MSE gradient profile (green). This suggests that variability in vertical advection is mainly explained by changes in vertical motion profile between moist and least aggregated states. This is observed robustly over other boxes as well (not shown).

Figure 4.6 also shows vertical profiles of mean vertical velocity (contour) and vertical MSE gradient (shading), and anomalous vertical velocity (contour) and vertical MSE gradient (shading) during most and least aggregated cases for IO in panel c. As expected we observe that the mean vertical velocity is ascending over the moist columns and

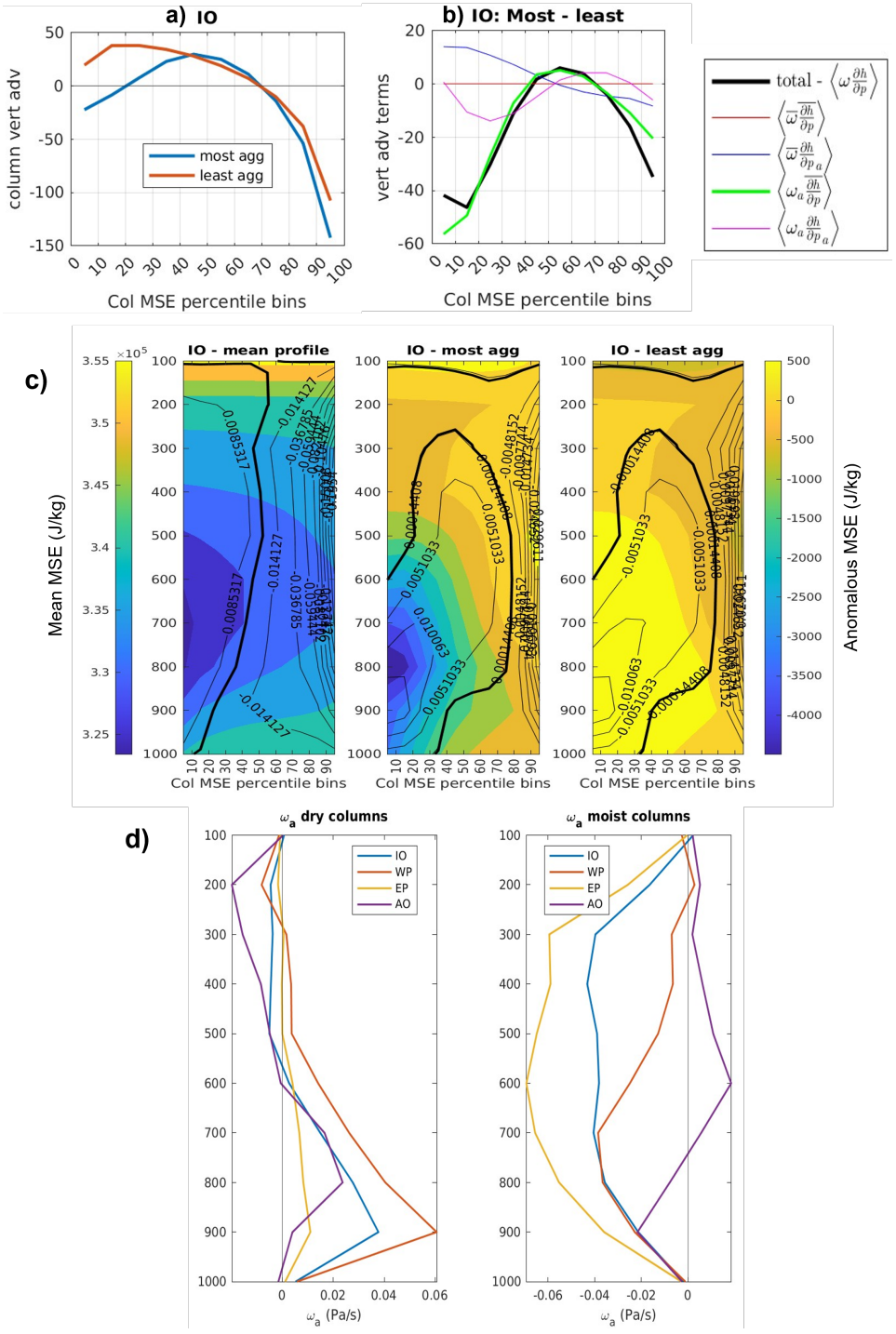

FIGURE 4.6: a) Mean column integrated vertical advection for deciles of column MSE in IO box when the domain is most aggregated (blue) and when it is least aggregated (red). b) Black - differences in total column vertical advection for a given col. MSE decile between most and least aggregated cases. Other colors represent the differences for various terms in vertical advection decompostion as per Equation 4.5. c) Mean and anomalous vertical velocity, Pa/s (contours), and MSE(shading) for the different column MSE deciles. Mean and anomalies consistent with Equation 4.5. Panels showing composite over the most and least aggregated cases shows anomalies with respect to the mean profile. Thick black contour corresponds to the zero contour.d) anomalous vertical velocity profiles in all four ocean basins over the two driest deciles (left) and two moistest deciles (right).

descending over the dry columns. We further observe that dry columns getting drier dominate the MSE profile changes as the domain gets more aggregated. Anomalous MSE change in moist columns is comparatively closer to zero. In terms of vertical velocity changes we observe a strong increase of low level subsidence over the dry regions consistent with previous idealized modeling studies. This increase in subsidence combined with the positive vertical MSE gradient at low levels contributes to anomalous negative advection or anomalous drying of the dry columns. Oppositely, we see an enhancement of upward vertical velocity over the moistest columns but it is not easy to make out if that is bottom or top heavy.

This is better visualized in panel d in Figure 4.6 which shows the mean anomalous vertical motion profile for the two driest and moistest bins from panel c. In consistency with Figure 4.6b, the anomalous vertical velocity plotted here is the difference between the most and least aggregated composites. Profiles from all four ocean basins are plotted for easy comparison. Figure 4.6d clearly shows a ubiquitous increase in low level subsidence in the dry columns in all ocean basins with aggregation. In contrast, changes over the moistest columns are not uniform. We observe that enhancement of upward motion has a relatively more bottom heavy profile in WP and AO as compared to IO and EP. As discussed previously, this tends to moisten the moist columns in WP and AO but, it tends to dry the moist columns in IO and EP. Together these differences can explain the differences in magnitude in contribution of vertical advection to maintenance of aggregation in Figure 4.3, while the uniform pattern of enhanced low level subsidence tending to dry the dry columns further explains the overall positive value.

Idealized modeling studies can disagree on what causes this increase of low level subsidence in dry regions. Muller and Held (2012) found this to be driven by enhanced low level radiative cooling in dry regions, whereas (Holloway and Woolnough, 2016) found the low level circulation to not be driven by radiative changes in their simulation. Understanding the exact relationship between vertical radiative cooling profiles and its impact on circulation and organization of convection is an big open area of current research. Our results support that such feedbacks are important for understanding maintenance of large-scale aggregation.

4.5 Conclusions

Through this study we wanted to establish a process oriented framework to visualize and understand aggregation of convection in the real world. To do so, we utilized spatial variance of MSE over ocean-wide large domains as our metric of aggregation. Although the physical basis of the framework itself is not new, but this is the first time it is being applied to observations or reanalysis. This serves multiple purposes.

- First, it defines aggregation in terms of its impact on the large-scale environment rather than properties of cloud clusters. This helps in making a more apples-to-apples type of comparison for aggregation across different conditions and regimes.
- Since MSE variance can be tracked through a budget equation (Equation 4.2 it adds a process-oriented view point to the approach. One can look more explicitly at the

system while it is aggregating or disaggregating in addition to when it is already aggregated or disaggregated.

- The ocean wide domain size allows for a somewhat more realistic comparison between idealized models and real world as larger domains are more closer to RCE in real world compared to smaller domains in previous studies.

- Time scale of aggregation with these larger domains is slower and more comparable to time scale in idealized models which has traditionally been a big point of difference between self aggregation and aggregation at cloud or mesoscale level in observations.

- Lastly, using the MSE variance budget allows for the possibility to put other studies looking at moisture modes and connect them with notion of aggregation.

We develop a new phase space to visualize the evolution of aggregation in the form of the MSE variance phase space. It puts domain MSE variance on the x-axis (extent of aggregation) and the tendency of MSE variance on y-axis (change in aggregation). A composite vector plot showing the evolution of aggregation on this phase space highlights that aggregation in real world is a transient process in the form of continuous aggregation-disaggregation cycles (Figure 4.2). This visualization encourages thinking about aggregation in real world as a cyclical mode which makes it more realistic compared to thinking of aggregation as a quasi-stationary equilibrium state based on the idealized model results.

We use the MSE variance budget to answer the question of what determines the extent of aggregation observed and what determines when the system aggregates or disaggregates during these cycles. Based on erefeq2, possible contributors are, variance in vertical advection of MSE - variance coming from transport of MSE by the overturning circulation and associated convergence, variance in the horizontal advection of MSE – variance coming from transport of MSE by the circulation in presence of horizontal gradients of MSE, variance in column radiative fluxes – variance coming from changes in radiative fluxes because moisture and clouds in the column are changing, variance in surface fluxes – variance coming from changes in latent and sensible heat fluxes between convecting and non-convecting regions.

Our results highlight that while all factors contribute significantly and systematically to determining the extent of aggregation, only variance from horizontal advection contributes to whether the domain aggregates or disaggregates (Figure 4.3). Key features observed throughout different regions in the tropics are listed below.

- We find that overall in the domain, surface fluxes seem to always tend to moisten the drier columns, radiative fluxes always tend to moisten/warm the moister columns and dry/cool the drier columns, and horizontal advection almost always tends to dry the moister columns.

- Further, when the domain is more aggregated, we find that surface fluxes tend to moisten the drier columns more strongly (negative feedback), radiative fluxes tend to warm the moister columns and cool the drier columns more strongly (positive

feedback), horizontal advection tends to dry the moister columns more strongly (negative feedback), and vertical advection tends to moisten the drier columns less (positive feedback). These are consistent across different regions for the most part, and only differ quantitatively rather than qualitatively.

- Whether the domain will further aggregate or disaggregate covaries strongest with the strength of the negative feedback from horizontal advection. When horizontal advection tends to strongly dry moist columns the domain disaggregates, and vice versa.

- Looking at the three dimensional structure of the circulation shows that horizontal circulation is anomalously from the dry to moist columns in lower levels when the domain is more aggregated, and anomalously from moist to dry columns when the domain is less aggregated. Also, low level subsidence over the drier columns gets enhanced when the domain is more aggregated which tends to dry the drier columns making vertical advection act as a positive feedback.

There are some interesting similarities and differences in the results from this study and expectations based on idealized model studies. Our results show that while radiative fluxes are important for maintenance of aggregation in observations similar to idealized models, that does not mean that they control when the domain will aggregate or disaggregate. Rather that is governed by horizontal advection. Therefore, understanding horizontal advection and how that will change with climate change will also be an important factor impacting the frequency or period of aggregation in real world. (Wing, 2019)

discuss how frequency of aggregation is important for its impact on climate and extreme precipitation events in the real world.

Our results support the findings from idealized studies that low level circulation in dry regions is an important feedback. We find that low level subsidence in dry regions changes in a more uniform and systematic manner with aggregation across different regions compared to changes in upward vertical motion profiles in the moist regions. Averaging over the full cycle shows that the overall impact is of the same sign as impact of changes over dry region even if changes over moist regions have the opposite effect.

Chapter 5

Summary and Discussion

This dissertation analyses various aspects of large-scale convective evolution in daily time series data on the GMS phase plane. Previous studies have shown that convective variability at these scales is characterized in the form of convective life-cycles or moisture recharge-discharge cycles (Inoue and Back, 2015, 2017). The recharge-discharge cycles are in the shape of counter-clockwise orbits on the phase plane. The direction of evolution is important because Wolding et al. (2020) show that it is the direction of evolution that the climate models get incorrect. In this study, we present new diagnostic frameworks and applications for the GMS phase plane to better understand what processes are important for the recharge-discharge cycle variability.

In chapter 2, we focused on the evolution of MSE budget terms during different phases of the recharge-discharge cycles. We used the geometrical aspect of the GMS phase plane to

define novel phase angle parameters to define state of the system and study its evolution. We highlight that evolution of the wave is primarily an angular feature so using a phase angle makes it easier to track and calculate composites over similar phases. Phase angle also allows us to convert the unbound GMS value, when convection is small, to a finite ranged angle value. This makes it possible to use this framework to study daily time series evolution of GMS, something that could not be done before directly. Overall, our results indicate that the advective terms act as primary drivers of the recharge-discharge cycles, while the diabatic flux terms act to slow it down. Further, the behavior of the cycles is largely consistent across different ocean basins in this framework having a sub-seasonal timescale of around 40 days.

Our results looking into the evolution of MSE budget show that both vertical and horizontal advection contribute to cyclic evolution of the cycle in terms of contributing non-negligibly towards the counter-clockwise evolution. This is a key result, because other studies seem to suggest that horizontal advection is more important for driving this variability (Inoue et al., 2021). This discrepancy results from the fact that in other studies, being the primary driver of the cycle is primarily a question of how well the particular term covaries with MSE tendency or y-axis of the phase plane. If horizontal advection is a good determinant of whether MSE tendency is positive or negative then it is the main driver the cycle. However, the GMS phase plane highlights that the cycle evolves in an angular direction and not just along one axis. Therefore, contribution to this angular evolution is also a way of contributing to it's propagation and the phase angle framework allows us to quantify that. This is relevant for model diagnostics as there could be errors

in vertical advection in the models and not just in horizontal advection for getting the direction of evolution correct. This could potentially also provides a way in which vertical and horizontal advection changes are both coupled to the local convective state leading to a ubiquitous pattern in different regions despite variations in environmental conditions.

In chapter 3, we focus on whether other faster moisture modes namely easterly waves in the Eastern Pacific also evolve as counter-clockwise trajectories on the phase space. While chapter 2 focused on composite cycles, chapter 3 focuses on case studies. We find that individual Easterly waves do resemble a counter-clockwise evolving orbit on the GMS phase plane as well. This is significant because it shows a potential for the GMS phase plane framework to be able to contribute to forecasting endeavours. We further find that the individual cycles also display an important role being played by advection of MSE in their propagation, similar to the composite cycles in chapter 2.

In chapter 4, we shift gears from GMS phase plane and propose a new MSE variance based framework to characterize the large-scale cyclic variability. The mean spatial variance of MSE over a domain will not vary in case of a horizontally propagating wave. It will only vary if strength of the wave changes with time. Therefore, the MSE variance based phase plane represents the cyclical evolution of strength of the wave without being affected by its propagation. Or in other words, it provides a more lagrangian perspective of the moisture recharge-discharge cycles. Drawing parallels to studies on self-aggregation of convection in idealized models, we can consider these cycles on the variance phase

plane as aggregation-disaggregation cycles, with domain mean MSE variance acting as our metric of aggregation.

This framework provides a new way of visualizing and representing aggregation in the real world, particularly one focused on large-scale aggregation. We find that whether convection tends to aggregate or disaggregate in the real world is primarily dictated by horizontal advection. This is in contrast to idealized modeling studies which seem to suggest that column radiative feedbacks are the main determinant. We find that in reanalysis data, the role of radiative feedbacks is more relevant for determining the mean strength of aggregation instead of the when.

We also look at the 3-dimensional structure of the circulation to understand how it changes as amount aggregation varies. We find that, low level subsidence in the dry columns is enhanced throughout the tropics when the domain is more aggregated. This subsidence anomaly is bottom-heavy. Hence, it tends to moisten the dry columns less as aggregation increases, making vertical advection a positive feedback on aggregation. It is interesting to note that this is a change that we see ubiquitously throughout the tropics pointing towards the importance of vertical motion in subsiding regions in understanding convective aggregation.

We also find that when the domain is less aggregated, there is a strong flow from moist to dry columns. This is consistent with a theoretical model of moisture mode eddies that are driven by strong MSE gradients and act to weaken the very thing that drives them. If true, this implies a fundamental shift in how we think about moisture modes

and relevance of aggregation in real world. We traditionally think of moisture modes to be a representation of self-aggregation in the real world, driven by moisture-precipitation feedback. However, this new framework instead suggests that moisture modes are in fact a disaggregation process which redistribute moisture in the domain. Self-aggregation instead, is a larger planetary scale feature with a strong tendency to initiate it's own disaggregation rather than a tendency to maintain itself as in idealized modeling studies.

Overall, this dissertation extends our understanding about the fundamental processes that contribute to generic organization of large-scale tropical convection. In that process, various new process oriented diagnostics are introduced. These can be used for diagnosing model biases and errors associated not just with recharge-discharge cycles but potentially also with other moisture driven variability. The ubiquitous nature of these processes emphasizes how fundamental they are to the tropics, making it even more important to ensure that our models get them right.

Bibliography

Adames, F., 2022: The Basic Equations under Weak Temperature Gradient Balance: Formulation, Scaling, and Types of Convectively Coupled Motions. *Journal of the Atmospheric Sciences*, **79**, 2087–2108, doi:10.1175/JAS-D-21-0215.1, publisher: American Meteorological Society Section: Journal of the Atmospheric Sciences.
URL https://journals.ametsoc.org/view/journals/atsc/79/8/JAS-D-21-0215.1.xml

Adames, F. and D. Kim, 2016: The MJO as a Dispersive, Convectively Coupled Moisture Wave: Theory and Observations. *Journal of the Atmospheric Sciences*, **73**, 913–941, doi:10.1175/JAS-D-15-0170.1.
URL https://journals.ametsoc.org/view/journals/atsc/73/3/jas-d-15-0170.1.xml

Adames, F., D. Kim, S. K. Clark, Y. Ming, and K. Inoue, 2019: Scale Analysis of Moist Thermodynamics in a Simple Model and the Relationship between Moisture Modes and Gravity Waves. *Journal of the Atmospheric Sciences*, **76**, 3863–3881, doi:10.1175/JAS-D-19-0121.1, publisher: American Meteorological Society Section:

Journal of the Atmospheric Sciences.

URL https://journals.ametsoc.org/view/journals/atsc/76/12/jas-d-19-0121.1.xml

Adames, F. and E. D. Maloney, 2021: Moisture Mode Theory's Contribution to Advances in our Understanding of the Madden-Julian Oscillation and Other Tropical Disturbances. *Current Climate Change Reports*, **7**, 72–85, doi:10.1007/s40641-021-00172-4.

URL https://doi.org/10.1007/s40641-021-00172-4

Adames, F. and Y. Ming, 2018: Moisture and Moist Static Energy Budgets of South Asian Monsoon Low Pressure Systems in GFDL AM4.0. *Journal of the Atmospheric Sciences*, **75**, 2107–2123, doi:10.1175/JAS-D-17-0309.1, publisher: American Meteorological Society Section: Journal of the Atmospheric Sciences.

URL https://journals.ametsoc.org/view/journals/atsc/75/6/jas-d-17-0309.1.xml

Adames-Corraliza, F. and V. Mayta, 2023: The Stirring Tropics. Part II: Theory of Moisture ModeHadley Cell Interactions. Publisher: EarthArXiv.

URL https://eartharxiv.org/repository/view/5166/

Ahn, M.-S., D. Kim, K. R. Sperber, I.-S. Kang, E. Maloney, D. Waliser, H. Hendon, and on behalf of WGNE MJO Task Force, 2017: MJO simulation in CMIP5 climate models: MJO skill metrics and process-oriented diagnosis. *Climate Dynamics*, **49**, 4023–4045, doi:10.1007/s00382-017-3558-4.

URL https://doi.org/10.1007/s00382-017-3558-4

Andersen, J. A. and Z. Kuang, 2012: Moist Static Energy Budget of MJO-like Disturbances in the Atmosphere of a Zonally Symmetric Aquaplanet. *Journal of Climate*, **25**, 2782–2804, doi:10.1175/JCLI-D-11-00168.1.

URL https://journals.ametsoc.org/view/journals/clim/25/8/jcli-d-11-00168.1.xml

Arnold, N. P. and D. A. Randall, 2015: Global-scale convective aggregation: Implications for the Madden-Julian Oscillation. *Journal of Advances in Modeling Earth Systems*, **7**, 1499–1518, doi:10.1002/2015MS000498, _eprint: https://onlinelibrary.wiley.com/doi/pdf/10.1002/2015MS000498.

URL https://onlinelibrary.wiley.com/doi/abs/10.1002/2015MS000498

Back, L. E. and C. S. Bretherton, 2005: The Relationship between Wind Speed and Precipitation in the Pacific ITCZ. *Journal of Climate*, **18**, 4317–4328, doi:10.1175/JCLI3519.1, publisher: American Meteorological Society Section: Journal of Climate.

URL https://journals.ametsoc.org/view/journals/clim/18/20/jcli3519.1.xml

— 2006: Geographic variability in the export of moist static energy and vertical motion profiles in the tropical Pacific. *Geophysical Research Letters*, **33**, doi:10.1029/2006GL026672.

URL https://onlinelibrary.wiley.com/doi/abs/10.1029/2006GL026672

Beucler, T. and T. W. Cronin, 2016: Moisture-radiative cooling instability. *Journal of Advances in Modeling Earth Systems*, **8**, 1620–1640, doi:10.1002/2016MS000763.

URL https://onlinelibrary.wiley.com/doi/abs/10.1002/2016MS000763

Bony, S., A. Semie, R. J. Kramer, B. Soden, A. M. Tompkins, and K. A. Emanuel, 2020: Observed Modulation of the Tropical Radiation Budget by Deep Convective Organization and Lower-Tropospheric Stability. *AGU Advances*, **1**, e2019AV000155, doi:10.1029/2019AV000155, _eprint: https://onlinelibrary.wiley.com/doi/pdf/10.1029/2019AV000155.

URL https://onlinelibrary.wiley.com/doi/abs/10.1029/2019AV000155

Bretherton, C. S., P. N. Blossey, and M. Khairoutdinov, 2005: An Energy-Balance Analysis of Deep Convective Self-Aggregation above Uniform SST. *Journal of the Atmospheric Sciences*, **62**, 4273–4292, doi:10.1175/JAS3614.1, publisher: American Meteorological Society Section: Journal of the Atmospheric Sciences.

URL https://journals.ametsoc.org/view/journals/atsc/62/12/jas3614.1.xml

Bretherton, C. S., M. E. Peters, and L. E. Back, 2004: Relationships between Water Vapor Path and Precipitation over the Tropical Oceans. *Journal of Climate*, **17**, 1517–1528, doi:10.1175/1520-0442(2004)017¡1517:RBWVPA¿2.0.CO;2.

URL https://journals.ametsoc.org/view/journals/clim/17/7/1520-0442_2004_017_1517_rbwvpa_2.0.co_2.xml

Bretherton, C. S. and A. H. Sobel, 2002: A Simple Model of a Convectively Coupled Walker Circulation Using the Weak Temperature Gradient Approximation. *Journal of*

Climate, **15**, 2907–2920, doi:10.1175/1520-0442(2002)015¡2907:ASMOAC¿2.0.CO;2.

URL https://journals.ametsoc.org/view/journals/clim/15/20/1520-0442_2002_015_2907_asmoac_2.0.co_2.xml

Chikira, M., 2014: Eastward-Propagating Intraseasonal Oscillation Represented by Chikira–Sugiyama Cumulus Parameterization. Part II: Understanding Moisture Variation under Weak Temperature Gradient Balance. *Journal of the Atmospheric Sciences*, **71**, 615–639, doi:10.1175/JAS-D-13-038.1, publisher: American Meteorological Society Section: Journal of the Atmospheric Sciences.

URL https://journals.ametsoc.org/view/journals/atsc/71/2/jas-d-13-038.1.xml

Coppin, D. and S. Bony, 2015: Physical mechanisms controlling the initiation of convective self-aggregation in a General Circulation Model. *Journal of Advances in Modeling Earth Systems*, **7**, 2060–2078, doi:10.1002/2015MS000571, _eprint: https://onlinelibrary.wiley.com/doi/pdf/10.1002/2015MS000571.

URL https://onlinelibrary.wiley.com/doi/abs/10.1002/2015MS000571

Cronin, T. W. and A. A. Wing, 2017: Clouds, Circulation, and Climate Sensitivity in a Radiative-Convective Equilibrium Channel Model. *Journal of Advances in Modeling Earth Systems*, **9**, 2883–2905, doi:10.1002/2017MS001111, number: 8 _eprint: https://onlinelibrary.wiley.com/doi/pdf/10.1002/2017MS001111.

URL https://onlinelibrary.wiley.com/doi/abs/10.1002/2017MS001111

Curry, J. A., A. Bentamy, M. A. Bourassa, D. Bourras, E. F. Bradley, M. Brunke, S. Castro, S. H. Chou, C. A. Clayson, W. J. Emery, L. Eymard, C. W. Fairall, M. Kubota, B. Lin, W. Perrie, R. A. Reeder, I. A. Renfrew, W. B. Rossow, J. Schulz, S. R. Smith, P. J. Webster, G. A. Wick, and X. Zeng, 2004: SEAFLUX. *Bulletin of the American Meteorological Society*, **85**, 409–424, doi:10.1175/BAMS-85-3-409.

URL https://journals.ametsoc.org/view/journals/bams/85/3/bams-85-3-409.xml

Dee, D. P., S. M. Uppala, A. J. Simmons, P. Berrisford, P. Poli, S. Kobayashi, U. Andrae, M. A. Balmaseda, G. Balsamo, P. Bauer, P. Bechtold, A. C. M. Beljaars, L. v. d. Berg, J. Bidlot, N. Bormann, C. Delsol, R. Dragani, M. Fuentes, A. J. Geer, L. Haimberger, S. B. Healy, H. Hersbach, E. V. Hólm, L. Isaksen, P. Kållberg, M. Köhler, M. Matricardi, A. P. McNally, B. M. Monge-Sanz, J.-J. Morcrette, B.-K. Park, C. Peubey, P. d. Rosnay, C. Tavolato, J.-N. Thépaut, and F. Vitart, 2011: The ERA-Interim reanalysis: configuration and performance of the data assimilation system. *Quarterly Journal of the Royal Meteorological Society*, **137**, 553–597, doi:10.1002/qj.828.

URL http://rmets.onlinelibrary.wiley.com/doi/abs/10.1002/qj.828

Fuchs, and D. J. Raymond, 2017: A simple model of intraseasonal oscillations. *Journal of Advances in Modeling Earth Systems*, **9**, 1195–1211, doi:10.1002/2017MS000963.

URL https://onlinelibrary.wiley.com/doi/abs/10.1002/2017MS000963

Fuchs-Stone, , D. J. Raymond, and S. Sentić, 2020: OTREC2019: Convection Over the East Pacific and Southwest Caribbean. *Geophysical Research Letters*, **47**, e2020GL087564, doi:10.1029/2020GL087564, _eprint: https://onlinelibrary.wiley.com/doi/pdf/10.1029/2020GL087564.

URL https://onlinelibrary.wiley.com/doi/abs/10.1029/2020GL087564

Hannah, W. M. and E. D. Maloney, 2014: The moist static energy budget in NCAR CAM5 hindcasts during DYNAMO. *Journal of Advances in Modeling Earth Systems*, **6**, 420–440, doi:10.1002/2013MS000272.

URL https://agupubs.onlinelibrary.wiley.com/doi/abs/10.1002/2013MS000272

Hannah, W. M., B. E. Mapes, and G. S. Elsaesser, 2016: A Lagrangian View of Moisture Dynamics during DYNAMO. *Journal of the Atmospheric Sciences*, **73**, 1967–1985, doi:10.1175/JAS-D-15-0243.1, publisher: American Meteorological Society Section: Journal of the Atmospheric Sciences.

URL https://journals.ametsoc.org/view/journals/atsc/73/5/jas-d-15-0243.1.xml

Held, I. M., R. S. Hemler, and V. Ramaswamy, 1993: Radiative-Convective Equilibrium with Explicit Two-Dimensional Moist Convection. *Journal of the Atmospheric Sciences*, **50**, 3909–3927, doi:10.1175/1520-0469(1993)050¡3909:RCEWET¿2.0.CO;2, publisher: American Meteorological Society Section: Journal of the Atmospheric Sciences.

URL https://journals.ametsoc.org/view/journals/atsc/50/23/1520-0469_1993_050_3909_rcewet_2_0_co_2.xml

Hersbach, H., B. Bell, P. Berrisford, S. Hirahara, A. Horányi, J. Muñoz-Sabater, J. Nicolas, C. Peubey, R. Radu, D. Schepers, A. Simmons, C. Soci, S. Abdalla, X. Abellan, G. Balsamo, P. Bechtold, G. Biavati, J. Bidlot, M. Bonavita, G. De Chiara, P. Dahlgren, D. Dee, M. Diamantakis, R. Dragani, J. Flemming, R. Forbes, M. Fuentes, A. Geer, L. Haimberger, S. Healy, R. J. Hogan, E. Hólm, M. Janisková, S. Keeley, P. Laloyaux, P. Lopez, C. Lupu, G. Radnoti, P. de Rosnay, I. Rozum, F. Vamborg, S. Villaume, and J.-N. Thépaut, 2020: The ERA5 global reanalysis. *Quarterly Journal of the Royal Meteorological Society*, **146**, 1999–2049, doi:10.1002/qj.3803, _eprint: https://onlinelibrary.wiley.com/doi/pdf/10.1002/qj.3803.

URL https://onlinelibrary.wiley.com/doi/abs/10.1002/qj.3803

Holloway, C. E., A. A. Wing, S. Bony, C. Muller, H. Masunaga, T. S. L'Ecuyer, D. D. Turner, and P. Zuidema, 2017: Observing Convective Aggregation. *Surveys in Geophysics*, **38**, 1199–1236, doi:10.1007/s10712-017-9419-1.

URL https://doi.org/10.1007/s10712-017-9419-1

Holloway, C. E. and S. J. Woolnough, 2016: The sensitivity of convective aggregation to diabatic processes in idealized radiative-convective equilibrium simulations. *Journal of Advances in Modeling Earth Systems*, **8**, 166–195, doi:10.1002/2015MS000511, _eprint: https://agupubs.onlinelibrary.wiley.com/doi/pdf/10.1002/2015MS000511.

URL https://agupubs.onlinelibrary.wiley.com/doi/abs/10.1002/2015MS000511

Huaman, L., E. D. Maloney, C. Schumacher, and G. N. Kiladis, 2021: Easterly Waves in the East Pacific during the OTREC 2019 Field Campaign. *Journal of the Atmospheric Sciences*, **78**, 4071–4088, doi:10.1175/JAS-D-21-0128.1, publisher: American Meteorological Society Section: Journal of the Atmospheric Sciences.

URL https://journals-ametsoc-org.ezproxy.library.wisc.edu/view/journals/atsc/78/12/JAS-D-21-0128.1.xml

Hung, M.-P., J.-L. Lin, W. Wang, D. Kim, T. Shinoda, and S. J. Weaver, 2013: MJO and Convectively Coupled Equatorial Waves Simulated by CMIP5 Climate Models. *Journal of Climate*, **26**, 6185–6214, doi:10.1175/JCLI-D-12-00541.1.

URL https://journals.ametsoc.org/view/journals/clim/26/17/jcli-d-12-00541.1.xml

Inoue, K., F. Adames, and K. Yasunaga, 2020: Vertical Velocity Profiles in Convectively Coupled Equatorial Waves and MJO: New Diagnoses of Vertical Velocity Profiles in the Wavenumber–Frequency Domain. *Journal of the Atmospheric Sciences*, **77**, 2139–2162, doi:10.1175/JAS-D-19-0209.1.

URL https://journals.ametsoc.org/view/journals/atsc/77/6/JAS-D-19-0209.1.xml

Inoue, K. and L. E. Back, 2015: Gross Moist Stability Assessment during TOGA COARE: Various Interpretations of Gross Moist Stability. *Journal of the Atmospheric*

Sciences, **72**, 4148–4166, doi:10.1175/JAS-D-15-0092.1.

URL https://journals.ametsoc.org/view/journals/atsc/72/11/jas-d-15-0092.1.xml

— 2017: Gross Moist Stability Analysis: Assessment of Satellite-Based Products in the GMS Plane. *Journal of the Atmospheric Sciences*, **74**, 1819–1837, doi:10.1175/JAS-D-16-0218.1.

URL https://journals.ametsoc.org/view/journals/atsc/74/6/jas-d-16-0218.1.xml

Inoue, K., M. Biasutti, and A. M. Fridlind, 2021: Evidence that Horizontal Moisture Advection Regulates the Ubiquitous Amplification of Rainfall Variability over Tropical Oceans. *Journal of the Atmospheric Sciences*, **78**, 529–547, doi:10.1175/JAS-D-20-0201.1.

URL https://journals.ametsoc.org/view/journals/atsc/78/2/jas-d-20-0201.1.xml

Jakob, C., M. S. Singh, and L. Jungandreas, 2019: Radiative Convective Equilibrium and Organized Convection: An Observational Perspective. *Journal of Geophysical Research: Atmospheres*, **124**, 5418–5430, doi:10.1029/2018JD030092, _eprint: https://onlinelibrary.wiley.com/doi/pdf/10.1029/2018JD030092.

URL https://onlinelibrary.wiley.com/doi/abs/10.1029/2018JD030092

Jiang, X., D. E. Waliser, P. K. Xavier, J. Petch, N. P. Klingaman, S. J. Woolnough, B. Guan, G. Bellon, T. Crueger, C. DeMott, C. Hannay, H. Lin, W. Hu, D. Kim,

C.-L. Lappen, M.-M. Lu, H.-Y. Ma, T. Miyakawa, J. A. Ridout, S. D. Schubert, J. Scinocca, K.-H. Seo, E. Shindo, X. Song, C. Stan, W.-L. Tseng, W. Wang, T. Wu, X. Wu, K. Wyser, G. J. Zhang, and H. Zhu, 2015: Vertical structure and physical processes of the Madden-Julian oscillation: Exploring key model physics in climate simulations. *Journal of Geophysical Research: Atmospheres*, **120**, 4718–4748, doi:10.1002/2014JD022375.

URL https://onlinelibrary.wiley.com/doi/abs/10.1002/2014JD022375

Juračić, A. and D. J. Raymond, 2016: The effects of moist entropy and moisture budgets on tropical cyclone development. *Journal of Geophysical Research: Atmospheres*, **121**, 9458–9473, doi:10.1002/2016JD025065.

URL https://onlinelibrary.wiley.com/doi/abs/10.1002/2016JD025065

Kadoya, T. and H. Masunaga, 2018: New Observational Metrics of Convective Self-Aggregation: Methodology and a Case Study. *Journal of the Meteorological Society of Japan. Ser. II*, **96**, 535–548, doi:10.2151/jmsj.2018-054.

URL https://www.jstage.jst.go.jp/article/jmsj/96/6/96_2018-054/_article

Kiladis, G. N., M. C. Wheeler, P. T. Haertel, K. H. Straub, and P. E. Roundy, 2009: Convectively coupled equatorial waves. *Reviews of Geophysics*, **47**, doi:10.1029/2008RG000266, number: 2.

URL https://onlinelibrary.wiley.com/doi/abs/10.1029/2008RG000266

Kim, D., P. Xavier, E. Maloney, M. Wheeler, D. Waliser, K. Sperber, H. Hendon, C. Zhang, R. Neale, Y.-T. Hwang, and H. Liu, 2014: Process-Oriented MJO Simulation Diagnostic: Moisture Sensitivity of Simulated Convection. *Journal of Climate*, **27**, 5379–5395, doi:10.1175/JCLI-D-13-00497.1.

URL https://journals.ametsoc.org/view/journals/clim/27/14/jcli-d-13-00497.1.xml

Kiranmayi, L. and E. D. Maloney, 2011: Intraseasonal moist static energy budget in reanalysis data. *Journal of Geophysical Research: Atmospheres*, **116**, doi:10.1029/2011JD016031.

URL https://onlinelibrary.wiley.com/doi/abs/10.1029/2011JD016031

Lebsock, M. D., T. S. L'Ecuyer, and R. Pincus, 2017: An Observational View of Relationships Between Moisture Aggregation, Cloud, and Radiative Heating Profiles. *Surveys in Geophysics*, **38**, 1237–1254, doi:10.1007/s10712-017-9443-1.

URL https://doi.org/10.1007/s10712-017-9443-1

L'Ecuyer, T. S. and G. L. Stephens, 2003: The Tropical Oceanic Energy Budget from the TRMM Perspective. Part I: Algorithm and Uncertainties. *Journal of Climate*, **16**, 1967–1985, doi:10.1175/1520-0442(2003)016¡1967:TTOEBF¿2.0.CO;2.

URL https://journals.ametsoc.org/view/journals/clim/16/12/1520-0442_2003_016_1967_ttoebf_2.0.co_2.xml

L'Ecuyer, T. S. and G. L. Stephens, 2007: The Tropical Atmospheric Energy Budget from the TRMM Perspective. Part II: Evaluating GCM Representations of the

Sensitivity of Regional Energy and Water Cycles to the 1998–99 ENSO Cycle. *Journal of Climate*, **20**, 4548–4571, doi:10.1175/JCLI4207.1.

URL https://journals.ametsoc.org/view/journals/clim/20/18/jcli4207.1.xml

Madden, R. A. and P. R. Julian, 1971: Detection of a 40–50 Day Oscillation in the Zonal Wind in the Tropical Pacific. *Journal of the Atmospheric Sciences*, **28**, 702–708, doi:10.1175/1520-0469(1971)028¡0702:DOADOI¿2.0.CO;2, publisher: American Meteorological Society Section: Journal of the Atmospheric Sciences.

URL https://journals.ametsoc.org/view/journals/atsc/28/5/1520-0469_1971_028_0702_doadoi_2_0_co_2.xml

Maithel, V. and L. Back, 2022: Moisture Recharge–Discharge Cycles: A Gross Moist Stability–Based Phase Angle Perspective. *Journal of the Atmospheric Sciences*, **79**, 2401–2417, doi:10.1175/JAS-D-21-0297.1, publisher: American Meteorological Society Section: Journal of the Atmospheric Sciences.

URL https://journals.ametsoc.org/view/journals/atsc/79/9/JAS-D-21-0297.1.xml

Maloney, E. D., 2009: The Moist Static Energy Budget of a Composite Tropical Intraseasonal Oscillation in a Climate Model. *Journal of Climate*, **22**, 711–729, doi:10.1175/2008JCLI2542.1, publisher: American Meteorological Society Section: Journal of Climate.

URL https://journals.ametsoc.org/view/journals/clim/22/3/2008jcli2542.1.xml

Mapes, B., S. Tulich, J. Lin, and P. Zuidema, 2006: The mesoscale convection life cycle: Building block or prototype for large-scale tropical waves? *Dynamics of Atmospheres and Oceans*, **42**, 3–29, doi:10.1016/j.dynatmoce.2006.03.003.

URL https://linkinghub.elsevier.com/retrieve/pii/S0377026506000340

Mapes, B. E., E. S. Chung, W. M. Hannah, H. Masunaga, A. J. Wimmers, and C. S. Velden, 2018: The Meandering Margin of the Meteorological Moist Tropics. *Geophysical Research Letters*, **45**, 1177–1184, doi:10.1002/2017GL076440, _eprint: https://onlinelibrary.wiley.com/doi/pdf/10.1002/2017GL076440.

URL https://onlinelibrary.wiley.com/doi/abs/10.1002/2017GL076440

Masunaga, H., 2013: A Satellite Study of Tropical Moist Convection and Environmental Variability: A Moisture and Thermal Budget Analysis. *Journal of the Atmospheric Sciences*, **70**, 2443–2466, doi:10.1175/JAS-D-12-0273.1, publisher: American Meteorological Society Section: Journal of the Atmospheric Sciences.

URL https://journals.ametsoc.org/view/journals/atsc/70/8/jas-d-12-0273.1.xml

Masunaga, H., C. E. Holloway, H. Kanamori, S. Bony, and T. H. M. Stein, 2021: Transient Aggregation of Convection: Observed Behavior and Underlying Processes. *Journal of Climate*, **34**, 1685–1700, doi:10.1175/JCLI-D-19-0933.1, publisher: American Meteorological Society Section: Journal of Climate.

URL https://journals.ametsoc.org/view/journals/clim/34/5/JCLI-D-19-0933.1.xml

Masunaga, H. and T. S. L'Ecuyer, 2014: A Mechanism of Tropical Convection Inferred from Observed Variability in the Moist Static Energy Budget. *Journal of the Atmospheric Sciences*, **71**, 3747–3766, doi:10.1175/JAS-D-14-0015.1.

URL https://journals.ametsoc.org/doi/10.1175/JAS-D-14-0015.1

Matsuno, T., 1966: Quasi-Geostrophic Motions in the Equatorial Area. *Journal of the Meteorological Society of Japan. Ser. II*, **44**, 25–43, doi:10.2151/jmsj1965.44.1$_2$5.

URL

Mayta, V. and F. A. Corraliza, 2023: The Stirring Tropics. Part I: The Ubiquity of Moisture Modes and Moisture-Vortex. Publisher: EarthArXiv.

https://eartharxiv.org/repository/view/5167/

Mayta, V. C., F. Adames, and F. Ahmed, 2022: Westward-Propagating Moisture Mode Over the Tropical Western Hemisphere. *Geophysical Research Letters*, **49**, e2022GL097799, doi:10.1029/2022GL097799, _eprint: https://onlinelibrary.wiley.com/doi/pdf/10.1029/2022GL097799.

https://onlinelibrary.wiley.com/doi/abs/10.1029/2022GL097799

Muller, C. J. and I. M. Held, 2012: Detailed Investigation of the Self-Aggregation of Convection in Cloud-Resolving Simulations. *Journal of the Atmospheric Sciences*, **69**, 2551–2565, doi:10.1175/JAS-D-11-0257.1, publisher: American Meteorological Society

Section: Journal of the Atmospheric Sciences.

https://journals.ametsoc.org/view/journals/atsc/69/8/jas-d-11-0257.1.xml

Neelin, J. D. and I. M. Held, 1987: Modeling Tropical Convergence Based on the Moist Static Energy Budget. *Monthly Weather Review*, **115**, 3–12, doi:10.1175/1520-0493(1987)115¡0003:MTC

https://journals.ametsoc.org/view/journals/mwre/115/1/1520-0493_1987_115_0003_mtcbot_2_0_co_2.xml

Neelin, J. D. and J.-Y. Yu, 1994: Modes of Tropical Variability under Convective Adjustment and the Madden–Julian Oscillation. Part I: Analytical Theory. *Journal of the Atmospheric Sciences*, **51**, 1876–1894, doi:10.1175/1520-0469(1994)051¡1876:MOTVUC¿2.0.CO;2, publisher: American Meteorological Society Section: Journal of the Atmospheric Sciences.

https://journals.ametsoc.org/view/journals/atsc/51/13/1520-0469_1994_051_1876_motvuc_2_0_co_2.xml

Neelin, J. D. and N. Zeng, 2000: A Quasi-Equilibrium Tropical Circulation Model—Formulation*. *Journal of the Atmospheric Sciences*, **57**, 1741–1766, doi:10.1175/1520-0469(2000)057¡1741:AQETCM¿2

http://journals.ametsoc.org/doi/10.1175/1520-0469(2000)057<1741:AQETCM>2.0.CO;2

Peters, M. E., Z. Kuang, and C. C. Walker, 2008: Analysis of Atmospheric Energy Transport in ERA-40 and Implications for Simple Models of the Mean Tropical Circulation. *Journal of Climate*, **21**, 5229–5241, doi:10.1175/2008JCLI2073.1, publisher: American

Meteorological Society Section: Journal of Climate.

https://journals.ametsoc.org/view/journals/clim/21/20/2008jcli2073.1.xml

Peters, O. and J. D. Neelin, 2006: Critical phenomena in atmospheric precipitation. *Nature Physics*, **2**, 393–396, doi:10.1038/nphys314, number: 6 Publisher: Nature Publishing Group.

https://www.nature.com/articles/nphys314

Pincus, R., A. Beljaars, S. A. Buehler, G. Kirchengast, F. Ladstaedter, and J. S. Whitaker, 2017: The Representation of Tropospheric Water Vapor Over Low-Latitude Oceans in (Re-)analysis: Errors, Impacts, and the Ability to Exploit Current and Prospective Observations. *Surveys in Geophysics*, **38**, 1399–1423, doi:10.1007/s10712-017-9437-z.

https://doi.org/10.1007/s10712-017-9437-z

Pope, K. N., C. E. Holloway, T. R. Jones, and T. H. M. Stein, 2021: Cloud-Radiation Interactions and Their Contributions to Convective Self-Aggregation. *Journal of Advances in Modeling Earth Systems*, **13**, e2021MS002535, doi:10.1029/2021MS002535, _eprint: https://onlinelibrary.wiley.com/doi/pdf/10.1029/2021MS002535.

https://onlinelibrary.wiley.com/doi/abs/10.1029/2021MS002535

— 2023: Radiation, Clouds, and Self-Aggregation in RCEMIP Simulations. *Journal of Advances in Modeling Earth Systems*, **15**, e2022MS003317, doi:10.1029/2022MS003317,

_eprint: https://onlinelibrary.wiley.com/doi/pdf/10.1029/2022MS003317.

https://onlinelibrary.wiley.com/doi/abs/10.1029/2022MS003317

Raymond, D. J., 2000: Thermodynamic control of tropical rainfall. *Quarterly Journal of the Royal Meteorological Society*, **126**, 889–898, doi:10.1002/qj.49712656406, _eprint: https://onlinelibrary.wiley.com/doi/pdf/10.1002/qj.49712656406.

https://onlinelibrary.wiley.com/doi/abs/10.1002/qj.49712656406

Raymond, D. J. and Fuchs, 2007: Convectively coupled gravity and moisture modes in a simple atmospheric model. *Tellus A: Dynamic Meteorology and Oceanography*, **59**, 627–640, doi:10.1111/j.1600-0870.2007.00268.x.

https://www.tandfonline.com/doi/full/10.1111/j.1600-0870.2007.00268.x

— 2009: Moisture Modes and the Madden–Julian Oscillation. *Journal of Climate*, **22**, 3031–3046, doi:10.1175/2008JCLI2739.1.

https://journals.ametsoc.org/view/journals/clim/22/11/2008jcli2739.1.xml

Raymond, D. J. and S. L. Sessions, 2007: Evolution of convection during tropical cyclogenesis. *Geophysical Research Letters*, **34**, doi:10.1029/2006GL028607, _eprint: https://onlinelibrary.wiley

https://onlinelibrary.wiley.com/doi/abs/10.1029/2006GL028607

Raymond, D. J., S. L. Sessions, and Fuchs, 2007: A theory for the spinup of tropical depressions. *Quarterly Journal of the Royal Meteorological Society*, **133**, 1743–1754,

doi:10.1002/qj.125, _eprint: https://rmets.onlinelibrary.wiley.com/doi/pdf/10.1002/qj.125.

https://rmets.onlinelibrary.wiley.com/doi/abs/10.1002/qj.125

Raymond, D. J., S. L. Sessions, A. H. Sobel, and Fuchs, 2009: The Mechanics of Gross Moist Stability. *Journal of Advances in Modeling Earth Systems*, **1**, doi:10.3894/JAMES.2009.1.9.

https://agupubs.onlinelibrary.wiley.com/doi/abs/10.3894/JAMES.2009.1.9

Raymond, D. J. and X. Zeng, 2005: Modelling tropical atmospheric convection in the context of the weak temperature gradient approximation. *Quarterly Journal of the Royal Meteorological Society*, **131**, 1301–1320, doi:10.1256/qj.03.97.

http://rmets.onlinelibrary.wiley.com/doi/abs/10.1256/qj.03.97

Riehl, H. and J. Malkus, 1958: On the heat balance in the equatorial trough zone. *Geophysica*, **6**, 503–538.

Rydbeck, A. V. and E. D. Maloney, 2015: On the Convective Coupling and Moisture Organization of East Pacific Easterly Waves. *Journal of the Atmospheric Sciences*, **72**, 3850–3870, doi:10.1175/JAS-D-15-0056.1, publisher: American Meteorological Society Section: Journal of the Atmospheric Sciences.

https://journals.ametsoc.org/view/journals/atsc/72/10/jas-d-15-0056.1.xml

Sakaeda, N. and G. Torri, 2022: The Behaviors of Intraseasonal Cloud Organization During DYNAMO/AMIE. *Journal of Geophysical Research: Atmospheres*, **127**, e2021JD035749,

doi:10.1029/2021JD035749, _eprint: https://agupubs.onlinelibrary.wiley.com/doi/pdf/10.1029/2021JD

http://onlinelibrary.wiley.com/doi/abs/10.1029/2021JD035749

Sessions, S. L., S. Sugaya, D. J. Raymond, and A. H. Sobel, 2010: Multiple equilibria in a cloud-resolving model using the weak temperature gradient approximation. *Journal of Geophysical Research: Atmospheres*, **115**, doi:10.1029/2009JD013376, _eprint: https://onlinelibrary.wiley.com/doi/pdf/10.1029/2009JD013376.

https://onlinelibrary.wiley.com/doi/abs/10.1029/2009JD013376

Sobel, A. and E. Maloney, 2013: Moisture Modes and the Eastward Propagation of the MJO. *Journal of the Atmospheric Sciences*, **70**, 187–192, doi:10.1175/JAS-D-12-0189.1.

https://journals.ametsoc.org/view/journals/atsc/70/1/jas-d-12-0189.1.xml

Sobel, A., S. Wang, and D. Kim, 2014: Moist Static Energy Budget of the MJO during DYNAMO. *Journal of the Atmospheric Sciences*, **71**, 4276–4291, doi:10.1175/JAS-D-14-0052.1, publisher: American Meteorological Society Section: Journal of the Atmospheric Sciences.

https://journals.ametsoc.org/view/journals/atsc/71/11/jas-d-14-0052.1.xml

Sobel, A. H. and C. S. Bretherton, 2000: Modeling Tropical Precipitation in a Single Column. *Journal of Climate*, **13**, 4378–4392, doi:10.1175/1520-0442(2000)013¡4378:MTPIAS¿2.0.CO;2.

https://journals.ametsoc.org/view/journals/clim/13/24/1520-0442_2000_013_4378_mtpias_2.0.co_2.xml

Sobel, A. H., J. Nilsson, and L. M. Polvani, 2001: The Weak Temperature Gradient Approximation and Balanced Tropical Moisture Waves. *Journal of the Atmospheric Sciences*, **58**, 3650–3665, doi:10.1175/1520-0469(2001)058¡3650:TWTGAA¿2.0.CO;2.
https://journals.ametsoc.org/view/journals/atsc/58/23/1520-0469_2001_058_3650_twtgaa_2.0.co_2.xml

Srinivasan, J., 2001: A simple thermodynamic model for seasonal variation of monsoon rainfall. *Current Science*, **80**, 73–77, publisher: Temporary Publisher.
https://www.jstor.org/stable/24105558

Stein, T. H. M., C. E. Holloway, I. Tobin, and S. Bony, 2017: Observed Relationships between Cloud Vertical Structure and Convective Aggregation over Tropical Ocean. *Journal of Climate*, **30**, 2187–2207, doi:10.1175/JCLI-D-16-0125.1, publisher: American Meteorological Society Section: Journal of Climate.
https://journals.ametsoc.org/view/journals/clim/30/6/jcli-d-16-0125.1.xml

Stevens, B. and S. Bony, 2013: What Are Climate Models Missing? *Science*, **340**, 1053–1054, doi:10.1126/science.1237554.
https://www.sciencemag.org/lookup/doi/10.1126/science.1237554

Su, H. and J. D. Neelin, 2002: Teleconnection Mechanisms for Tropical Pacific Descent Anomalies during El Niño. *Journal of the Atmospheric Sciences*, **59**, 2694–2712, doi:10.1175/1520-0469(2002)059¡2694:TMFTPD¿2.0.CO;2.

https://journals.ametsoc.org/view/journals/atsc/59/18/1520-0469_2002_059_2694_tmftpd_2.0.co_2.xml

Tobin, I., S. Bony, and R. Roca, 2012: Observational Evidence for Relationships between the Degree of Aggregation of Deep Convection, Water Vapor, Surface Fluxes, and Radiation. *Journal of Climate*, **25**, 6885–6904, doi:10.1175/JCLI-D-11-00258.1, publisher: American Meteorological Society Section: Journal of Climate.
https://journals.ametsoc.org/view/journals/clim/25/20/jcli-d-11-00258.1.xml

Tompkins, A. M. and A. G. Semie, 2017: Organization of tropical convection in low vertical wind shears: Role of updraft entrainment. *Journal of Advances in Modeling Earth Systems*, **9**, 1046–1068, doi:10.1002/2016MS000802, _eprint: https://onlinelibrary.wiley.com/doi/pdf/10.10
https://onlinelibrary.wiley.com/doi/abs/10.1002/2016MS000802

Tsai, W.-M. and B. E. Mapes, 2022: Evidence of Aggregation Dependence of 5°-Scale Tropical Convective Evolution Using a Gross Moist Stability Framework. *Journal of the Atmospheric Sciences*, **79**, 1385–1404, doi:10.1175/JAS-D-21-0253.1, publisher: American Meteorological Society Section: Journal of the Atmospheric Sciences.
https://journals.ametsoc.org/view/journals/atsc/79/5/JAS-D-21-0253.1.xml

Wang, S., A. H. Sobel, and J. Nie, 2016: Modeling the MJO in a cloud-resolving model with parameterized large-scale dynamics: Vertical structure, radiation, and horizontal advection of dry air. *Journal of Advances in Modeling Earth Systems*, **8**, 121–139,

doi:10.1002/2015MS000529.

https://agupubs.onlinelibrary.wiley.com/doi/abs/10.1002/2015MS000529

Webster, P. J. and R. Lukas, 1992: TOGA COARE: The Coupled Ocean–Atmosphere Response Experiment. *Bulletin of the American Meteorological Society*, **73**, 1377–1416, doi:10.1175/1520-0477(1992)073¡1377:TCTCOR¿2.0.CO;2, publisher: American Meteorological Society Section: Bulletin of the American Meteorological Society.

https://journals.ametsoc.org/view/journals/bams/73/9/1520-0477_1992_073_1377_tctcor_2_0_co_2.xml

Wentz, F., C. Gentemann, and K. Hilburn, 2015: Remote Sensing Systems TRMM TMI Daily Environmental Suite on 0.25 deg grid, Version 7.1. Remote Sensing Systems, Santa Rosa, CA. Available online at www.remss.com/missions/tmi. Accessed 04 OCT 2021.

Wentz, F., K. Hilburn, and D. Smith, 2012: Remote Sensing Systems DMSP SSM/I Daily Environmental Suite on 0.25 deg grid, Version 7. Remote Sensing Systems, Santa Rosa, CA. Available online at www.remss.com/missions/ssmi. Accessed 04 OCT 2021.

Wentz, F., T. Meissner, C. Gentemann, and M. Brewer, 2014: Remote Sensing Systems AQUA AMSR-E Daily Environmental Suite on 0.25 deg grid, Version 7.0. Remote Sensing Systems, Santa Rosa, CA. Available online at www.remss.com/missions/amsr. Accessed 04 OCT 2021.

Wheeler, M. and G. N. Kiladis, 1999: Convectively Coupled Equatorial Waves: Analysis of Clouds and Temperature in the Wavenumber–Frequency Domain. *Journal of the Atmospheric Sciences*, **56**, 374–399, doi:10.1175/1520-0469(1999)056¡0374:CCEWAO¿2.0.CO;2, publisher: American Meteorological Society Section: Journal of the Atmospheric Sciences.
https://journals.ametsoc.org/view/journals/atsc/56/3/1520-0469_1999_056_0374_ccewao_2.0.co_2.xml

Wing, A. A., 2019: Self-Aggregation of Deep Convection and its Implications for Climate. *Current Climate Change Reports*, **5**, 1–11, doi:10.1007/s40641-019-00120-3.
https://doi.org/10.1007/s40641-019-00120-3

Wing, A. A. and T. W. Cronin, 2016: Self-aggregation of convection in long channel geometry. *Quarterly Journal of the Royal Meteorological Society*, **142**, 1–15, doi:10.1002/qj.2628, _eprint: https://onlinelibrary.wiley.com/doi/pdf/10.1002/qj.2628.
https://onlinelibrary.wiley.com/doi/abs/10.1002/qj.2628

Wing, A. A., K. Emanuel, C. E. Holloway, and C. Muller, 2017: Convective Self-Aggregation in Numerical Simulations: A Review. *Surveys in Geophysics*, **38**, 1173–1197, doi:10.1007/s10712-017-9408-4.
http://link.springer.com/10.1007/s10712-017-9408-4

Wing, A. A. and K. A. Emanuel, 2014: Physical mechanisms controlling self-aggregation

of convection in idealized numerical modeling simulations. *Journal of Advances in Modeling Earth Systems*, **6**, 59–74, doi:10.1002/2013MS000269.

https://onlinelibrary.wiley.com/doi/abs/10.1002/2013MS000269

Wolding, B., J. Dias, G. Kiladis, F. Ahmed, S. W. Powell, E. Maloney, and M. Branson, 2020: Interactions between Moisture and Tropical Convection. Part I: The Coevolution of Moisture and Convection. *Journal of the Atmospheric Sciences*, **77**, 1783–1799, doi:10.1175/JAS-D-19-0225.1.

http://journals.ametsoc.org/doi/10.1175/JAS-D-19-0225.1

Wolding, B., S. W. Powell, F. Ahmed, J. Dias, M. Gehne, G. Kiladis, and J. D. Neelin, 2022: Tropical Thermodynamic–Convection Coupling in Observations and Reanalyses. *Journal of the Atmospheric Sciences*, **79**, 1781–1803, doi:10.1175/JAS-D-21-0256.1, publisher: American Meteorological Society Section: Journal of the Atmospheric Sciences.

https://journals.ametsoc.org/view/journals/atsc/79/7/JAS-D-21-0256.1.xml

Wolding, B. O. and E. D. Maloney, 2015: Objective Diagnostics and the Madden–Julian Oscillation. Part II: Application to Moist Static Energy and Moisture Budgets. *Journal of Climate*, **28**, 7786–7808, doi:10.1175/JCLI-D-14-00689.1, publisher: American Meteorological Society Section: Journal of Climate.

https://journals.ametsoc.org/view/journals/clim/28/19/jcli-d-14-00689.1.xml

Wolding, B. O., E. D. Maloney, and M. Branson, 2016: Vertically resolved weak temperature gradient analysis of the Madden-Julian Oscillation in SP-CESM. *Journal of Advances in Modeling Earth Systems*, **8**, 1586–1619, doi:10.1002/2016MS000724, _eprint: https://onlinelibrary.wiley.com/doi/pdf/10.1002/2016MS000724.
https://onlinelibrary.wiley.com/doi/abs/10.1002/2016MS000724

Wu, X. and L. Deng, 2013: Comparison of Moist Static Energy and Budget between the GCM-Simulated Madden–Julian Oscillation and Observations over the Indian Ocean and Western Pacific. *Journal of Climate*, **26**, 4981–4993, doi:10.1175/JCLI-D-12-00607.1, publisher: American Meteorological Society Section: Journal of Climate.
https://journals.ametsoc.org/view/journals/clim/26/14/jcli-d-12-00607.1.xml

Yanai, M., S. Esbensen, and J.-H. Chu, 1973: Determination of Bulk Properties of Tropical Cloud Clusters from Large-Scale Heat and Moisture Budgets. *Journal of the Atmospheric Sciences*, **30**, 611–627, doi:10.1175/1520-0469(1973)030¡0611:DOBPOT¿2.0.CO;2, publisher: American Meteorological Society Section: Journal of the Atmospheric Sciences.
https://journals.ametsoc.org/view/journals/atsc/30/4/1520-0469_1973_030_0611_dobpot_2_0_co_2.xml

Yano, J.-I. and M. Bonazzola, 2009: Scale Analysis for Large-Scale Tropical Atmospheric Dynamics. *Journal of the Atmospheric Sciences*, **66**, 159–172, doi:10.1175/2008JAS2687.1, publisher: American Meteorological Society Section: Journal of the Atmospheric Sciences.
https://journals.ametsoc.org/view/journals/atsc/66/1/2008jas2687.1.xml

Yasunaga, K., S. Yokoi, K. Inoue, and B. E. Mapes, 2019: Space–Time Spectral Analysis of the Moist Static Energy Budget Equation. *Journal of Climate*, **32**, 501–529, doi:10.1175/JCLI-D-18-0334.1.

https://journals.ametsoc.org/view/journals/clim/32/2/jcli-d-18-0334.1.xml

Yu, J.-Y., C. Chou, and J. D. Neelin, 1998: Estimating the Gross Moist Stability of the Tropical Atmosphere. *Journal of the Atmospheric Sciences*, **55**, 1354–1372, doi:10.1175/1520-0469(1998)055¡1354:ETGMSO¿2.0.CO;2, publisher: American Meteorological Society Section: Journal of the Atmospheric Sciences.

https://journals.ametsoc.org/view/journals/atsc/55/8/1520-0469_1998_055_1354_etgmso_2.0.co_2.xml

Yu, J.-Y. and J. D. Neelin, 1997: Analytic Approximations for Moist Convectively Adjusted Regions. *Journal of the Atmospheric Sciences*, **54**, 1054–1063, doi:10.1175/1520-0469(1997)054¡1054:AAFMCA¿2.0.CO;2, publisher: American Meteorological Society Section: Journal of the Atmospheric Sciences.

https://journals.ametsoc.org/view/journals/atsc/54/8/1520-0469_1997_054_1054_aafmca_2.0.co_2.xml

Zhang, M. H. and J. L. Lin, 1997: Constrained Variational Analysis of Sounding Data Based on Column-Integrated Budgets of Mass, Heat, Moisture, and Momentum: Approach and Application to ARM Measurements. *Journal of the Atmospheric Sciences*, **54**, 1503–1524, doi:10.1175/1520-0469(1997)054¡1503:CVAOSD¿2.0.CO;2.

https://journals.ametsoc.org/view/journals/atsc/54/11/1520-0469_1997_054_1503_cvaosd_2.0.co_2.xml